SANDIA REPORT

SAND79—0414 • UC—34a
Unlimited Release
Reprinted February 1987

Calorimetric Measurement of Electron Energy Deposition in Extended Media—Theory vs Experiment

Grant J. Lockwood, Laurence E. Ruggles,
Glenn H. Miller, John A. Halbleib

Prepared by
Sandia National Laboratories
Albuquerque, New Mexico 87185 and Livermore, California 94550
for the United States Department of Energy
under Contract DE-AC04-76DP00789

SF2900Q(8-81)

Issued by Sandia Laboratories, operated for the United States Department of Energy by Sandia Corporation.

NOTICE

This report was prepared as an account of work sponsored by the United States Government. Neither the United States nor the Department of Energy, nor any of their employees, nor any of their contractors, subcontractors, or their employees, makes any warranty, express or implied, or assumes any legal liability or responsibility for the accuracy, completeness or usefulness of any information, apparatus, product or process disclosed, or represents that its use would not infringe privately owned rights.

Printed in the United States of America

Available from
National Technical Information Service
U. S. Department of Commerce
5285 Port Royal Road
Springfield, VA 22161

Price: Printed Copy $7.25; Microfiche $3.00

SAND79-0414
Unlimited Release
Printed January 1980
Reprinted February 1987

CALORIMETRIC MEASUREMENT OF ELECTRON ENERGY DEPOSITION IN EXTENDED MEDIA-- THEORY VS EXPERIMENT

Grant J. Lockwood
Laurence E. Ruggles
Beam Source Applications Division 4232

Glenn H. Miller
Laser Application and Spectroscopy Division 4216

John A. Halbleib
Theoretical Division 4231

Sandia Laboratories
Albuquerque, NM 87185

ABSTRACT

A new calorimetric technique has been developed for measuring electron energy deposition profiles in one dimension. The experimental procedures and theoretical analyses required in the application of the new method are reviewed. We present extensive results for electron energy deposition profiles in semi-infinite homogeneous and multilayer configurations. These data cover a range of elements from beryllium through uranium at source energies from 0.3 to 1.0 MeV (selected data at 0.5 and 0.1 MeV) and at incident angles from 0° to 60°. In every case, the experimental profiles are compared with the predictions of a coupled electron/photon Monte Carlo transport code. Overall agreement between theory and experiment is very good. However, there appears to be a tendency for the theoretical profiles to be higher near the peaks and lower near the tails, especially in high-Z materials. There is also a discrepancy between theory and experiment in low-Z materials near high-Z/low-Z interfaces.

ACKNOWLEDGMENT

It is a pleasure to make note of the assistance provided by Allyn R. Phillips, who provided the programming for the on-line computer.

CONTENTS

CONTENTS (Cont)

ILLUSTRATIONS

ILLUSTRATIONS (Cont)

ILLUSTRATIONS (Cont)

CALORIMETRIC MEASUREMENT OF ELECTRON ENERGY DEPOSITION IN EXTENDED MEDIA-- THEORY VS EXPERIMENT

I. Introduction

The energy deposited in extended media by electrons with kinetic energies in the megaelectron-volt (MeV) range has been studied extensively over the past few decades. Extended-media targets imply geometries with dimensions that are a significant fraction of the ranges of the source electrons, so that the predictions of one-step multiple interaction methods such as the continuous-slowing-down-approximation (CSDA) or energy-loss straggling theories cannot be relied upon. In recent years, investigation of these phenomena has received impetus from such areas as health physics research, space shielding problems, and the myriad of applications of pulsed relativistic electron beam technology (electron-beam fusion, gas-laser excitation, simulation of nuclear and space radiation effects, and others).

Traditional methods of measuring electron energy deposition profiles have included ionization chambers,[1-11] passive dosimetry,[12-18] solid-state detectors,[19-21] and luminescence.[22] The classic work of Spencer[23] was the first serious theoretical technique. Today, however, the method of condensed-history Monte Carlo[24] has all but replaced Spencer's moments method.

Despite all of this activity, there remain substantial ambiguities among various experimental results that preclude the kind of definitive verification of theoretical models that is warranted. This situation is illustrated quite vividly in Figure I. 1. Shown here are five experimental measurements[7, 8, 11, 20, 25] and the theoretical prediction from a condensed-history Monte Carlo model[26] of the electron energy deposition profile in a semi-infinite medium of Al for normally incident, 0.5-MeV electrons. Shown also are Spencer's results[23] for a plane parallel source of 0.5-MeV electrons in an infinite medium of Al. It is this kind of scatter in such basic transport data that motivated the present work.

A critical review of data available through the early 1970s leads to an awareness of certain deficiencies:

1. Much of the data is not absolute in the sense that often some response profile other than energy deposition is reported, or else the response profile is arbitrarily normalized to agree with existing theoretical or experimental energy deposition data.

2. Many of the results were obtained by using infinite rather than semi-infinite geometries. This was done either to simplify the measurement or to facilitate comparison with Spencer's early calculations.[23] In any case, the semi-infinite geometry is of more practical importance.

3. In the case of semi-infinite geometries, there are very little data for electron energies less than 1.0 MeV for nonnormal incidence, and for multislab media.

4. Spatial resolution near the surface of semi-infinite geometries is poor, especially for high-atomic-number media.

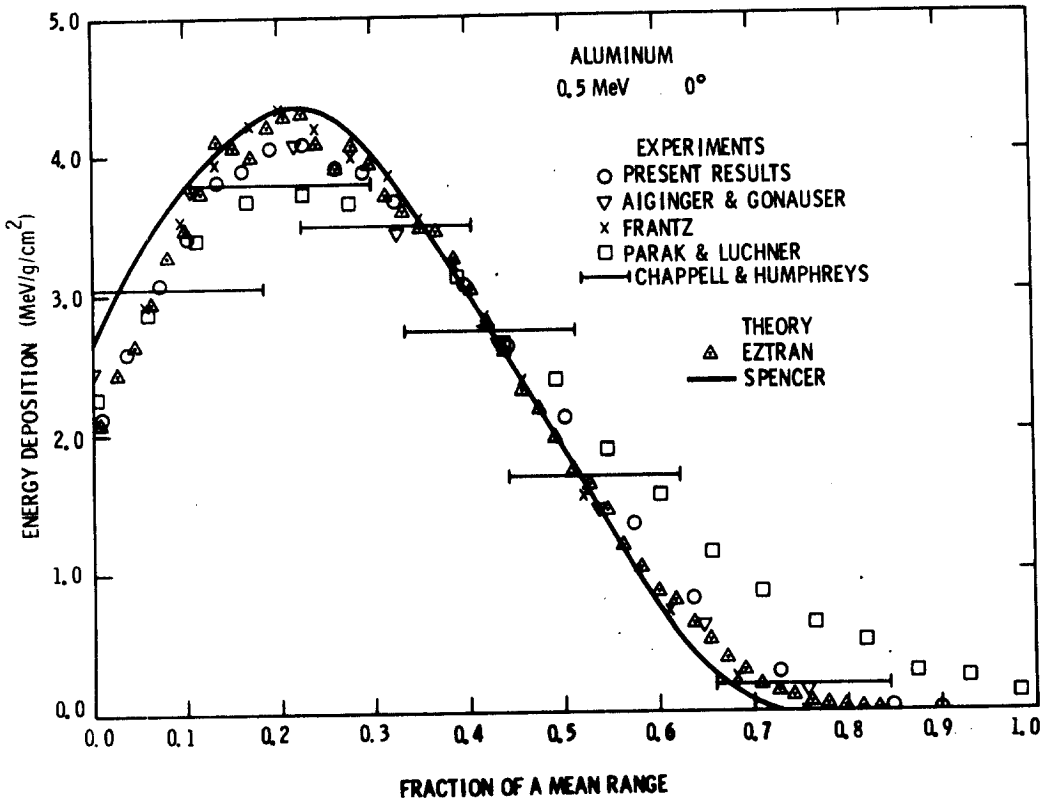

Figure I.1. Comparison of Experimental Measurements and Theoretical Predictions of Energy Deposition Profiles in Semi-Infinite Aluminum by Normally Incident 0.5-MeV Electrons

On the basis of this review, a commitment was made to a program having as its objective the measurement of absolute, high-resolution electron energy deposition profiles in a wide range of materials (varying atomic number) at source energies up to 1.0 MeV and at various angles of incidence for homogeneous semi-infinite and multilayer configurations. In addition to their inherent value as basic transport data, these results would also be useful for the verification of state-of-the-art transport codes.

Most of the existing data had been obtained with the use of thin gas-filled ionization chambers or passive dosimeters. During the early stages of the present program, the ionization method was

employed.[27] However, three rather serious problems were encountered. First, it was necessary to surround the entire chamber with the fill-gas at the same pressure, since the necessarily very thin front electrode could not withstand significant pressure difference without bowing. This, in turn, required a thin window between the gas-filled region and the electron accelerator. This window scattered the beam and had to be considered a part of the stopping material. It was difficult to account for these effects in the analysis. Second, the process of making the measurement was complicated, requiring that saturation be verified and that several extraneous effects be treated. In order to accomplish the latter, it was necessary to make measurements as a function of gas pressure, thus aggravating the window problem noted in the first point. Third, the gas used did not have the same atomic number as the material under investigation, necessitating a correction for difference in stopping powers. This correction was difficult and could have introduced significant inaccuracy.

The first and second difficulties could have been eliminated by using passive dosimetry. However, the third problem is likely to have been worse, since the atomic numbers available for passive dosimeters are very limited. Further, the measurement would not have been prompt; a significant time would have elapsed between completion of the experiment and reduction of the data. Only one experiment could have been conducted for each dosimeter. Excellent quality control and extensive calibration would have been required. Finally, the beam would have to be uniformly distributed over a sizeable area.

It was found that to a large degree a thin-foil calorimetric technique could nullify all these objections. If the material under investigation were a stable metal, then the calorimeter could be made of that material, thus avoiding any stopping power correction. This method could be used in vacuo, so that no window would be required. The data could be collected and analyzed by an on-line computer so that the results would be available in a matter of seconds following a measurement. Calibration would be straightforward and accurate. Because of these advantages, consideration of other methods was abandoned in favor of the development of a sophisticated calorimetric technique with on-line data analysis.

This report is a comprehensive review of the calorimetric measurement of electron energy deposition profiles and of the comparison of these experimental data with the predictions of the TIGER code,[26] a one-dimensional, coupled electron/photon Monte Carlo transport code. Portions of this material have appeared in previous publications.[25, 27, 28, 29] Section II provides a detailed discussion of the calorimetric method. A complete description of the experimental apparatus is given in Section III. Application of the TIGER code to predict the energy deposition profiles is discussed in Section IV. Section V presents graphical and tabular comparisons of experimental and theoretical results ranging over source energies, incident angles, and target atomic numbers of 0.3 to 1.0 MeV (selected data at 0.05 and 0.1 MeV), 0° to 60° and 4 to 92, respectively. Concluding remarks are contained in Section VI.

II. Calorimetric Method

A. General Considerations

In the previous section, the requirements for the energy-deposition measurement technique were reviewed. The available methods were surveyed with the result that none satisfied all of the requirements. Of those examined, it appeared that calorimetry offered the greatest promise. Therefore, the development of an improved technique based on this method was pursued.

At the outset, it was clear that this approach had several advantages. First, it was absolute. The sensitivity could be calculated from the geometry and known material properties. In addition to this, an experimental calibration could be made so that an independent check should be available. Second, it appeared that thin-foil calorimeters could be made of most metals, so that a variety of materials could be studied. In most cases of interest, no correction for relative stopping power would be required; at worst, the correction would be small and contribute little to the error. Third, the method was active rather than passive and had the possibility for rapid measurement and automatic data reduction.

On the other hand, there were some possible difficulties and uncertainties. It appeared that the signal might be small and that there might be a signal/noise ratio problem. The most likely means of temperature measurement appeared to be the use of thermocouples, so that one might be measuring 10^{-5}- to 10^{-4}-V signals in a radiation (Bremsstrahlung) environment. Further, it was not clear that there would not be a long-period thermal drift, making the measurement time-consuming and destroying the precision. Such a drift could occur due to the heat flow to the calorimeter support structure and an imperfect heat sink for the thermocouple reference junction. Finally, the response of the calorimeter might very well be dependent not only on the input power level but also on the geometrical extent and location of the deposition region. As the calorimeter was moved through the material thickness corresponding to movement through the electron range, the diameter of the energy deposition region changed. Further, the electron beam axis might not coincide with that of the calorimeter. In the case of nonnormal incidence, the projection of a cylindrical beam is elliptical. If these factors influenced the sensitivity, a true "calibration constant" would not exist.

The first of these problems was nonexistent. Even at low deposition rates, the signal/noise ratio was adequate, so that temperature measurement by thermocouples was quite satisfactory. The long-period thermal drift problem was present and would have caused great difficulty. However, it was possible to modulate the electron beam and measure the periodic thermocouple signal thus obtained. By making the modulation period short compared to the very long (of the order of 10^3 s) thermal-drift time constant, the effect was largely eliminated. The third problem, dependence of sensitivity on energy deposition geometry, was present and did perturb the results.

Sensitivity variation was eliminated by not using the amplitude of the periodic thermocouple signal but using instead the time derivative, taken at a prescribed time in the modulation cycle. The reason for the success of this can be seen from the analysis and will be pointed out later.

We now proceed to perform the analysis. Following this we will discuss the design considerations. Some unforeseen difficulties arose during the course of the experiments, and these will be examined also.

B. Theory of Calorimeter Response

Consider a circular foil of thickness w, radius r_o, density ρ, specific heat c, thermal conductivity K_1, and emissivity ϵ (centimetre-gram-second units are used throughout). Assume that the foil is supported by some number of wires resulting in a total cross sectional area A and each having a length L. The thermal conductivity of the wire is K_2. These wires are assumed to terminate in a perfect heat sink. The temperature at r_o is monitored as a function of time. It is assumed that there is no azimuthal temperature variation. The temperature relative to the heat-sink temperature at radius r and time t is given by u(r, t).

The differential equation is given by*

$$\frac{1}{r}\frac{\partial}{\partial r}\left(r\frac{\partial u}{\partial r}\right) - \alpha^2 u = \beta^2\frac{\partial u}{\partial t} - \frac{\dot{q}(r,t)}{wK_1} \quad , \tag{1}$$

where

$$\alpha^2 = \frac{8\sigma\epsilon T_o^3}{wK_1} \qquad \text{and} \qquad \beta^2 = \frac{\rho c}{K_1} \quad .$$

In the expressions all symbols have been defined except σ, which is the Stefan-Boltzmann constant; T_o, which is the Kelvin temperature of the enclosure and heat sink; and $\dot{q}(r, t)$, which is the rate of heat input per unit area. Note that $T^4 - T_o^4$ has been approximated by $4T_o^3 u$.

The function $\dot{q}(r, t)$ has the following time dependence

$$\begin{aligned} &\dot{q}(r,t) = \dot{q}(r) \qquad \text{for} \quad Nt_o < t \le (N + 1/2)t_o \\ &\dot{q}(r,t) = 0 \qquad\quad \text{for} \quad (N + 1/2)t_o < t \le (N + 1)t_o \quad . \end{aligned} \tag{2}$$

*See Appendix for the derivation of this equation.

Here N is an integer and t_o is the modulation period. The initial condition is

$$u(r, 0) = 0 \quad . \tag{3}$$

The boundary condition is given by

$$\left.\frac{\partial u(r, t)}{\partial r}\right|_{r=r_o} = -\gamma^2 u(r_o, t) \quad , \tag{4}$$

where

$$\gamma^2 = \frac{K_2 A/L}{2\pi r_o w K_1}$$

The equilibrium solutions ($N \to \infty$) to Eq (1) are given by

$$u(r, t) = \sum_{n=1}^{\infty} A_n J_o(k_n r) \left[1 - \mu_n e^{-t'/\tau_n}\right] \quad , \qquad Nt_o < t \leq (N + 1/2)t_o$$

and (5)

$$u(r, t) = \sum_{n=1}^{\infty} A_n J_o(k_n r) \mu_n e^{-t''/\tau_n}, \qquad (N + 1/2)t_o < t \leq (N + 1)t_o \quad .$$

Here t' and t'' are the times measured from Nt_o and $(N + 1/2)t_o$, respectively. The k_n's are the roots of Eq (4), which becomes

$$k_n J_1(k_n r_o) = \gamma^2 J_o(k_n r_o) \quad , \tag{6}$$

and the τ_n's are given by

$$\tau_n = \frac{\beta^2}{\alpha^2 + k_n^2} \quad . \tag{7}$$

The μ_n's are defined by

$$\mu_n = \left[1 + e^{-t_o/2\tau_n}\right]^{-1} \quad . \tag{8}$$

J_o and J_1 are the zero and first order Bessel functions. The A_n's are the Fourier-Bessel coefficients which are given by

$$A_n = \frac{2\tau_n}{w\rho c r_o^2} \frac{1}{J_o^2(k_n r_o) + J_1^2(k_n r_o)} \int_o^{r_m} \dot{q}(r) J_o(k_n r) r dr \quad , \tag{9}$$

where r_m is the maximum radius at which there is heat input. It is convenient to define an f(r), such that

$$q(r) = \frac{\dot{Q}_o}{\pi r_m^2} f(r), \text{ and } \int_o^{r_m} f(r) 2\pi r dr = \pi r_m^2 \quad . \tag{10}$$

Here $\dot{Q}_o$ is the total rate of heat input. Then we obtain

$$A_n = \frac{2\dot{Q}_o \tau_n}{\pi r_o^2 w\rho c} \frac{1}{\left[J_o^2(k_n r_o) + J_1^2(k_n r_o)\right]} \frac{1}{r_m^2} \int_o^{r_m} f(r) J_o(k_n r) r dr \quad . \tag{11}$$

For the special case where f(r) = 1 (i.e., the energy is put in uniformly over a circle of radius r_m), we obtain

$$A_n = \frac{2\dot{Q}_o \tau_n}{\pi r_o^2 w\rho c} \frac{1}{\left[J_o^2(k_n r_o) + J_1^2(k_n r_o)\right]} \frac{J_1(k_n r_m)}{k_n r_m} \quad . \tag{12}$$

We will assume such an input for the discussion which follows. At critical points the consequences of this assumption will be noted.

The most obvious method of obtaining the energy deposition from a calorimeter used in the time-modulated mode is to measure the amplitude of the resulting signal. Using Eq (5), we find that the amplitude is the maximum (with t′) of the function

$$\Delta u = \sum_{n=1}^{\infty} A_n J_o(k_n r_o) \left[2\mu_n e^{-t'/\tau_n} - 1\right] \quad . \tag{13}$$

The difficulty with this can be seen from Eq (12). A_n varies as

$$\frac{2J_1(k_n r_m)}{k_n r_m} \quad .$$

For $k_n r_m \ll 1$, this factor is nearly unity. However, for larger values of the argument, the factor may become small or negative. Thus as r_m is allowed to increase toward r_o, the sensitivity changes. Measurement of the amplitude is therefore not satisfactory, and we must consider other techniques.

Equation (7) indicates that the time constants of the successive terms in Eq (5) decrease rapidly as k_n increases. Examination of a table of roots of Eq (6)[30] shows that k_n increases rapidly with n, thus causing a rapid decrease in τ_n. In a typical case, successive time constants were calculated to be 75, 1.25, 0.4, and 0.2 s for n = 1, 2, 3, and 4, respectively. This immediately suggests that, due to the negative exponential, all terms other than the first can be depressed by taking the time derivative at a time in each half-cycle that is large compared to τ_2. We would then have

$$\left.\frac{du}{dt}\right|_{t=t_d} = \pm\sum A_n J_o(k_n r_o) \frac{\mu_n}{\tau_n} e^{-t_d/\tau_n} \quad . \tag{14}$$

The plus or minus algebraic signs are obtained for the two half-cycles in Eq (5). If the condition $t_d \gg \tau_2$, τ_3, etc, prevails, then

$$\left.\frac{du}{dt}\right|_{t=t_d} \cong \pm A_1 J_o(k_1 r_o) \frac{\mu_1}{\tau_1} e^{-t_d/\tau_1} \quad . \tag{15}$$

This solves no problem unless A_1 is a constant, independent of r_m. This is, in fact, a good approximation. Since $r_m \leq r_o$, we consider the range of $k_1 r_o$.

Due to the small value of $k_1 r_o$ (< 2.405), the value of the factor

$$\frac{2J_1(k_1 r_o)}{k_1 r_o}$$

is limited by

$$1 \geq \frac{2J_1(k_1 r_m)}{k_1 r_m} \geq 0.43 \quad ,$$

with the limits arranged in order of increasing $k_1 r_o$. While this is a large change, it is also unrealistic. In general the characteristics of the support wires, which determine γ^2 in Eq (6), will be chosen so that $k_1 r_o$ will be no more than about 0.5, resulting in a lower limit of

$$\frac{2J_1(k_1 r_o)}{k_1 r_o} = 0.97$$

Thus we find that the effect of varying r_m from zero to r_o is

$$1 \geq \frac{2J_1(k_1 r_m)}{k_1 r_m} \geq 0.97 \quad .$$

While this is very satisfactory, it is still overly generous. In most cases r_m will never be greater than $0.3\, r_o$. Then the lower limit is about 0.997 instead of 0.97.

The foregoing makes it clear that the derivative method provides a sensitivity which is very nearly constant. One must reexamine at this point the assumption that the energy is deposited in a manner which is independent of azimuth. Without attempting to solve the more general problem where $\dot{q} = \dot{q}(r, \phi)$, we can make an observation. If there is a ϕ-dependence either by displacing the deposition axis or by making the beam asymmetrical, then the result is to introduce Bessel functions of order greater than zero into the series of Eq (5). These terms will also have time constants short compared to τ_1, and hence will be removed by the derivative process. Experimentally, the beam position was varied over a wide range ($\sim$ 30% of r_o) with only small ($\sim$ 2%) variations in sensitivity. Typically the alignment in an experiment is maintained to within $0.05\, r_o$. Asymmetries may become large for oblique incidence, however.

From Eqs (12) and (15), one may now obtain an expression for Q_o. The approximations

$$\frac{2J_1(k_1 r_m)}{k_1 r_m} = 1 \quad ,$$

and

$$\frac{J_o(k_1 r)}{J_o^2(k_1 r_o) + J_1^2(k_1 r_o)} = 1$$

are made. These are both good within a few tenths of a percent for typical cases. This gives

$$Q_o = \pi r_o^2 w \rho c \left(1 + e^{-t_o/2\tau_1}\right) e^{t_d/\tau_1} \left.\frac{du}{dt}\right|_{t=t_d} \quad . \qquad (1$$

C. Data Analysis

Equation (16) indicates that one is to take the derivative at $t = t_d$, calculate e^{t_d/τ_1} and insert these as factors into the equation. Several factors enter into the choice of t_d. Certainly it must be large compared to τ_2. In addition, however, it might be chosen to minimize variations in

(or errors in the value of) τ_1. By differentiating the τ_1-dependent factors with respect to τ_1 and setting the derivative equal to zero, one finds that

$$t_d = \frac{t_o}{2} e^{-t_o/2\tau_1} \left[1 + e^{-t_o/2\tau_1} \right]^{-1} .$$

This criterion is not generally compatible with $t_d \gg \tau_2$, however. This problem was solved in the following manner. The data were processed in real time by an on-line digital computer (see Section III). The derivative was calculated continuously for $t_d >> \tau_2$, and the computer produced a least-squares linear fit on $\ln\left(\frac{du}{dt}\right)$ as a function of t_d. From this, the derivative could be calculated at any given time (even at $t_d \leq \tau_2$) with maximum precision, since all available data were used. This procedure evolved during the course of the measurements reported here so that the precision differs for the various results. In each set of results presented in Section V, the precision and method of analysis are indicated.

D. Calibration

In order to calibrate any of the calorimeters, it was necessary to deposit energy in it at a known rate. More specifically, it was very desirable that the same modulation period and the same data reduction procedure be used as that employed in the electron energy deposition measurements. This was accomplished by using ions of known energy and current from a separate accelerator. Ions are very suitable for the following reasons.

1. At the energies used, 10 to 100 keV, the range is much less than the calorimeter thickness. Thus none of the energy is transmitted through the back surface.
2. The backscatter is very small, and hence no correction for it is necessary.
3. Bremsstrahlung production is negligible, so there is no significant energy loss from the foil by this process.

E. Design Considerations

A number of factors influence the design of a calorimeter. In this part, the principal ones will be discussed.

1. Foil Radius. As the radius is decreased, more energy is lost by electrons scattered through large angles. The larger the space between elements (front foils, calorimeter, "infinite" plate) the more serious this effect. If the radius is too large, it may be too difficult to insure a planar orientation. Thus a compromise is necessary.

2. Foil Thickness. This also requires a compromise. The thinner the foil, the better the energy resolution. On the other hand, τ_1 is very dependent on foil thickness. Equation (7) may be rewritten as

$$\tau_n = \frac{\rho c w}{8\sigma \epsilon T_o^3 + w K_1 k_n^2} \quad .$$

For τ_1, the second term in the denominator may be made negligible, indicating that $\tau_1 \propto w$. For τ_2, the second term may be much more important, in which case τ_2 does not depend on w. Thus, the condition $\tau_1 >> \tau_2$ may not apply for very thin foils.

3. Foil Material. A major advantage cited for the calorimetric method was the possibility that the sensor was of the same material as, or close in atomic number to, that for which the deposition profile was to be obtained. Thus, one usually uses the metal closest in Z to the material involved. One can still specify the properties which are important, however. The thermal conductivity should be high. This permits small values of τ_2, τ_3, etc, while having very little influence on τ_1. The thermal emissivity ϵ should be low. This permits a large value of τ_1, without affecting τ_2, τ_3, etc. It is important that ϵ remain constant. A small value of ϵ is important in minimizing the thermal feed-through problem, which will be discussed in the next subsection. Low density is also desirable, since this feature leads to good energy resolution and high sensitivity. In general, Al, Cu, Ag, and Au are "good" while Fe, Pt, Ta, and U are "poor." However, any of the so-called "poor" materials can be used satisfactorily for most purposes.

4. Support Wires. In addition to maintaining the foil in a rigid position, the support wires provide heat-conducting paths and add to the thermal capacity. A more detailed analysis has been performed[31] with the result that the thermal capacity of the foil should have half of the support wire thermal capacity added to it. However, if the length of the wires becomes too great, then the correction is more complicated. The condition that the simple correction applies is that the time constant of the wires should be small compared to that of the foil, so that the temperature along the wires should be a linear function of the length coordinate. In general, the wire material and diameter may be chosen as a matter of convenience. Cu and Ta have been used where large or small thermal conductance, respectively, was desired.

5. Thermocouple. The thermocouple wires should have low thermal conductance and low thermal capacity. This is equivalent to requiring the minimum reasonable wire diameter. Chromel-Constantan has been found to be very satisfactory. It can be obtained in small diameter (No. 40 wire size) and has good sensitivity, about 60 μV/°C. The mounting of the junctions is important. The reference junction

should be imbedded in the support structure which holds the foil. Thus, if the temperature of this structure changes, the reference junction temperature will also change, tending to compensate for the effect. The active junction may be attached to the foil either by spot-welding or by a vacuum epoxy. In the latter case, the thermocouple can be electrically isolated, permitting the use of several thermocouples in series. The location of the active junction is particularly important. Since each term of the series in $J_o(k_n r)$ has n - 1 zeros in $0 \leq r \leq r_o$, one can locate the junction in a position to suppress the n^{th} term. For n = 1, the value of $J_o(k_1 r)$ is nearly unity throughout the domain of r, so the location is not important to this term. The usual practice has been to locate the junction at the edge, $r = r_o$. However, for a material such as tantalum, it has been very helpful to locate the junction near the zero of $J_o(k_2 r)$. This is usually at about $0.65\ r_o$. This results in a more rapid decay of the transient signal after beam switch, so that a larger fraction of the data can be used in determining the linear least-squares fit to $\ln\left(\frac{du}{dt}\right)$ as a function of t_d.

6. Modulation Period. The choice of t_o is restricted by the time constants. Values of $t_o \gg \tau_1$ are not beneficial because the derivative is too small. Further, thermal drift becomes important at very large t_o. On the lower end, there may not be enough time after the higher-order terms have decayed to acquire meaningful data. In general, t_o should be chosen to be a few times τ_1. Within this restriction the actual value is not critical.

F. The Thermal Coupling Problem

An important effect in the use of a thin foil calorimeter to measure energy deposition profiles was the radiant transfer of energy between the calorimeter and the adjacent surfaces. In this case, the thin foils in front of the calorimeter underwent the same periodic temperature changes because the modulated electron beam heated them also. Since emissivity and absorptivity are closely related, energy was transferred to the calorimeter at a rate proportional to

$$\epsilon_1 \epsilon_2 T_o^3 \Delta u(t) \ ,$$

where ϵ_1 and ϵ_2 are the emissivities of the two surfaces and $\Delta u(t)$ is the temperature difference between the two. The factor involving the absolute temperature T_o is included since it offers an obvious means of reducing the effect. Since this effect is also modulated with the period t_o, it is not directly distinguishable from energy deposition by electrons. Quite clearly the situation is bad for (1) materials of high emissivity, or (2) foils of low areal density. For the homogeneous case, i.e., material under test and calorimeter of the same material, the effect goes as ϵ^2 so that there is high premium on low emissivity. The lower the areal density, the greater the fraction of total energy deposited which the thermal coupling represents. (The energy deposited by electrons is proportional to areal density, while the thermal coupling is a surface effect.)

There are a number of ways of dealing with the problem. Reducing the average temperature T_o has been noted. While this should be very effective, one would like to avoid the additional experimental complexity. Two other approaches have been used. In the first, a thin thermal shield was placed between the calorimeter and adjacent surfaces. This was a foil of low emissivity, with a sufficiently small areal density so that the perturbation produced on the energy deposition profile was negligible. The thermally coupled signal transmitted through the shield from an adjacent foil to the calorimeter was thus attenuated, having been effectively multiplied by ϵ_s^2 (ϵ_s is the emissivity of the shield). For ϵ_s about 2×10^{-2}, typical of bright aluminum, the unwanted signal was multiplied by a factor of 4×10^{-4}. This method was used in the normal incidence data for tantalum and for the Ta/Al combination. In this case, the coupling effect was about 10% of the desired signal, and the shield reduced it to a value well below the measurement limit. The second approach used was that of removing the unwanted signal by data correction. The coupling coefficient was determined experimentally, and each datum corrected accordingly. In this case, the same thin foil was always used adjacent to the calorimeter. The assumption was made that the energy deposition rate in this foil was the same as that in the calorimeter so that a constant correction factor could be used. This approach is limited to those cases where the effect is small. The correction is probably subject to about a 10% uncertainty so that in the case of a 20% correction an error of about 2% results. Each of the two methods outlined here places additional requirements on the calibration procedure. These will be discussed in Section III.

III. Apparatus and Procedures

The apparatus used to make the measurements has undergone a series of improvements over the past several years. These improvements resulted from a desire to obtain the data with higher accuracy, efficiency, and convenience, and not as a result of any fundamental change in the experimental technique. Thus, only the latest version of the apparatus will be treated. However, in the data section, earlier systems will be discussed where they bear on the data presented. The apparatus consists of a 1-MeV electron accelerator, a large vacuum chamber with a beam-measuring Faraday cup, and an experimental package.

The electron accelerator delivers monoenergetic electron beams of up to 34 μA. The energy range is from 0.025 to 1.2 MeV. Because of the design of the charging system, the voltage ripple is less than 100 V at 1.0 MeV. A Sandia-designed voltage regulator has been incorporated which provides regulation of ±1 kV at 1.0 MeV. The beam energy has been measured by using a thick beryllium calorimeter[32] and is known to approximately 0.1%.

The stainless-steel vacuum chamber is 1.22 m in diameter and contains a Faraday cup and experiment mounting platform (see Figure III.1). The Faraday cup which is in line with the beam precedes the mounting platform and is equipped with a solenoid-actuated end plate. This door is used to electromechanically modulate the beam which is measured by the cup during the "off" half-cycle. Since the cup subtends only a very small solid angle for electrons backscattered from the

experimental package (located on the mounting platform), there is negligible probability of interference in the measurement of the deposited energy. The position of the mounting platform following the Faraday cup is adjustable in the X, Y, Z, and θ directions. This permits the experimental package to be located on the beam axis and positioned at the axis of rotation of the platform. With this arrangement, the experimental package can be rotated about the beam axis in order to vary the angle of incidence. Note that with the separated in-line Faraday cup, the beam current measurement is not affected by the position of the experimental package. The angular position of the mounting platform is continuously adjustable from the control room and the angle of rotation is measured to 0.1° with a shaft encoder. The beam axis is defined by the aperture located in front of the Faraday cup and a similar aperture on a movable mount at the front edge of the platform. The second aperture is moveable so that it can be used to locate the beam on axis and then be moved from the beam path so that electron scattering from it and its mount does not affect the measurement.

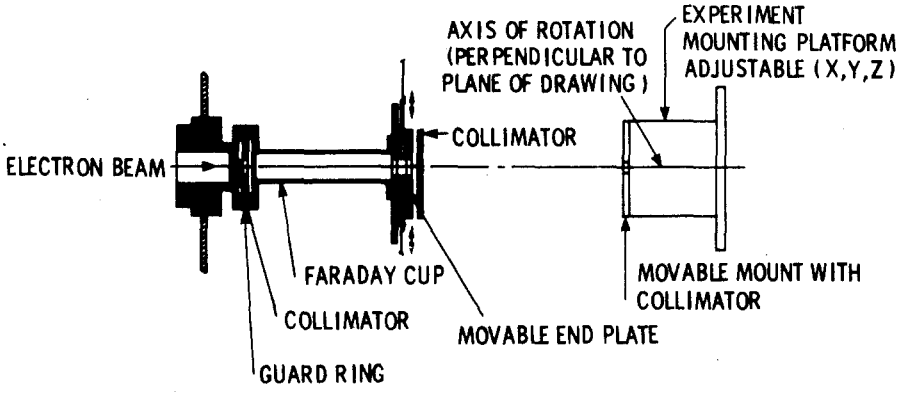

Figure III.1. Faraday Cup and Experimental Mounting Platform

The experimental apparatus developed to make dose-depth profile measurements by using a thin calorimeter is shown in Figure III.2. The main components are the front foil, calorimeter foil, "infinite" plate, thermocouple, and reference junction.

The front foil, which is positioned 0.1 cm in front of the calorimeter foil, consists of either a single foil (see Figure III.3) or a stack of two or more foils of the material in which the measurement is being made. Because the thickness of the front foil is varied, the calorimeter foil measures energy deposition as a function of depth in the material. Thus, in determining the depth at which the dose is measured, one-half the calorimeter foil thickness is added to the thickness of the front foil. The minimum measurable depth is obtained with no front foil present, so that the electron beam strikes the calorimeter foil directly.

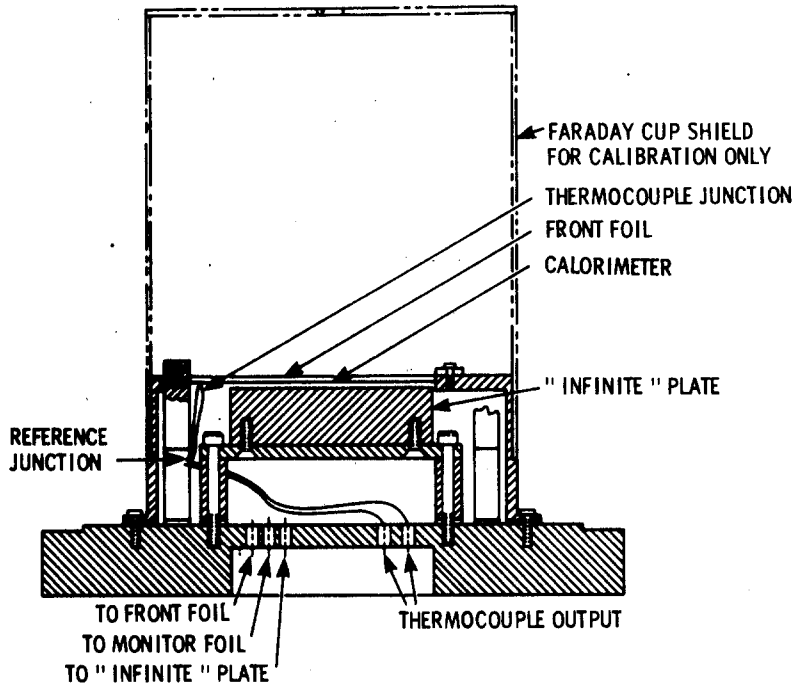

Figure III. 2. Experimental Apparatus

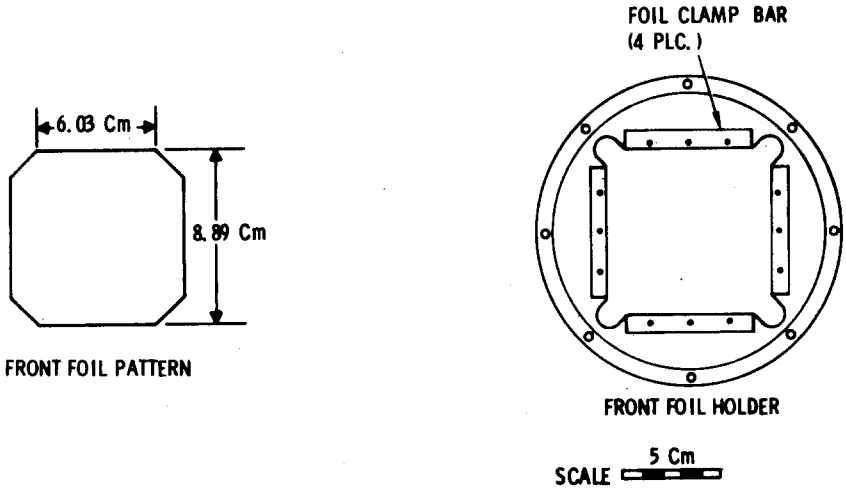

Figure III. 3. Front Foil

When the electron beam is on, energy is deposited in the front foil and the foil heats up. To keep this to a minimum, the front foil is clamped, on four sides, to a foil holder (see Figure III. 3) of sufficient mass to act as a heat sink. However, thermal coupling to the calorimeter from adjacent foils has been observed with material having high thermal emissivity and low thermal conductivity. It was noted in the preceding section that two methods have been used successfully to make measurements when thermal coupling was a problem. In the first method used when thermal coupling is small, a thin foil of the same material as that of the calorimeter is positioned adjacent to the calorimeter for all measurements except the minimal depth measurement for which there is no front foil. The energy "feed through" from this foil was determined with the aid of an ion beam (see calibration). The ion beam was allowed to impinge on this front foil and the calorimeter output was measured. Thus, the energy "feed through" was determined for a known rate of energy input into the adjacent foil. Each point on the deposition curves was then corrected to account for the thermal transfer to or from the calorimeter as indicated by this measurement. The correction using this method was 3% or less. When thermal coupling was large, very thin aluminum (2.3×10^{-4} g/cm^2) heat shields were placed on either side of the calorimeter to obtain thermal isolation.

The calorimeter was made of a thin foil of the material under investigation. The shape and mounting of the calorimeter foil is shown in Figure III. 4. The foil thickness and support wires were chosen to obtain a reasonable value of the first time constant τ_1, as discussed in the previous section. The temperature of the calorimeter foil was measured with a thermocouple. The choice of the thermocouple wires is treated in the previous section. Number 40 wire size Chromel-Constantan thermocouple was used with the junction located at 2. 3 cm from the center of the calorimeter foil, and the reference junction was located in the mounting ring heat sink (see Figure III. 4). The calorimeter foil is held by its support wires 0. 1 cm in front of the "infinite" plate.

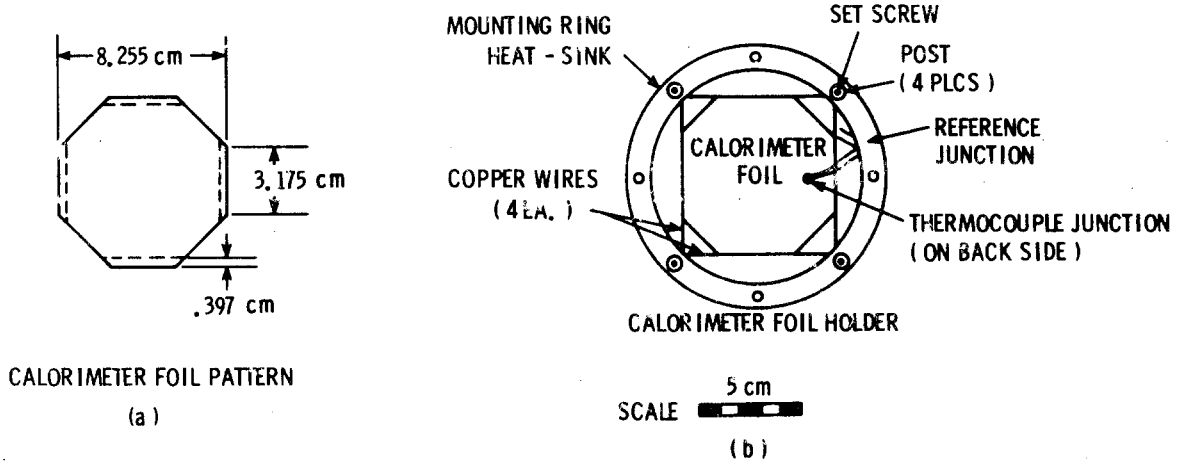

Figure III. 4. Calorimeter Foil

The "infinite" plate was a 7.62-cm-diameter disc of the same material as the front foils and calorimeter. It is called an "infinite" plate because its thickness exceeds the range of the most energetic electrons utilized.

The front foil, calorimeter foil, and "infinite" plate were mounted to a base plate but electrically insulated from it. Each element was connected to a hermetically sealed BNC connector mounted in the base plate. This allowed the elements to be externally connected to measure total electron current or currents to individual components. The base plate was compatible with the mounting platform in the vacuum chamber and the vacuum chamber on the heavy-ion accelerator used for calibration. This arrangement allowed the experimental apparatus to be moved from the electron accelerator to the heavy-ion accelerator without disturbing any of the internal electrical connections.

Calibration of the calorimeter foil was accomplished by means of a heavy-ion accelerator. Since the range of kiloelectronvolt heavy ions is much less than the thickness of any of the calorimeters and the reflection coefficient is very small, the energy deposited in the calorimeter foil was obtained from the product of the incident beam current times the accelerating potential. The beam current measurement was made by using a Faraday-cup shield (FCS) attached to the experimental apparatus (Figure III.3). The FCS satisfied the requirement for a deep Faraday cup, insuring that the escape of secondary electrons ejected from the calorimeter foil by impact of the heavy ion was negligible. The accelerating potential was measured with a calibrated voltage divider and corrected for ion source potentials and is known to ±1%. In the calibration, the incident ion beam was modulated to produce a symmetric square wave having the same period used with the electron measurements. Thus, the response of the calorimeter was determined for a well-defined rate of energy input, and the system was calibrated. For materials which had small thermal coupling between the front foils and the calorimeter, an additional measurement was necessary with the ion beam incident on a thin foil positioned adjacent to the calorimeter as discussed earlier. For materials which had large thermal coupling, thus requiring aluminum heat shields, the calibration was accomplished as follows: First, using the heavy-ion accelerator, the calorimeter was calibrated without the front heat shield, and a calibration constant was determined. Then a second calibration constant was obtained with a thin aluminum foil in front which had a small hole to allow the ion beam to reach the calorimeter. Thus, two different constants were obtained. It was necessary to demonstrate that the hole in the shield did not affect the calibration since, for electron deposition, the shield would not have this hole. This was accomplished by measuring the electron energy deposition at the surface of the material without a shield and again with a complete no-hole heat shield. Using the first calibration constant for the no-shield case and the calibration constant obtained for an incomplete shield (with hole) for the second, agreement to within the accuracy of the measurement was obtained for all electron energies. Therefore, we conclude that the hole in the shield does not significantly affect the calibration constant. In one case only, that of carbon, an indirect calibration was obtained. The carbon calorimeter was loosely enclosed in a very thin aluminum shroud which served as a heat shield. The contact between the carbon and the aluminum was sufficiently poor so that negligible conduction occurred. However, this shroud could not be

easily removed to calibrate as described above. Instead a total-stopping carbon calorimeter requiring no shields was constructed and calibrated by the first procedure. It was then used to measure total electron energy deposition. The Al-shrouded carbon calorimeter was used to measure the relative electron energy deposition in carbon. The energy deposited was integrated over the electron range and normalized to the value obtained with the total-stopping calorimeter. The calibration factor thus obtained was used in all subsequent measurements with this calorimeter.

The data were collected and processed by an on-line computer. A block diagram of this system is shown in Figure III. 5. All measuring instruments used in the calibration are the same as those used to obtain the experimental data. The beam modulation period t_o was selected to satisfy the requirement that t_o should be a few times the first time constant τ_1 of the calorimeter. Several cycles were examined by the computer. The rate of change of the thermocouple voltage with time (t_d), normalized to the beam current (i_B), was calculated continuously for times much greater than τ_2, and the computer produced a linear least-squares fit of $\ln\left(\frac{1}{i_B}\frac{du}{dt}\right)$ as a function of t_d. From this, the derivative could be calculated at any given time with maximum precision, since all available data were used. In practice, the derivative was calculated at $t_d = 0$ (the intercept) and this was corrected for variation in the first time constant τ_1 as indicated by Eq (16) of the previous section. Thus a quantity S is defined as

$$S = \text{Intercept}\left(1 + e^{-t_o/2\tau_1}\right) .$$

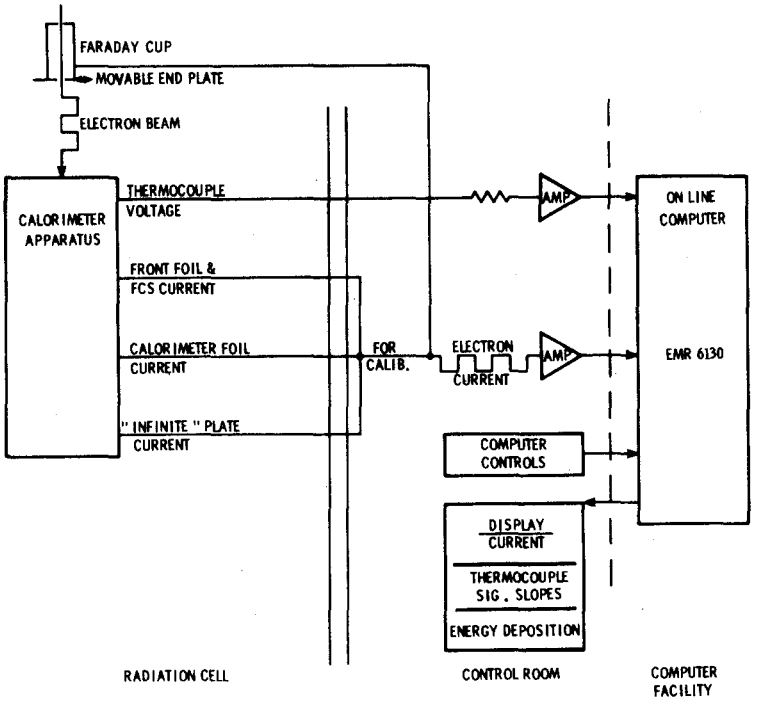

Figure III. 5. Data Collection and Processing System

IV. Theoretical Profiles

All theoretical electron energy deposition profiles were obtained by using the one-dimensional coupled electron/photon Monte Carlo transport code, TIGER.[26] The TIGER code describes the generation and transport of the electron/photon cascade in multislab geometries from several megaelectronvolts down to 1.0 keV for electrons and to 10.0 keV for photons. It combines condensed-history electron Monte Carlo[24] with conventional single-scattering photon Monte Carlo. The electron transport includes energy-loss straggling, elastic scattering, and the production of knock-on electrons, continuous Bremsstrahlung radiation, characteristic x-rays, and annihilation radiation. Photon transport includes the photoelectric, Compton, and pair-production interactions along with the production of the corresponding secondary particles. Electron cross sections and sampling distributions are obtained from DATAPAC-4 and LIBRARY TAPE 2 of the ETRAN Monte Carlo code system.[33] Photon cross sections are the analytical fits of Biggs and Lighthill.[34] The method is more accurate at higher energies, with less rigorous description of the particle cascade at energies where the atomic shell structure of the transport media becomes important. The only shell effects considered are ionization of, fluorescence of, and Auger emission from the K-shell of the highest-atomic-number element in each material.

All theoretical profiles are based upon at least 5,000 primary electron histories and an electron cutoff energy that is, at most, 5% of the source electron kinetic energy. Upon reaching cutoff, an electron is transported a final spatial increment equal to its residual practical range, and its energy is deposited at a random position along this increment. Subzoning within a material layer was chosen to yield spatial resolution commensurate with available experimental resolution and/or the expected degree of spatial variation. Under the foregoing conditions, the best estimates of the statistical standard errors of the theoretical data plotted and tabulated in the following section are generally less than 5%, except for those results corresponding to depths where the predictions are well below the surface deposition.

V. Results

Absolute electron energy deposition profiles have been measured for eight semi-infinite homogenous media and seven semi-infinite multilayer configurations. Measurements were made as a function of energy and angle of incidence. The energy range was from 0.05 to 1.0 MeV. The incident angles studied were 0°, 30°, and 60°. These measurements are compared with the predictions of the electron-photon Monte Carlo transport code, TIGER.[26] The results are presented graphically and tabulated in subsections V.A through V.O at the end of this section. In each section, variations in the experimental system which affect the data are listed.

In all cases, a square-wave modulated beam was employed and the time derivative of the thermocouple signal was examined to obtain the energy deposition. Historically three different

methods were used to analyze the data. The first method (A) obtained the time derivative from a small sample of the data in each half cycle. In the second method (B), the derivative was calculated continuously for times greater than the second time constant (see Section II), and the computer produced a least-squares linear fit of the natural log of the derivative as a function of time for each half cycle. From this, the derivative was calculated at the desired time with maximum precision since all available data were used. The third method (C) obtained the data as in the second method (B), but in this case the derivative was calculated at zero time (the intercept), and this was corrected for variation in the first time constant (see Section III).

The energy deposition is shown as a function of depth expressed as a fraction of the continuous slowing-down approximation range (fraction of a mean range, FMR). The values of the FMR used correspond to the thickness of the front foils plus one-half the thickness of the calorimeter employed. In those cases where aluminum shields were used for thermal isolation of the calorimeter, the FMR of the front shield is included. The thickness of the front foils, shields, and calorimeters, in units of grams per centimeter squared, were determined from the ratio of the measured mass and area. The mass was measured with a balance to ±0.0002 g and the area was determined by averaging several measurements of the length and width to $\pm 10^{-3}$ cm^2.

As discussed in Sections II and III, thermal coupling to the calorimeter from adjacent foils was observed for some materials. To correct this situation, two different methods were used. In the first method (A) a correction term was determined for thermal coupling from a fixed thin foil of the same material as the calorimeter and placed immediately in front of it. The second method (B) used very thin aluminum (2.3×10^{-4} g/cm^2) heat shields to thermally isolate the calorimeter. The front heat shield is included in the calculated FMR as noted above.

When energy deposition profiles were measured for incident angles other than 0°, two methods of setting and determining the angle were employed. At first (A) the angle was set by physically rotating the experimental package and reading the angle from a scale and vernier located on the shaft. Since the radiation cell had to be entered to change angles, the data were taken with the angle set to one side of 0° only. This meant that if there was a small uncertainty in 0° which would not affect the normal incidence data, this uncertainty would be added to the angle determination. The angle was read to ±0.5°, and we estimate the uncertainty in 0° to be ±0.5°. To correct this problem, a new system (B) was installed. The angular position of the experimental package was made continuously adjustable from the control room by means of an electric drive motor, and the angle of rotation was measured to 0.1° with a shaft encoder. With this arrangement, all angular measurements were obtained from the average of two determinations made with the package set at the desired angle on either side of 0°. Thus, a small uncertainty in 0° would be essentially removed by this method.

A high-precision calorimetric system was developed for determining beam energy.[32] Prior to this development, the electron energy was calibrated by comparing pulses produced in a solid ion chamber by electrons from thin conversion sources with those produced by electrons from the

accelerator. The energy determined by this system was found to be a few percent high (i.e., 1.033, 0.521, 0.314, 0.109, and 0.058 MeV). Thus, measurements in Be, Al, Ta with Al shields, and the Ta/Al multi-layer were made with electrons of higher than nominal energy. For these results, the data are plotted at an FMR adjusted for the actual beam energy. Thus, a universal curve is obtained for comparison with the theoretical results at the nominal energies of 1.0, 0.5, 0.3, 0.1, and 0.05 MeV.

Thermophysical constants for each material were used in designing the different calorimeters. However, since the calorimeters were all calibrated by using a heavy ion accelerator as discussed in Section III, the constants do not enter in any of the data analysis and will not be made a part of this report.

In all of the data figures, the theoretical results appear as histograms and the experimental results as circles. On all plots the thickness of the calorimeter used is listed in units of grams per centimeter squared, and a horizontal bar is drawn which represents the FMR associated with the full calorimeter thickness.

For each material and multilayered configuration presented, a list is given which identifies the analysis method, angle determination method, and thermal coupling correction method. This identification (A, B, or C) refers to the descriptions above. In each of the tables of data for the theoretical profiles we have indicated the depth beyond which the estimated one-sigma statistical uncertainty exceeds some specified percent, as well as the estimated one-sigma statistical uncertainty in the predicted total deposition. These uncertainties are given to the nearest 0.5% so that an estimated value of less than 0.5% is shown as 0%.

For each experimental profile in a homogeneous material, the total energy deposited has been determined and is presented in the tables. Smooth curves were drawn as average data curves, and the integration was preformed by constructing a histogram with an increment of one calorimeter thickness and summing the area[25] under the histogram. In all cases, the statistical uncertainty in the determination of the total energy deposited is less than 0.25%; and thus, no uncertainty is listed with the total deposition presented in the tables.

The uncertainty in the experimental data has been determined by taking the square root of the sum of the squares of the uncertainties for the individual terms. The energy deposition is determined from a product of the calibration constant and the normalized signal from electron energy deposition. The precision of the signal is approximately 0.5% for all material used. The calibration constant requires that we determine the ion accelerator voltage, calorimeter areal density, and the normalized signal from ion energy deposition. The accelerator voltage is known to 1%, and the calorimeter areal density is known to better than 0.1%. The precision of the ion energy deposition signal varied from 0.5% to 2% depending on the material under study. This small variation is reflected in the estimated uncertainty listed in each data table.

A. Electron Energy Deposition in Beryllium

Energies (MeV):* 1.033, 0.521, 0.314, 0.109, and 0.058

Angles (°): 0

Analysis Method: B

Angle Determination Method: N/A

Thermal Coupling Correction Method: A

Continuous Slowing Down Approximation Range

Energy (MeV)	Range (g/cm^2)
1.033	5.54×10^{-1}
0.521	2.24×10^{-1}
0.314	1.07×10^{-1}
0.109	1.89×10^{-2}
0.058	6.04×10^{-3}

*Data plotted at nominal energy after adjusting FMR as discussed in introduction of this section.

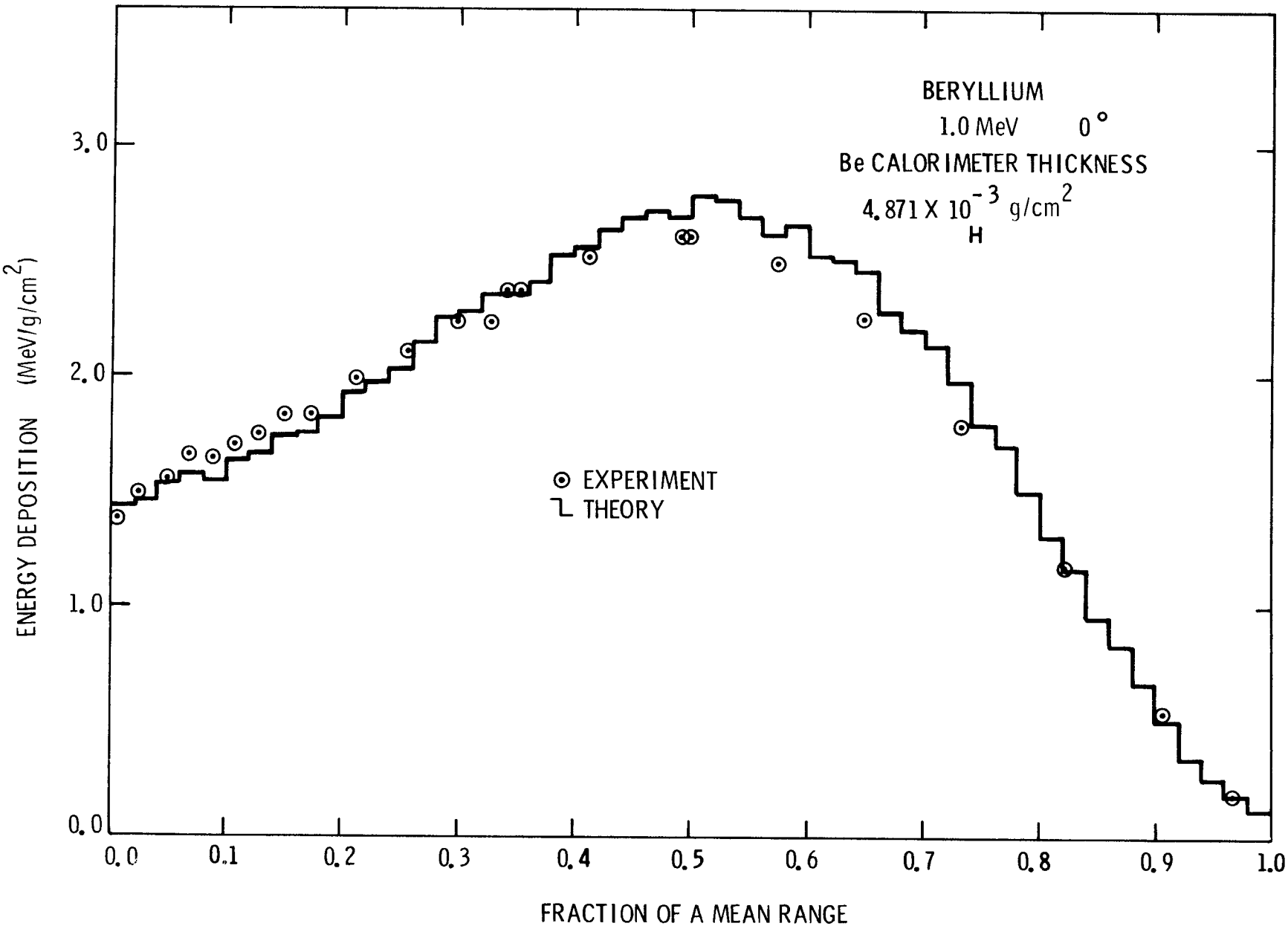

Figure V. A.1. Comparison of Experimental and Theoretical Energy Deposition Profiles in Semi-Infinite Beryllium for 1.0-MeV Electrons Incident at an Angle of 0°

Table V. A.1

Electron Energy Deposition in Beryllium[1, 2, 3]

Experimental Results 1.033 MeV, 0°		Theoretical Results 1.0 MeV, 0°			
FMR	J	FMR	J	FMR	J
0.004	1.38	0.02	1.44	0.56	2.69
0.025	1.49	0.04	1.45	0.58	2.62
0.049	1.55	0.06	1.53	0.60	2.66
0.069	1.65	0.08	1.57	0.62	2.52
0.089	1.64	0.10	1.54	0.64	2.51
0.109	1.70	0.12	1.63	0.66	2.46
0.128	1.74	0.14	1.66	0.68	2.28
0.150	1.83	0.16	1.74	0.70	2.21
0.174	1.83	0.18	1.75	0.72	2.14
0.213	1.99	0.20	1.82	0.74	1.98
0.257	2.10	0.22	1.93	0.76	1.79
0.298	2.24	0.24	1.97	0.78	1.70
0.328	2.23	0.26	2.03	0.80	1.50
0.345	2.37	0.28	2.15	0.82	1.31
0.353	2.38	0.30	2.26	0.84	1.16
0.413	2.51	0.32	2.28	0.86	0.95
0.492	2.61	0.34	2.35	0.88*	0.83
0.499	2.61	0.36	2.36	0.90	0.67
0.575	2.49	0.38	2.41	0.92	0.50
0.648	2.25	0.40	2.52	0.94	0.34
0.733	1.79	0.42	2.56	0.96	0.26
0.822	1.17	0.44	2.63	0.98	0.18
0.907	0.54	0.46	2.69	1.00	0.12
0.968	0.18	0.48	2.71	1.02	0.07
1.059	0.05	0.50	2.69	1.04	0.03
		0.52	2.78	1.06	0.02
Total Deposition = 1.022 MeV		0.54	2.77	1.08	0.01

Total Deposition = 0.995 MeV ±0%

1. FMR is fraction of a mean range.
2. J is energy deposited in MeV/g/cm^2.
3. Estimated experimental uncertainty is 1.6%.

*Estimated one-sigma statistical uncertainty exceeds 3% at larger FMR.

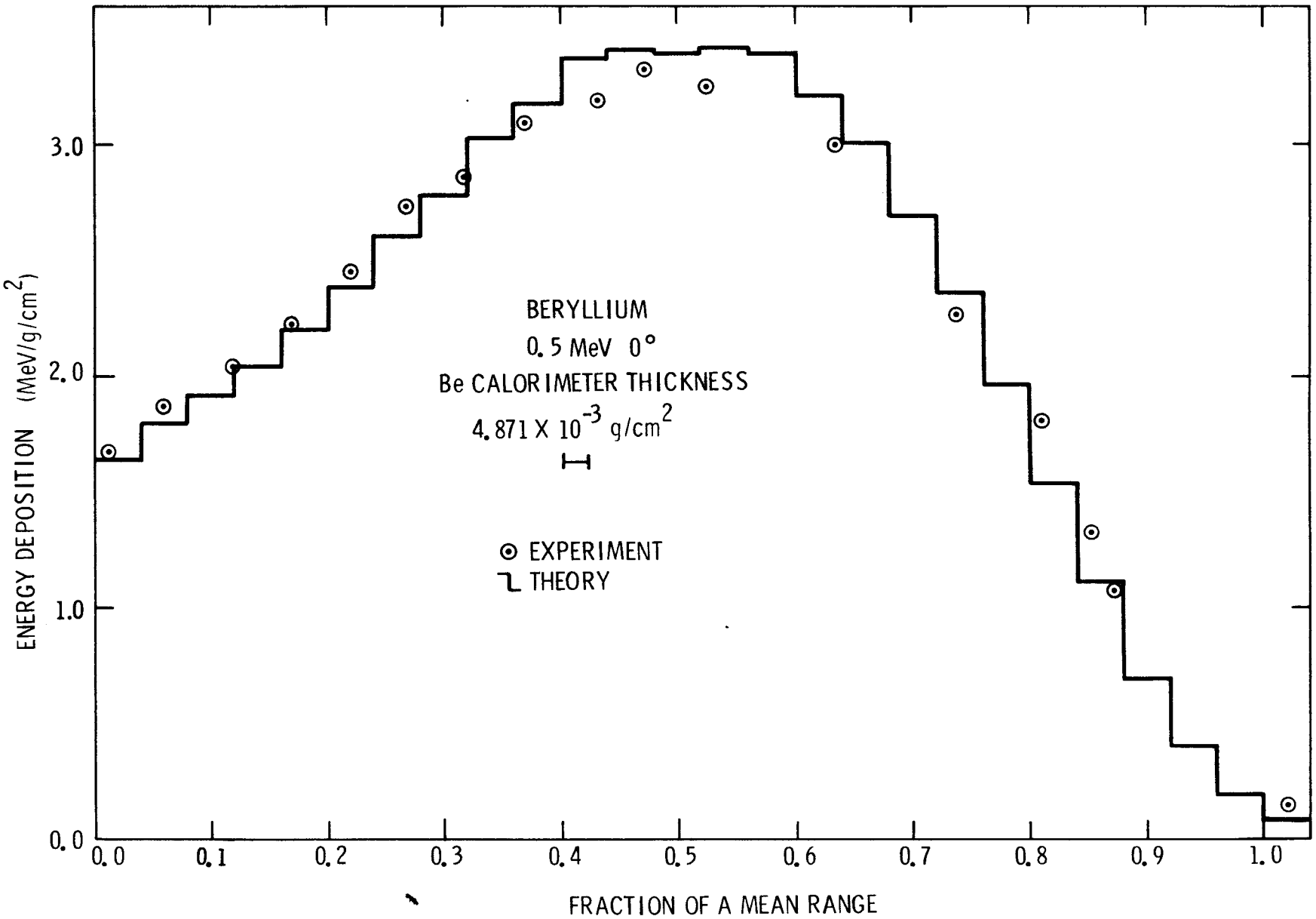

Figure V. A. 2. Comparison of Experimental and Theoretical Energy Deposition Profiles in Semi-Infinite Beryllium for 0.5-MeV Electrons Incident at an Angle of 0°

Table V. A.2

Electron Energy Deposition in Beryllium[1,2,3]

Experimental Results 0.521 MeV, 0°		Theoretical Results 0.5 MeV, 0°			
FMR	J	FMR	J	FMR	J
0.011	1.67	0.04	1.64	0.60	3.39
0.061	1.87	0.08	1.80	0.64	3.21
0.120	2.03	0.12	1.91	0.68	3.00
0.170	2.22	0.16	2.04	0.72	2.69
0.219	2.45	0.20	2.20	0.76	2.36
0.268	2.73	0.24	2.39	0.80	1.96
0.316	2.85	0.28	2.60	0.84	1.53
0.369	3.09	0.32	2.78	0.88*	1.10
0.431	3.19	0.36	3.02	0.92	0.69
0.471	3.32	0.40	3.17	0.96	0.40
0.525	3.24	0.44	3.37	1.00	0.19
0.634	2.98	0.48	3.40	1.04	0.08
0.736	2.26	0.52	3.39	1.08	0.02
0.811	1.80	0.56	3.40		
0.853	1.32				
0.872	1.07				
1.019	0.14	Total Deposition = 0.497 MeV ±0%			
Total Deposition = 0.520 MeV					

1. FMR is fraction of a mean range.
2. J is energy deposited in MeV/g/cm^2.
3. Estimated experimental uncertainty is 1.6%.

* Estimated one-sigma statistical uncertainty exceeds 3% at larger FMR.

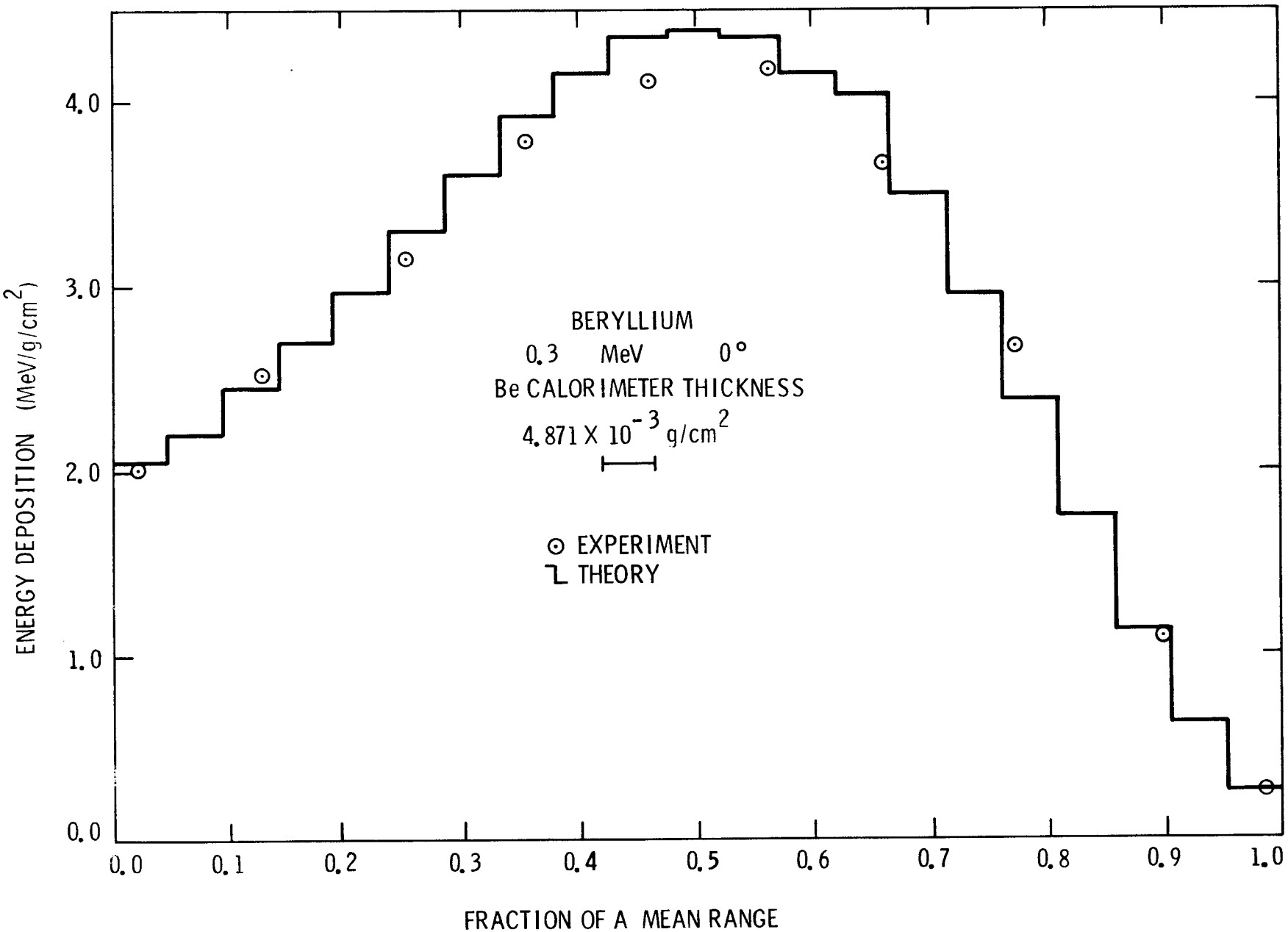

Figure V. A.3. Comparison of Experimental and Theoretical Energy Deposition Profiles in Semi-Infinite Beryllium for 0.3-MeV Electrons Incident at an Angle of 0°

Table V. A.3

Electron Energy Deposition in Beryllium[1,2,3]

Experimental Results 0.314 MeV, 0°		Theoretical Results 0.3 MeV, 0°			
FMR	J	FMR	J	FMR	J
0.022	2.01	0.048	2.04	0.571	4.35
0.128	2.52	0.095	2.19	0.619	4.14
0.251	3.15	0.143	2.44	0.666	3.91
0.355	3.78	0.190	2.69	0.714	3.49
0.459	4.10	0.238	2.97	0.761	2.96
0.563	4.18	0.286	3.29	0.809	2.37
0.662	3.65	0.333	3.61	0.857	1.74
0.773	2.66	0.381	3.92	0.904	1.13
0.901	1.09	0.428	4.14	0.952*	0.62
0.985	0.26	0.476	4.35	0.999	0.26
		0.523	4.38		
Total Deposition = 0.312 MeV		Total Deposition = 0.298 MeV ±0%			

1. FMR is fraction of a mean range.
2. J is energy deposited in $MeV/g/cm^2$.
3. Estimated experimental uncertainty is 1.6%.

*Estimated one-sigma statistical uncertainty exceeds 3% at larger FMR.

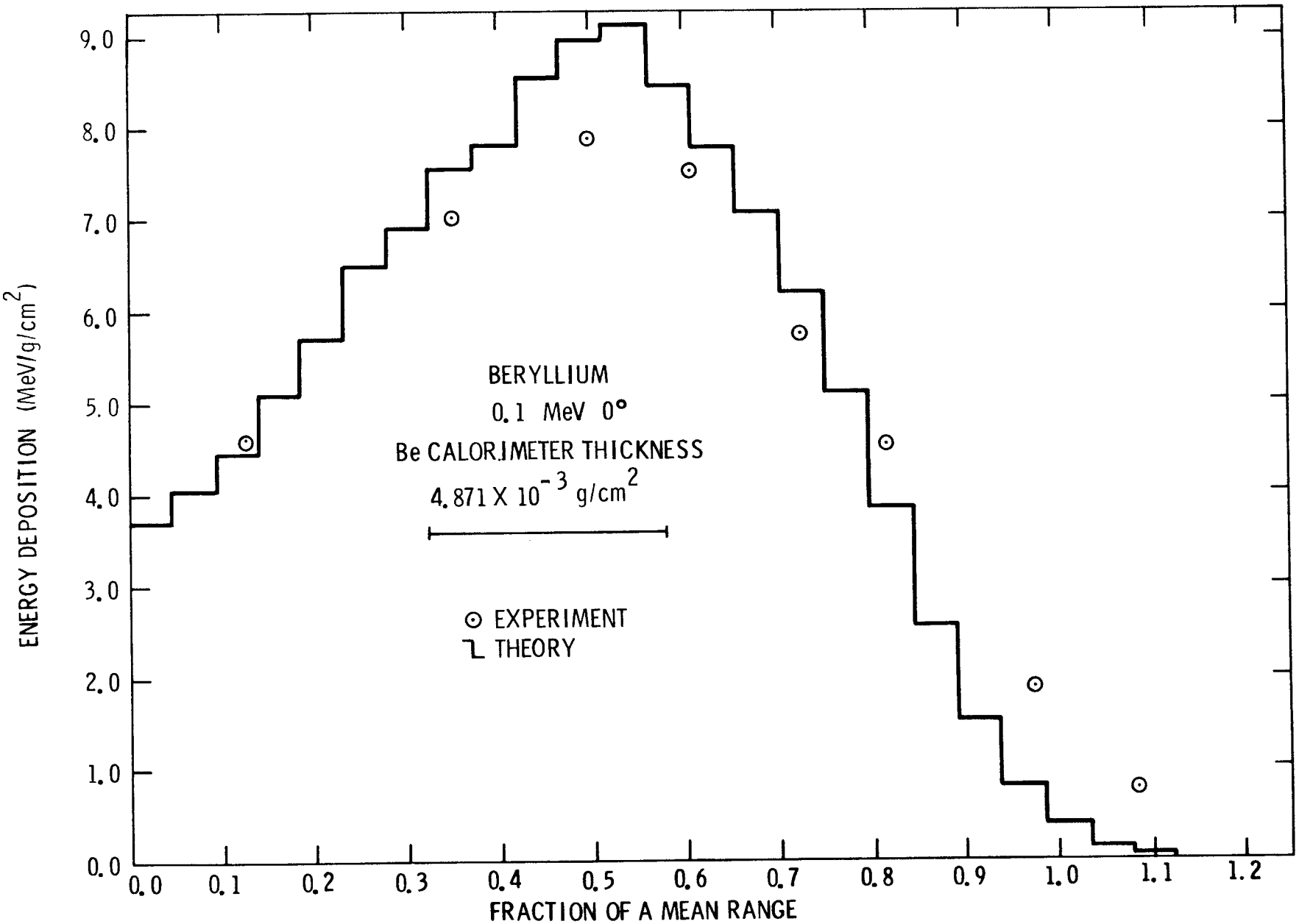

Figure V. A.4. Comparison of Experimental and Theoretical Energy Deposition Profiles in Semi-Infinite Beryllium for 0.1-MeV Electrons Incident at an Angle of 0°

Table V. A.4

Electron Energy Deposition in Beryllium[1, 2, 3]

Experimental Results 0.109 MeV, 0°		Theoretical Results 0.1 MeV, 0°			
FMR	J	FMR	J	FMR	J
0.127	4.59	0.047	3.69	0.609	8.42
0.353	6.98	0.094	4.04	0.656	7.77
0.499	7.87	0.141	4.44	0.703	7.07
0.608	7.50	0.187	5.08	0.750	6.18
0.726	5.74	0.234	5.69	0.797	5.09
0.819	4.51	0.281	6.50	0.844	3.84
0.973	1.86	0.328	6.90	0.891*	2.56
1.083	0.76	0.375	7.55	0.937	1.51
		0.422	7.78	0.984	0.80
Total Deposition = 0.109 MeV		0.469	8.53	1.031	0.37
		0.516	8.94	1.078	0.12
		0.562	9.10	1.125	0.04
		Total Deposition = 0.0991 MeV ±0%			

1. FMR is fraction of a mean range.
2. J is energy deposited in MeV/g/cm^2.
3. Estimated experimental uncertainty is 1.6%.

*Estimated one-sigma statistical uncertainty exceeds 3% at larger FMR.

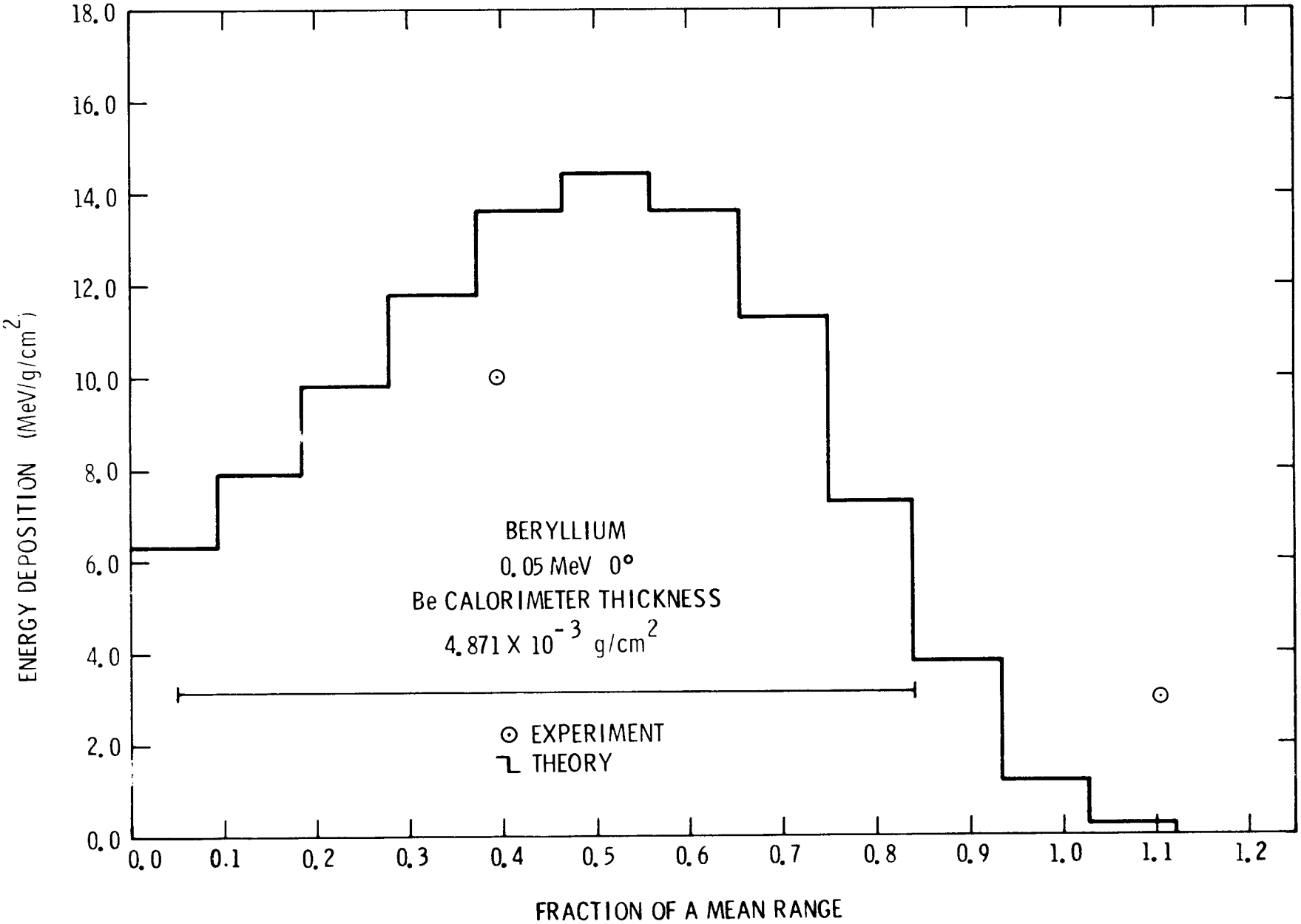

Figure V. A. 5. Comparison of Experimental and Theoretical Energy Deposition Profiles in Semi-Infinite Beryllium for 0.05-MeV Electrons Incident at an Angle of 0°

Table V. A.5

Electron Energy Deposition in Beryllium[1,2,3]

Experimental Results 0.058 MeV, 0°		Theoretical Results 0.05 MeV, 0°			
FMR	J	FMR	J	FMR	J
0.396	10.023	0.093	6.32	0.654	13.6
1.104	2.99	0.187	7.90	0.748	11.3
		0.280	9.79	0.841*	7.30
		0.374	11.8	0.935	3.78
		0.467	13.6	1.028	1.18
		0.561	14.4	1.122	0.24

Total Deposition = 0.0494 MeV ±0%

1. FMR is fraction of a mean range.
2. J is energy deposited in MeV/g/cm^2.
3. Estimated experimental uncertainty is 1.6%.

*Estimated one-sigma statistical uncertainty exceeds 3% for larger FMR.

B. Electron Energy Deposition in Carbon

Energies (MeV):	1.0
Angles (°):	0
Analysis Method:	C
Angle Determination Method:	N/A
Thermal Coupling Correction Method:	B

Continuous Slowing Down Approximation Range

Energy (MeV)	Range (g/cm^2)
1.0	4.89×10^{-1}

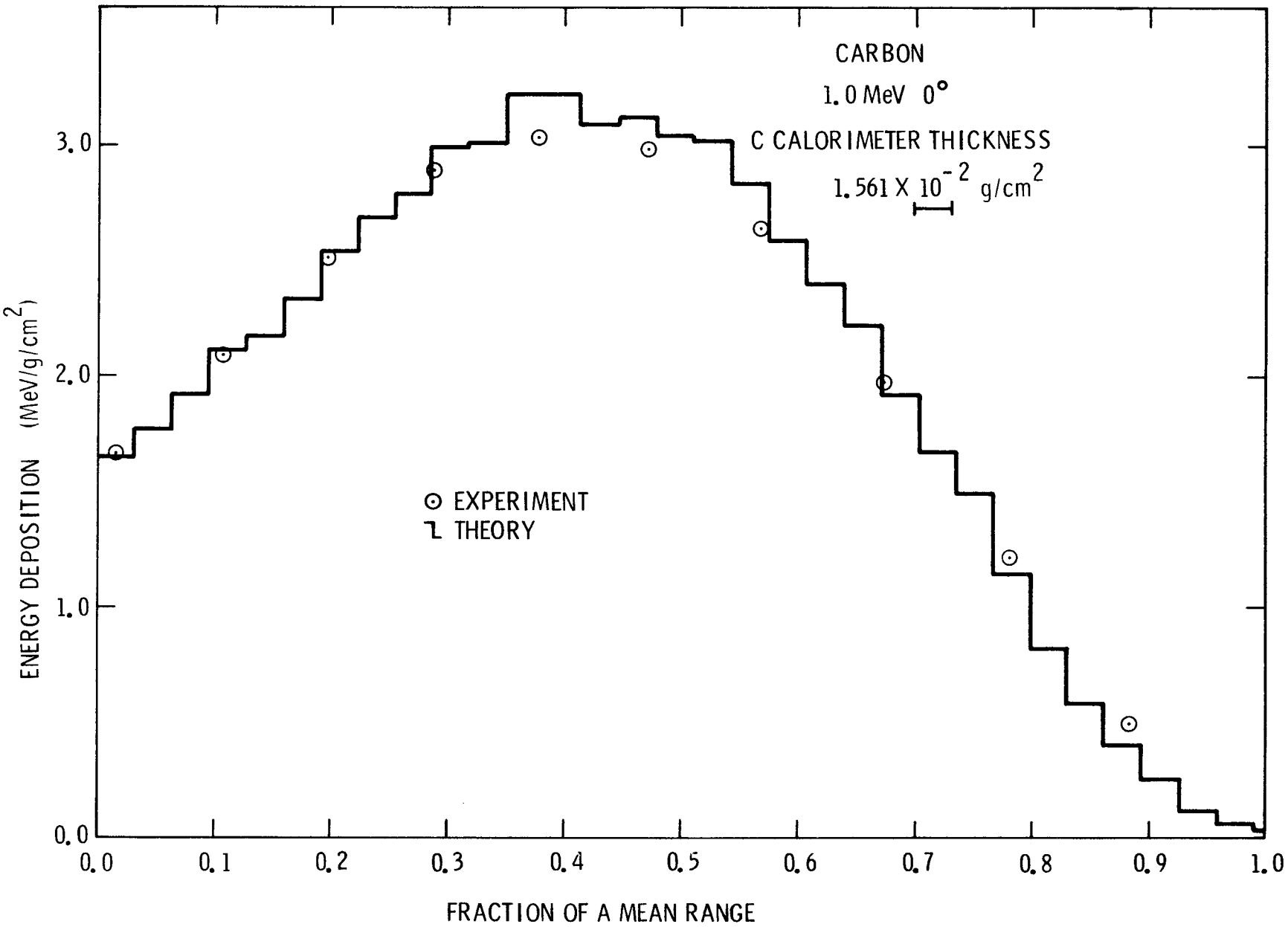

Figure V. B. 1. Comparison of Experimental and Theoretical Energy Deposition Profiles in Semi-Infinite Carbon for 1.0-MeV Electrons Incident at an Angle of 0°

Table V. B.1

Electron Energy Deposition in Carbon[1, 2, 3]

Experimental Results 1.0 MeV, 0°		Theoretical Results 1.0 MeV, 0°			
FMR	J	FMR	J	FMR	J
0.016	1.66	0.032	1.65	0.543	3.02
0.107	2.09	0.064	1.77	0.575	2.84
0.198	2.50	0.096	1.92	0.607	2.59
0.289	2.89	0.128	2.11	0.639	2.40
0.378	3.03	0.160	2.17	0.671	2.22
0.472	2.98	0.192	2.33	0.703	1.92
0.568	2.64	0.224	2.54	0.735	1.67
0.673	1.97	0.256	2.69	0.767	1.49
0.781	1.21	0.287	2.79	0.799	1.14
0.883	0.49	0.319	2.99	0.830*	0.82
		0.351	3.01	0.862	0.58
		0.383	3.22	0.894	0.40
		0.415	3.22	0.926	0.25
		0.447	3.09	0.958	0.11
		0.479	3.12	0.990	0.06
		0.511	3.04	1.022	0.03

Total Deposition = 0.987 MeV ±0%

1. FMR is fraction of a mean range.
2. J is energy deposited in MeV/g/cm^2.
3. Estimated experimental uncertainty is 2.0%.

*Estimated one-sigma statistical uncertainty exceeds 3% at larger FMR.

C. Electron Energy Deposition in Aluminum

Energies (MeV):* 1.033, 0.521, 0.314, 0.109, and 0.058

Angles (°): 0 and 60

Analysis Method: A

Angle Determination Method: A

Thermal Coupling Correction Method: None required

Continuous Slowing Down Approximation Range

Energy (MeV)	Range (g/cm^2)
1.033	5.69×10^{-1}
0.521	2.34×10^{-1}
0.314	1.13×10^{-1}
0.109	2.03×10^{-2}
0.058	6.63×10^{-3}

*Data plotted at nominal energy after adjusting FMR as discussed in introduction of this section.

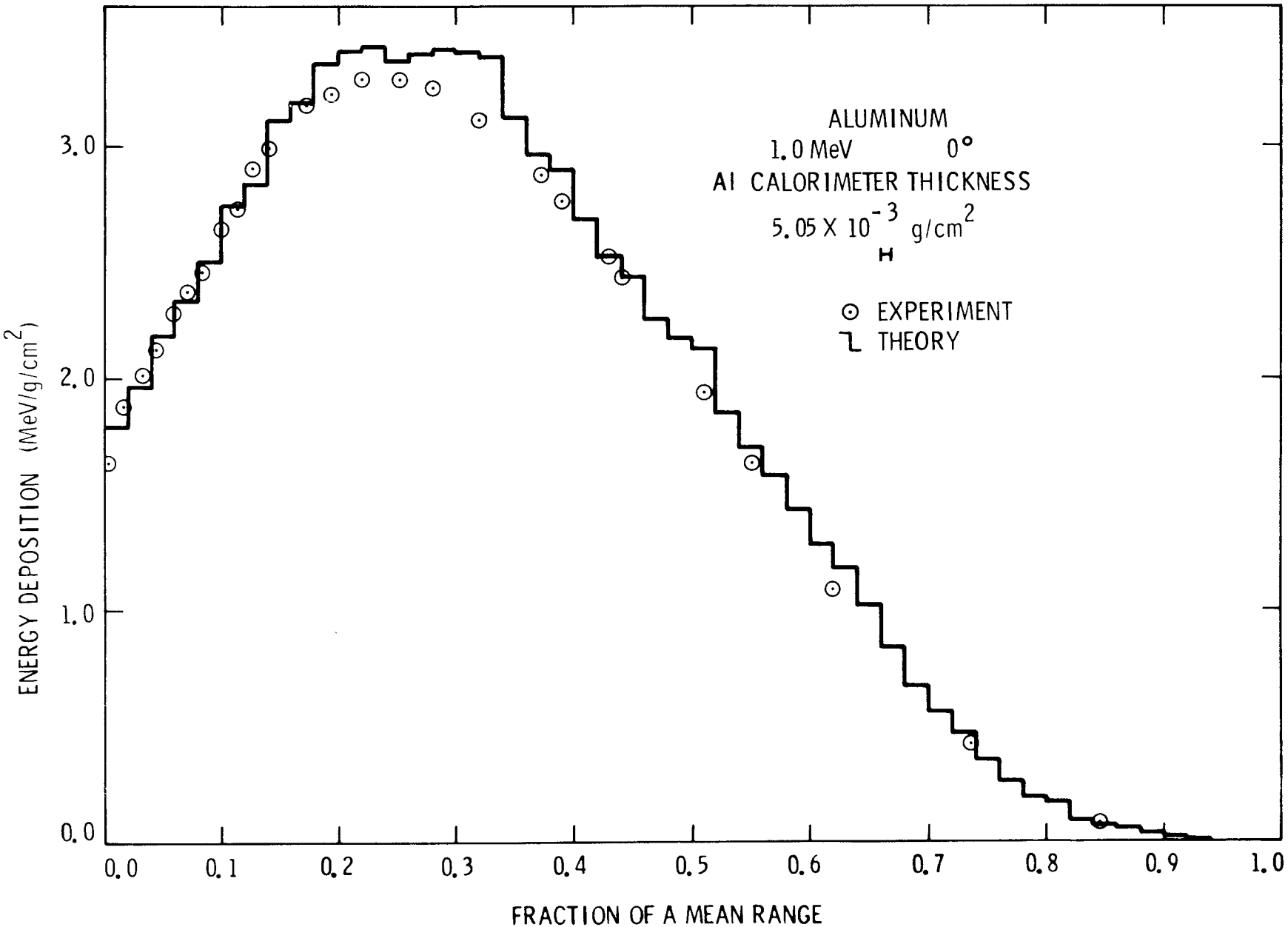

Figure V. C.1. Comparison of Experimental and Theoretical Energy Deposition Profiles in Semi-Infinite Aluminum for 1.0-MeV Electrons Incident at an Angle of 0°

Table V. C.1

Electron Energy Deposition in Aluminum[1, 2, 3]

Experimental Results 1.033 MeV, 0°		Theoretical Results 1.0 MeV, 0°			
FMR	J	FMR	J	FMR	J
0.0045	1.63	0.02	1.79	0.50	2.17
0.0165	1.87	0.04	1.96	0.52	2.12
0.0317	2.01	0.06	2.18	0.54	1.85
0.0448	2.12	0.08	2.33	0.56	1.70
0.0591	2.28	0.10	2.50	0.58	1.58
0.0707	2.37	0.12	2.74	0.60	1.43
0.0836	2.45	0.14	2.83	0.62	1.28
0.0987	2.64	0.16	3.10	0.64	1.18
0.115	2.73	0.18	3.18	0.66	1.02
0.127	2.90	0.20	3.35	0.68*	0.84
0.142	2.98	0.22	3.40	0.70	0.67
0.174	3.17	0.24	3.42	0.72	0.56
0.195	3.22	0.26	3.36	0.74	0.47
0.221	3.28	0.28	3.39	0.76	0.35
0.253	3.28	0.30	3.41	0.78	0.26
0.280	3.25	0.32	3.40	0.80	0.19
0.320	3.11	0.34	3.38	0.82	0.17
0.373	2.87	0.36	3.12	0.84	0.10
0.391	2.76	0.38	2.96	0.86	0.07
0.431	2.52	0.40	2.89	0.88	0.06
0.443	2.43	0.42	2.68	0.90	0.03
0.511	1.93	0.44	2.52	0.92	0.02
0.552	1.63	0.46	2.43	0.94	0.01
0.621	1.09	0.48	2.25		
0.736	0.42				
0.846	0.08	Total Deposition = 0.954 MeV ±0%			

Total Deposition = 0.970 MeV

1. FMR is fraction of a mean range.
2. J is energy deposited in MeV/g/cm^2.
3. Estimated experimental uncertainty is 1.4%.

*Estimated one-sigma statistical uncertainty exceeds 3% at larger FMR.

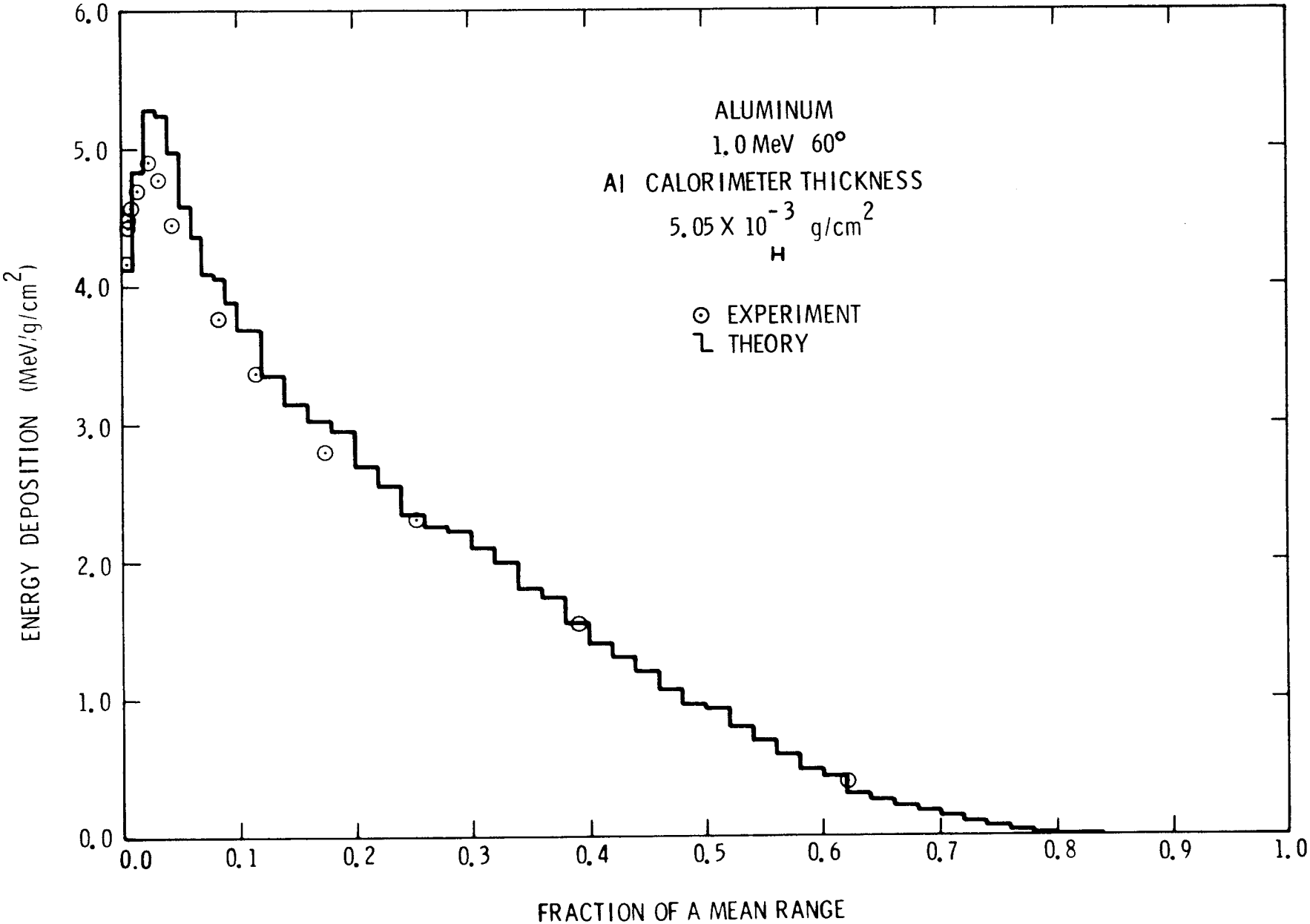

Figure V. C. 2. Comparison of Experimental and Theoretical Energy Deposition Profiles in Semi-Infinite Aluminum for 1.0-MeV Electrons Incident at an Angle of 60°

Table V. C.2

Electron Energy Deposition in Aluminum[1,2,3]

Experimental Results 1.033 MeV, 60°		Theoretical Results 1.0 MeV, 60°			
FMR	J	FMR	J	FMR	J
0.005	4.16	0.01	4.12	0.40	1.54
0.007	4.44	0.02	4.82	0.42	1.41
0.007	4.47	0.03	5.28	0.44*	1.31
0.009	4.57	0.04	5.24	0.46	1.20
0.013	4.67	0.05	4.97	0.48	1.06
0.024	4.90	0.06	4.58	0.50	0.96
0.032	4.75	0.07	4.36	0.52	0.92
0.045	4.44	0.08	4.08	0.54	0.79
0.084	3.76	0.09	4.06	0.56	0.69
0.115	3.36	0.10	3.88	0.58	0.59
0.174	2.79	0.12	3.68	0.60	0.48
0.253	2.30	0.14	3.35	0.62	0.44
0.391	1.54	0.16	3.14	0.64	0.31
0.621	0.38	0.18	3.03	0.66	0.27
		0.20	2.95	0.68	0.22
Total Deposition =		0.22	2.70	0.70	0.18
0.759 MeV		0.24	2.55	0.72	0.14
		0.26	2.34	0.74	0.10
		0.28	2.25	0.76	0.07
		0.30	2.23	0.78	0.04
		0.32	2.10	0.80	0.02
		0.34	1.99	0.82	0.02
		0.36	1.79	0.84	0.02
		0.38	1.74		
		Total Deposition = 0.785 MeV ±1%			

1. FMR is fraction of a mean range.
2. J is energy deposited in MeV/g/cm^2.
3. Estimated experimental uncertainty is 1.4%.

*Estimated one-sigma statistical uncertainty exceeds 3% at larger FMR.

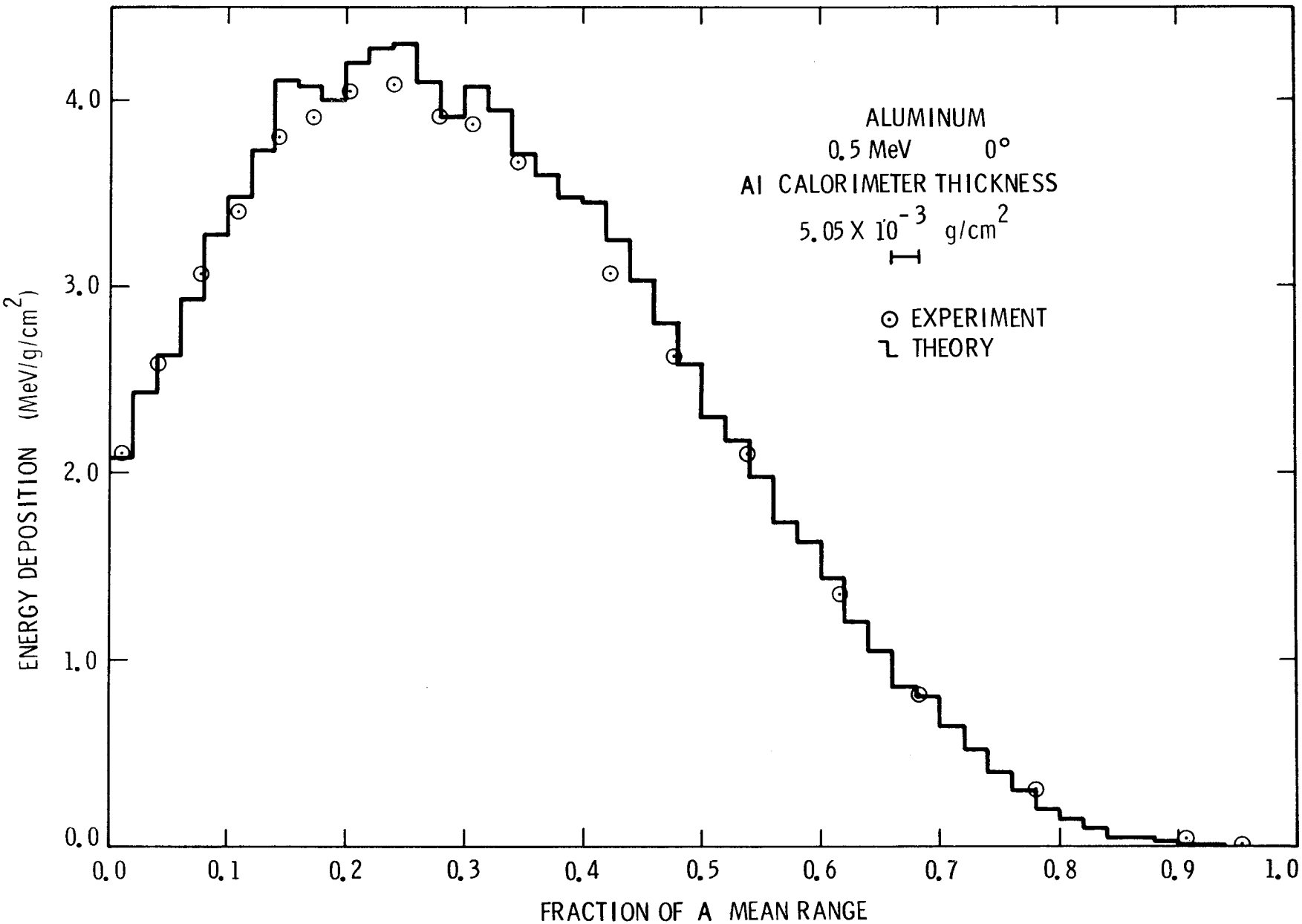

Figure V. C. 3. Comparison of Experimental and Theoretical Energy Deposition Profiles in Semi-Infinite Aluminum for 0.5-MeV Electrons Incident at an Angle of 0°

Table V. C. 3

Electron Energy Deposition in Aluminum[1, 2, 3]

Experimental Results 0.521 MeV, 0°		Theoretical Results 0.5 MeV, 0°			
FMR	J	FMR	J	FMR	J
0.0108	2.11	0.02	2.08	0.50	2.58
0.0403	2.58	0.04	2.43	0.52	2.30
0.0771	3.07	0.06	2.63	0.54	2.17
0.109	3.40	0.08	2.93	0.56	1.97
0.143	3.81	0.10	3.27	0.58	1.73
0.173	3.90	0.12	3.47	0.60	1.63
0.203	4.05	0.14	3.73	0.62	1.43
0.242	4.08	0.16	4.10	0.64	1.20
0.279	3.91	0.18	4.07	0.66	1.04
0.308	3.87	0.20	3.99	0.68*	0.86
0.345	3.66	0.22	4.20	0.70	0.80
0.424	3.07	0.24	4.28	0.72	0.64
0.475	2.62	0.26	4.30	0.74	0.52
0.538	2.10	0.28	4.09	0.76	0.40
0.615	1.34	0.30	3.91	0.78	0.30
0.682	0.81	0.32	4.07	0.80	0.20
0.780	0.30	0.34	3.94	0.82	0.15
0.908	0.04	0.36	3.71	0.84	0.11
0.953	0.00	0.38	3.59	0.86	0.06
		0.40	3.47	0.88	0.05
Total Deposition =		0.42	3.45	0.90	0.03
0.479 MeV		0.44	3.25	0.92	0.01
		0.46	3.03	0.94	0.01
		0.48	2.79		

Total Deposition = 0.471 MeV ±0%

1. FMR is fraction of a mean range.
2. J is energy deposited in $MeV/g/cm^2$.
3. Estimated experimental uncertainty is 1.4%.

*Estimated one-sigma statistical uncertainty exceeds 3% at larger FMR.

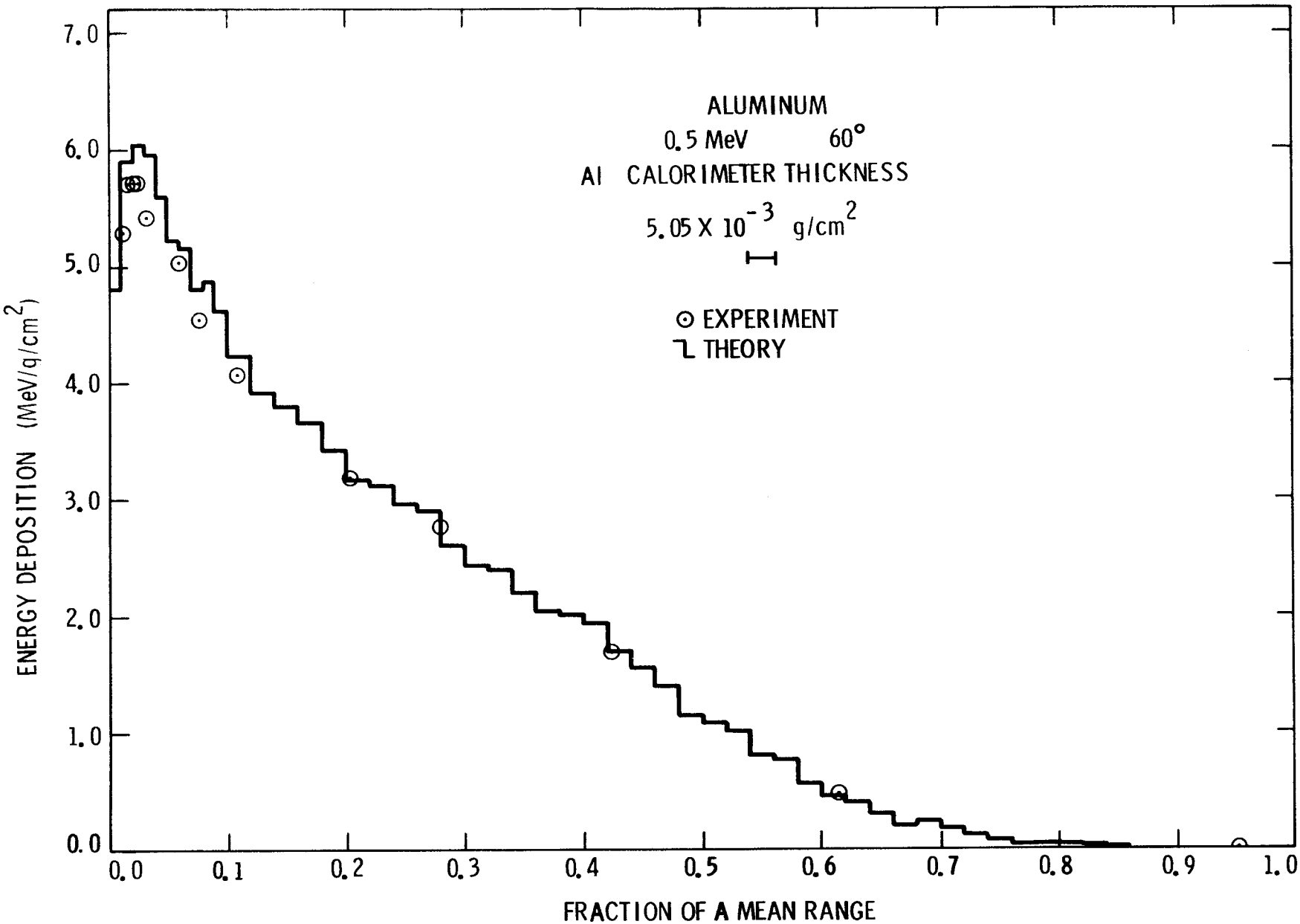

Figure V. C.4. Comparison of Experimental and Theoretical Energy Deposition Profiles in Semi-Infinite Aluminum for 0.5-MeV Electrons Incident at an Angle of 60°

Table V. C.4

Electron Energy Deposition in Aluminum[1,2,3]

Experimental Results 0.521 MeV, 60°		Theoretical Results 0.5 MeV, 60°			
FMR	J	FMR	J	FMR	J
0.011	5.28	0.01	4.81	0.40	2.01
0.016	5.70	0.02	5.89	0.42	1.94
0.018	5.71	0.03	6.04	0.44	1.70
0.023	5.72	0.04	5.95	0.46	1.55
0.032	5.41	0.05	5.59	0.48	1.39
0.059	5.03	0.06	5.22	0.50*	1.14
0.077	4.54	0.07	5.15	0.52	1.08
0.109	4.07	0.08	4.80	0.54	1.01
0.203	3.18	0.09	4.87	0.56	0.80
0.279	2.76	0.10	4.62	0.58	0.76
0.424	1.69	0.12	4.23	0.60	0.55
0.615	0.48	0.14	3.92	0.62	0.45
0.953	0.0	0.16	3.80	0.64	0.39
1.520	0.0	0.18	3.66	0.66	0.30
		0.20	3.42	0.68	0.20
Total Deposition =		0.22	3.16	0.70	0.23
0.391 MeV		0.24	3.12	0.72	0.18
		0.26	2.95	0.74	0.12
		0.28	2.90	0.76	0.07
		0.30	2.61	0.78	0.03
		0.32	2.43	0.80	0.04
		0.34	2.40	0.82	0.04
		0.36	2.20	0.84	0.03
		0.38	2.04	0.86	0.01

Total Deposition = 0.382 MeV ±1%

1. FMR is fraction of a mean range.
2. J is energy deposited in MeV/g/cm^2.
3. Estimated experimental uncertainty is 1.4%.

*Estimated one-sigma statistical uncertainty exceeds 3% at larger FMR.

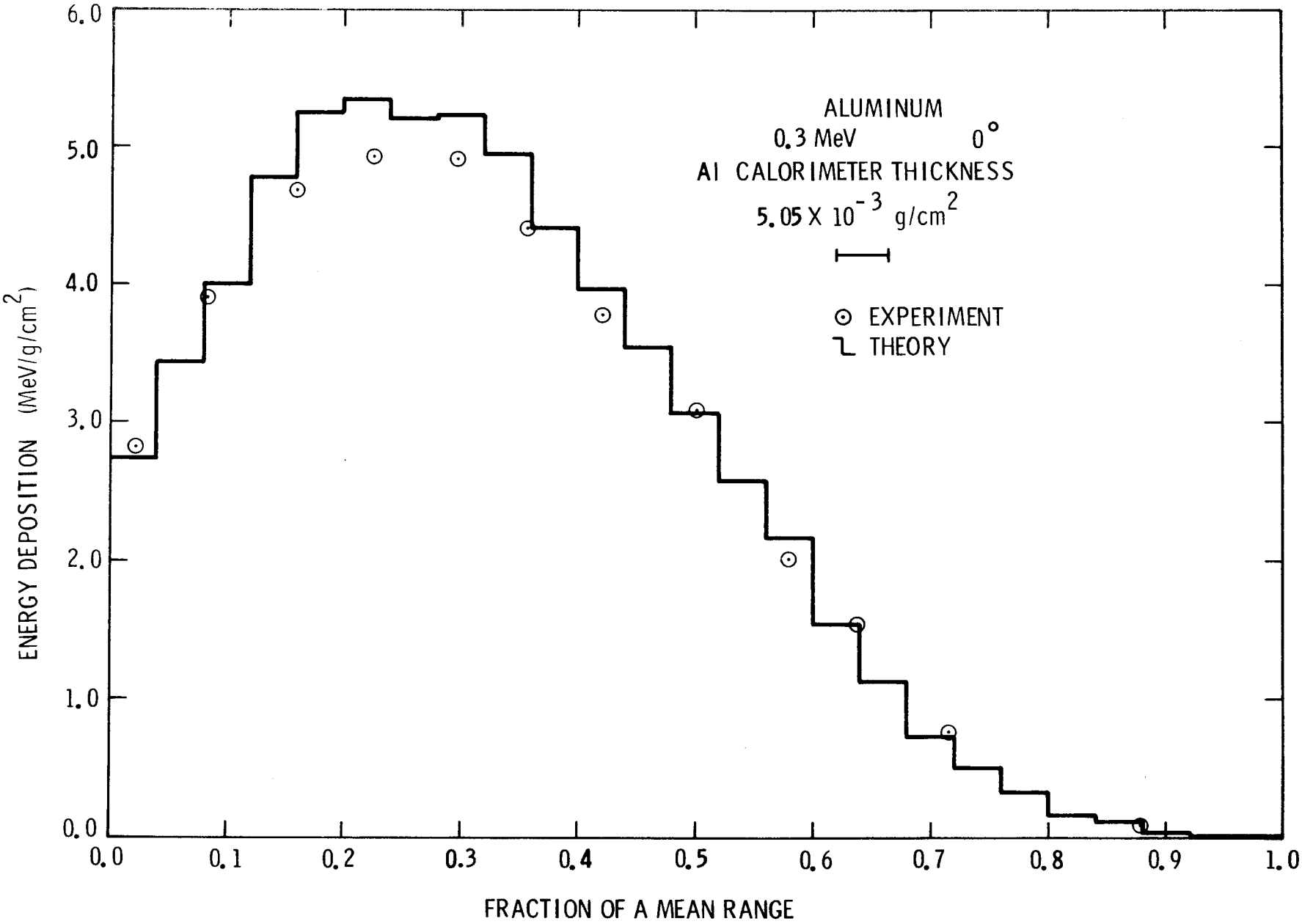

Figure V. C.5. Comparison of Experimental and Theoretical Energy Deposition Profiles in Semi-Infinite Aluminum for 0.3-MeV Electrons Incident at an Angle of 0°

Table V. C. 5

Electron Energy Deposition in Aluminum[1, 2, 3]

Experimental Results 0.314 MeV, 0°		Theoretical Results 0.3 MeV, 0°			
FMR	J	FMR	J	FMR	J
0.0224	2.82	0.04	2.74	0.56	2.57
0.0831	3.91	0.08	3.43	0.60	2.16
0.160	4.67	0.12	4.00	0.64	1.54
0.226	4.92	0.16	4.77	0.68*	1.12
0.297	4.90	0.20	5.24	0.72	0.72
0.357	4.40	0.24	5.34	0.76	0.50
0.422	3.77	0.28	5.20	0.80	0.32
0.501	3.08	0.32	5.23	0.84	0.17
0.579	2.00	0.36	4.94	0.88	0.11
0.638	1.54	0.40	4.41	0.92	0.04
0.717	0.76	0.44	3.96	0.96	0.01
0.879	0.08	0.48	3.54	1.00	0.01
Total Deposition = 0.285 MeV		0.52	3.06		
		Total Deposition = 0.280 MeV ±0%			

1. FMR is fraction of a mean range.
2. J is energy deposited in MeV/g/cm^2.
3. Estimated experimental uncertainty is 1.4%.

*Estimated one-sigma statistical uncertainty exceeds 3% at larger FMR.

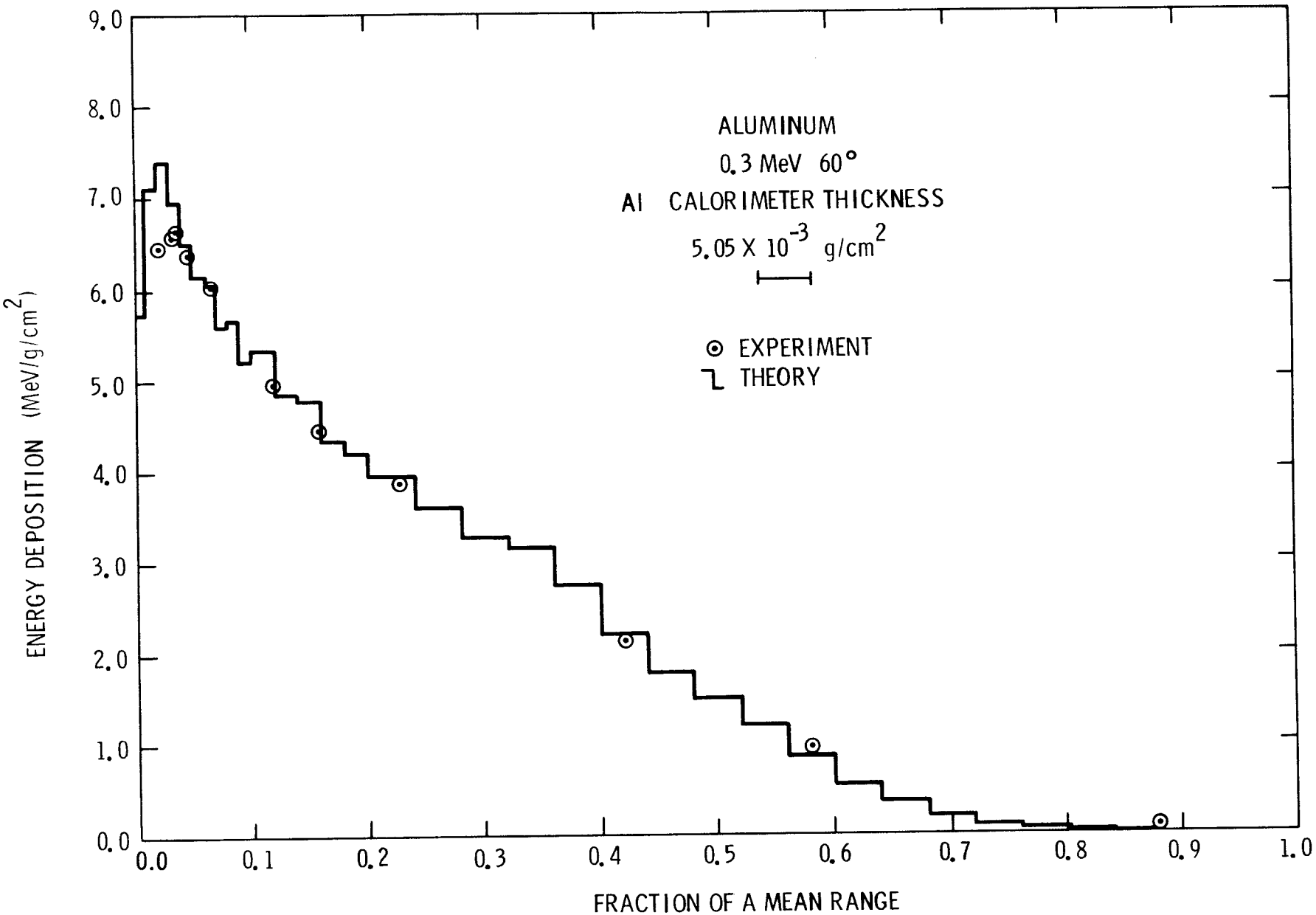

Figure V. C.6. Comparison of Experimental and Theoretical Energy Deposition Profiles in Semi-Infinite Aluminum for 0.3-MeV Electrons Incident at an Angle of 60°

Table V. C.6

Electron Energy Deposition in Aluminum[1, 2, 3]

Experimental Results 0.314 MeV, 60°		Theoretical Results 0.3 MeV, 60°			
FMR	J	FMR	J	FMR	J
0.022	6.45	0.01	5.70	0.28	3.61
0.033	6.56	0.02	7.10	0.32	3.28
0.037	6.63	0.03	7.38	0.36	3.15
0.047	6.35	0.04	6.95	0.40	2.75
0.066	6.05	0.05	6.48	0.44*	2.22
0.121	4.94	0.06	6.14	0.48	1.78
0.160	4.43	0.07	6.08	0.52	1.50
0.226	3.88	0.08	5.59	0.56	1.20
0.422	2.13	0.09	5.64	0.60	0.85
0.579	0.95	0.10	5.22	0.64	0.56
0.879	0.03	0.12	5.33	0.68	0.35
Total Deposition = 0.230 MeV		0.14	4.86	0.72	0.22
		0.16	4.77	0.76	0.11
		0.18	4.34	0.80	0.06
		0.20	4.19	0.84	0.03
		0.24	3.95	0.88	0.01
		Total Deposition = 0.228 MeV ±1%			

1. FMR is fraction of a mean range.
2. J is energy deposited in MeV/g/cm^2.
3. Estimated experimental uncertainty is 1.4%.

*Estimated one-sigma statistical uncertainty exceeds 3% at larger FMR.

Table V. C.7

Electron Energy Deposition in Aluminum[1,2,3]

Experimental Results 0°		Theoretical Results 0°	
0.109 MeV	0.058 MeV	0.1 MeV	0.05 MeV
J	J	J	J
7.78	9.65	8.18*	9.12*

1. Measured and calculated energy deposited in a calorimeter thickness (5.05×10^{-3} g/cm^2) of aluminum followed by an infinite thickness of aluminum.
2. J is energy deposited in MeV/g/cm^2.
3. Estimated experimental uncertainty is 1.4%.

*Estimated one-sigma statistical uncertainty is 1%.

D. Electron Energy Deposition in Iron

Energies (MeV):	1.0, 0.5, and 0.3
Angles (°):	0
Analysis Method:	C
Angle Determination Method:	N/A
Thermal Coupling Correction Method:	None required

Continuous Slowing Down Approximation Range

Energy (MeV)	Range (g/cm^2)
1.0	6.06×10^{-1}
0.5	2.49×10^{-1}
0.3	1.21×10^{-1}

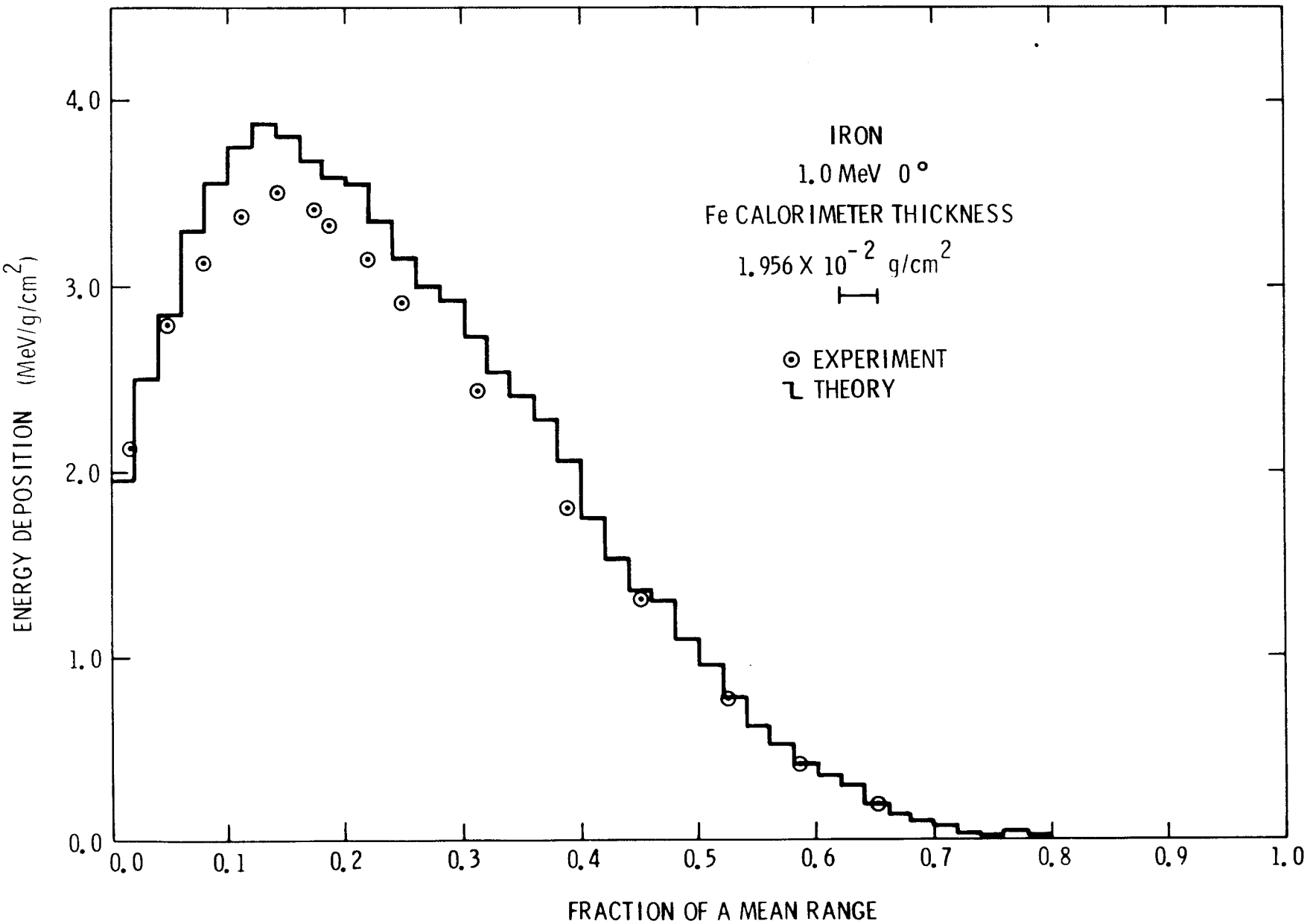

Figure V. D.1. Comparison of Experimental and Theoretical Energy Deposition Profiles in Semi-Infinite Iron for 1.0-MeV Electrons Incident at an Angle of 0°

Table V. D.1

Electron Energy Deposition in Iron[1,2,3]

Experimental Results 1.0 MeV, 0°		Theoretical Results 1.0 MeV, 0°			
FMR	J	FMR	J	FMR	J
0.016	2.12	0.02	1.96	0.42*	1.74
0.048	2.78	0.04	2.50	0.44	1.53
0.078	3.12	0.06	2.84	0.46	1.36
0.111	3.37	0.08	3.29	0.48	1.30
0.142	3.50	0.10	3.56	0.50	1.09
0.174	3.41	0.12	3.74	0.52	0.96
0.186	3.32	0.14	3.87	0.54	0.78
0.218	3.14	0.16	3.80	0.56	0.62
0.248	2.90	0.18	3.67	0.58	0.52
0.312	2.43	0.20	3.58	0.60	0.42
0.388	1.79	0.22	3.55	0.62	0.34
0.451	1.30	0.24	3.34	0.64	0.31
0.526	0.77	0.26	3.14	0.66	0.20
0.588	0.42	0.28	2.99	0.68	0.16
0.652	0.19	0.30	2.92	0.70	0.11
		0.32	2.72	0.72	0.08
Total Deposition = 0.804 MeV		0.34	2.53	0.74	0.04
		0.36	2.41	0.76	0.03
		0.38	2.28	0.78	0.04
		0.40	2.05	0.80	0.01

Total Deposition = 0.879 MeV ±2-1/2%

1. FMR is fraction of a mean range.
2. J is energy deposited in MeV/g/cm^2.
3. Estimated experimental uncertainty is 1.2%.

*

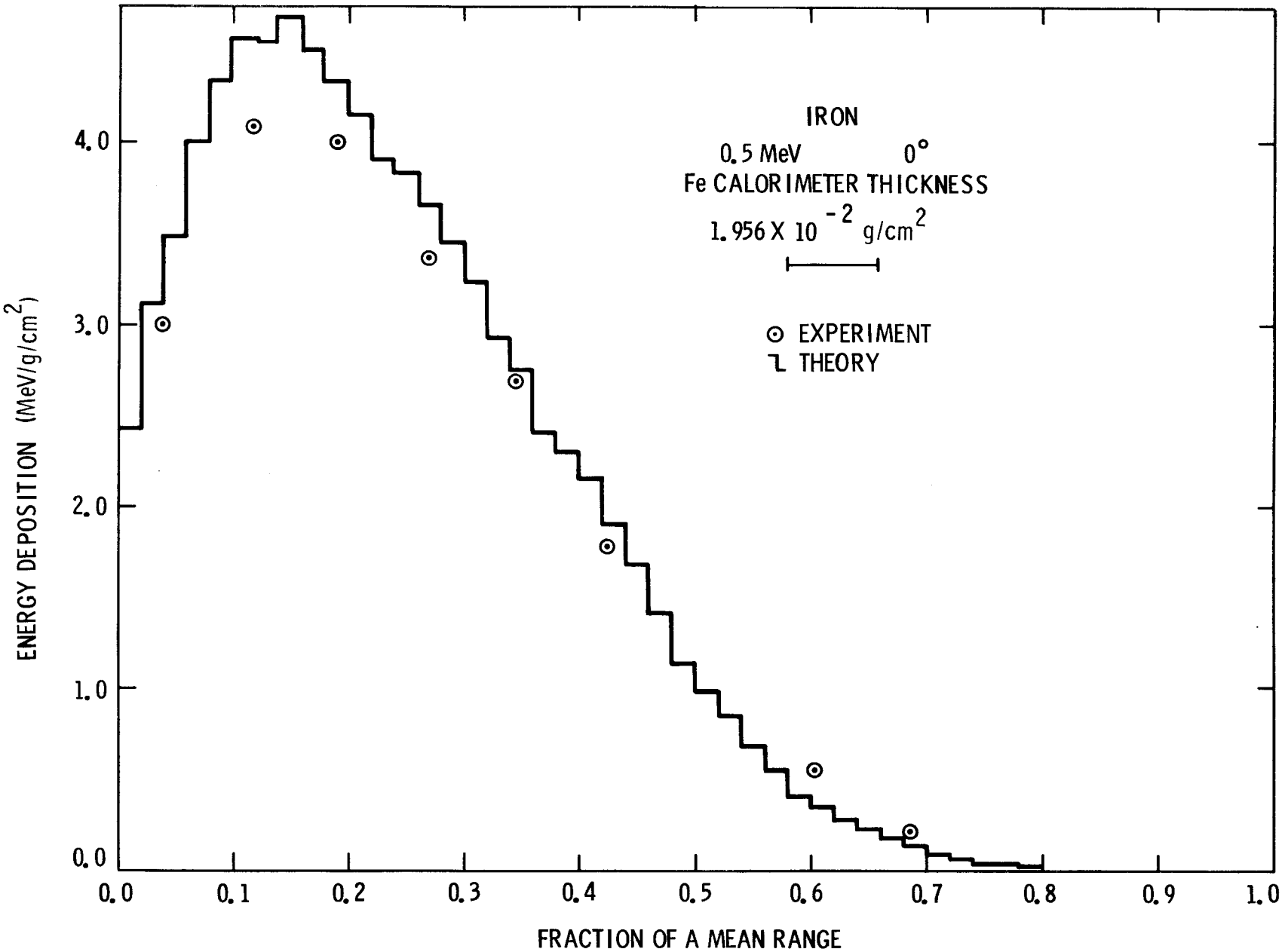

Figure V. D.2. Comparison of Experimental and Theoretical Energy Deposition Profiles in Semi-Infinite Iron for 0.5-MeV Electrons Incident at an Angle of 0°

Table V. D.2

Electron Energy Deposition in Iron[1, 2, 3]

Experimental Results 0.5 MeV, 0°		Theoretical Results 0.5 MeV, 0°			
FMR	J	FMR	J	FMR	J
0.039	2.99	0.02	2.43	0.42*	2.15
0.118	4.08	0.04	3.11	0.44	1.91
0.191	3.99	0.06	3.48	0.46	1.68
0.270	3.37	0.08	3.99	0.48	1.41
0.345	2.68	0.10	4.33	0.50	1.13
0.424	1.78	0.12	4.55	0.52	0.98
0.531	0.97	0.14	4.54	0.54	0.84
0.603	0.54	0.16	4.70	0.56	0.68
0.687	0.21	0.18	4.50	0.58	0.54
		0.20	4.33	0.60	0.39
Total Deposition = 0.404 MeV		0.22	4.14	0.62	0.34
		0.24	3.91	0.64	0.27
		0.26	3.83	0.66	0.22
		0.28	3.66	0.68	0.17
		0.30	3.44	0.70	0.13
		0.32	3.23	0.72	0.08
		0.34	2.92	0.74	0.05
		0.36	2.76	0.76	0.03
		0.38	2.41	0.78	0.03
		0.40	2.31	0.80	0.01

Total Deposition = 0.427 MeV ±0%

1. FMR is fraction of a mean range.
2. J is energy deposited in MeV/g/cm^2.
3. Estimated experimental uncertainty is 1.2%.

*Estimated one-sigma statistical uncertainty exceeds 3% at larger FMR.

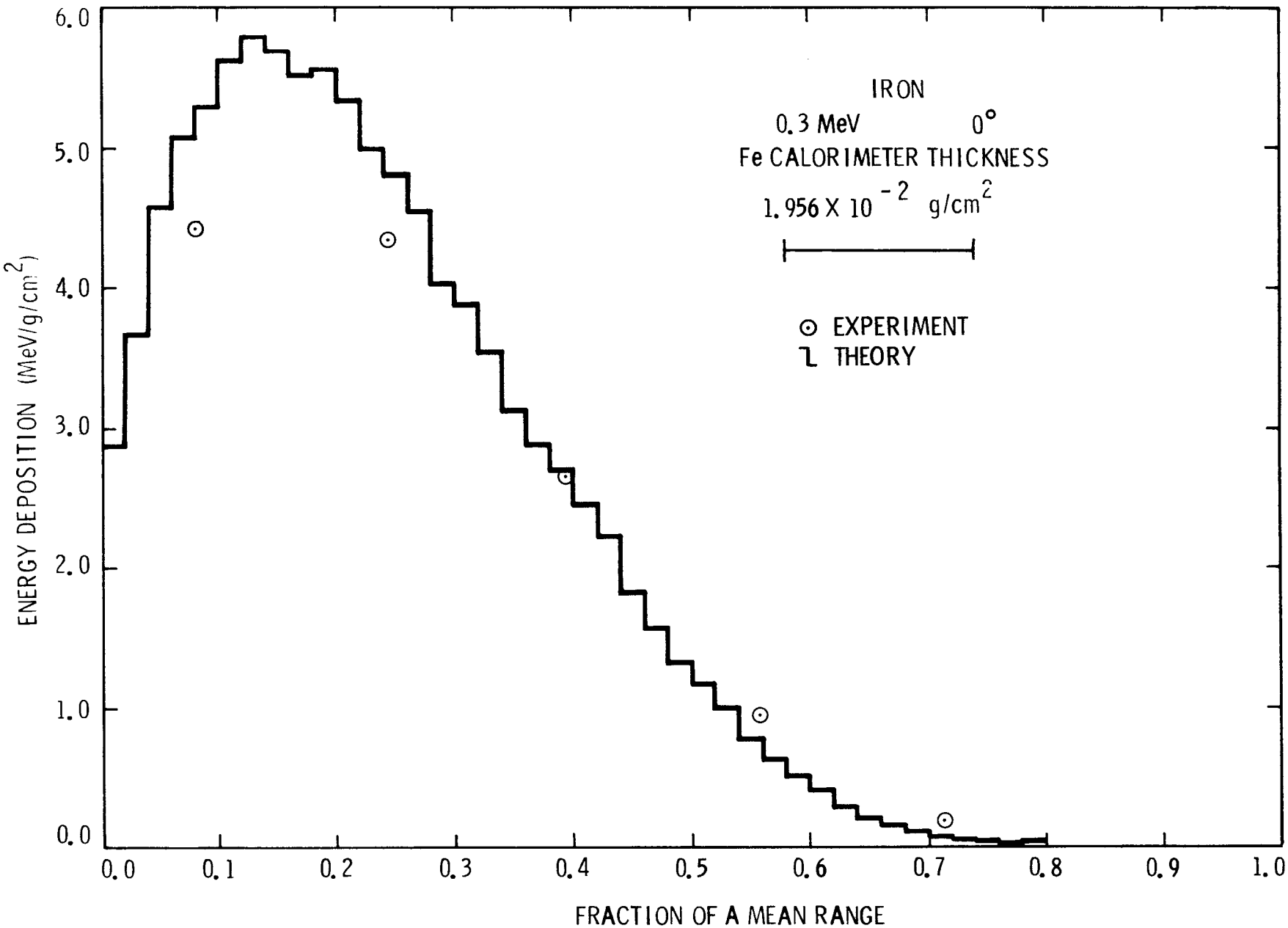

Figure V. D.3. Comparison of Experimental and Theoretical Energy Deposition Profiles in Semi-Infinite Iron for 0.3-MeV Electrons Incident at an Angle of 0°

Table V. D.3

Electron Energy Deposition in Iron[1, 2, 3]

Experimental Results 0.3 MeV, 0°		Theoretical Results 0.3 MeV, 0°			
FMR	J	FMR	J	FMR	J
0.081	4.43	0.02	2.87	0.42	2.45
0.244	4.34	0.04	3.84	0.44	2.23
0.395	2.66	0.06	4.57	0.46	1.82
0.558	0.95	0.08	5.07	0.48	1.57
0.714	0.19	0.10	5.29	0.50	1.33
		0.12	5.62	0.52	1.17
Total Deposition = 0.242 MeV		0.14	5.79	0.54	1.00
		0.16	5.69	0.56	0.77
		0.18	5.52	0.58	0.62
		0.20	5.55	0.60	0.51
		0.22	5.33	0.62	0.41
		0.24	4.98	0.64	0.28
		0.26	4.80	0.66	0.20
		0.28	4.54	0.68	0.15
		0.30	4.03	0.70	0.12
		0.32	3.88	0.72	0.07
		0.34	3.54	0.74	0.04
		0.36	3.12	0.76	0.03
		0.38*	2.88	0.78	0.02
		0.40	2.71	0.80	0.03
		Total Deposition = 0.252 MeV ±1%			

1. FMR is fraction of a mean range.
2. J is energy deposited in MeV/g/cm^2.
3. Estimated experimental uncertainty is 1.2%.

E. Electron Energy Deposition in Copper

Energies (MeV): 1.0, 0.5, and 0.3

Angle (°): 0

Analysis Method: C

Angle Determination Method: N/A

Thermal Coupling Correction Method: None required

Continuous Slowing Down Approximation Range

Energy (MeV)	Range (g/cm^2)
1.0	6.25×10^{-1}
0.5	2.58×10^{-1}
0.3	1.25×10^{-1}

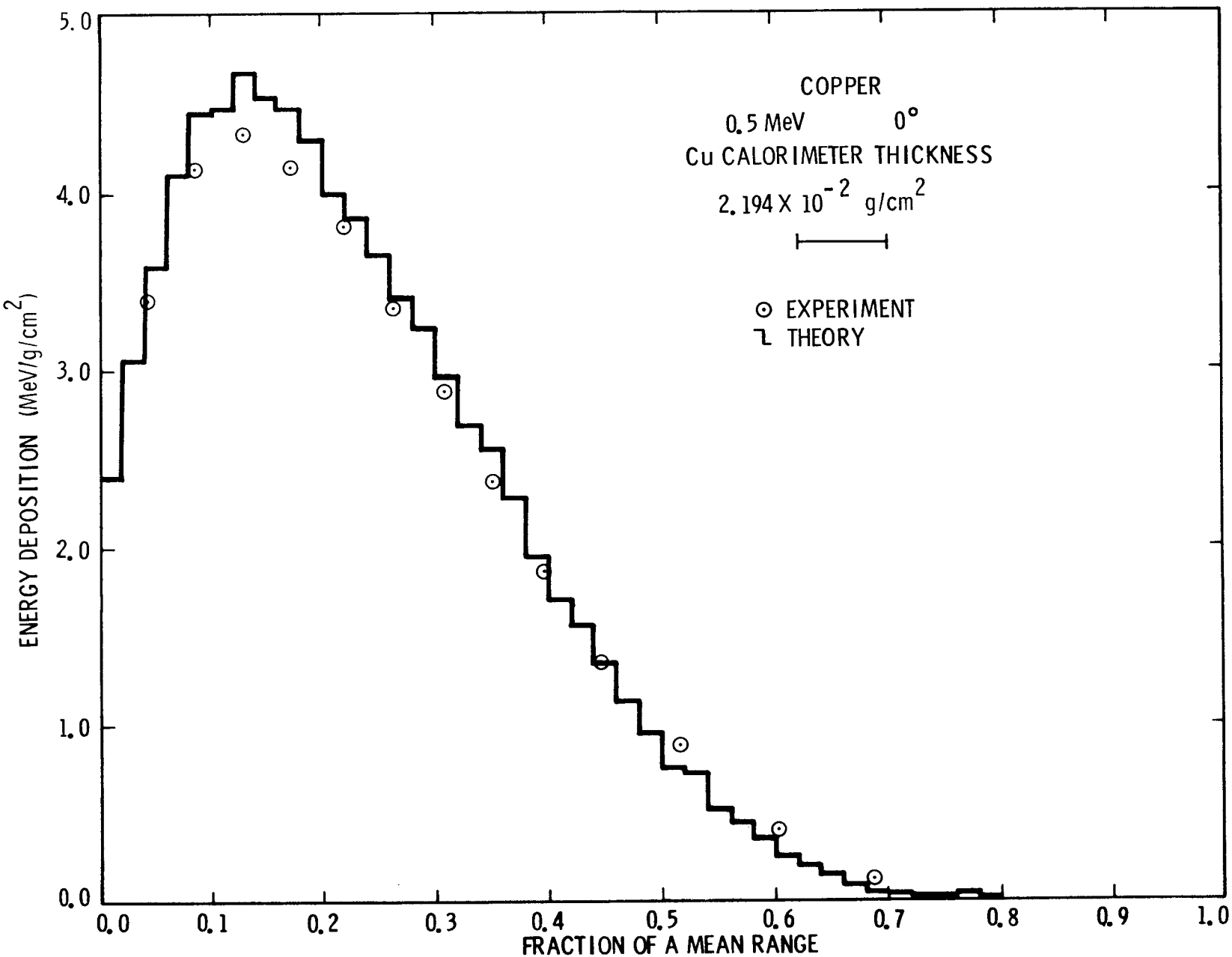

Figure V. E. 2. Comparison of Experimental and Theoretical Energy Deposition Profiles in Semi-Infinite Copper for 0.5-MeV Electrons Incident at an Angle of 0°

Table V. E. 2

Electron Energy Deposition in Copper[1, 2, 3]

Experimental Results 0.5 MeV, 0°		Theoretical Results 0.5 MeV, 0°			
FMR	J	FMR	J	FMR	J
0.042	3.39	0.02	2.39	0.42	1.70
0.086	4.14	0.04	3.06	0.44	1.56
0.129	4.33	0.06	3.58	0.46	1.34
0.173	4.14	0.08	4.10	0.48	1.13
0.220	3.80	0.10	4.46	0.50	0.94
0.264	3.35	0.12	4.47	0.52	0.74
0.307	2.88	0.14	4.68	0.54	0.73
0.351	2.37	0.16	4.55	0.56	0.52
0.397	1.87	0.18	4.47	0.58	0.44
0.447	1.35	0.20	4.29	0.60	0.35
0.516	0.89	0.22	3.99	0.62	0.25
0.602	0.41	0.24	3.86	0.64	0.20
0.689	0.13	0.26	3.64	0.66	0.15
		0.28	3.41	0.68	0.08
Total Deposition = 0.412 MeV		0.30	3.23	0.70	0.05
		0.32	2.96	0.72	0.03
		0.34	2.68	0.74	0.02
		0.36	2.55	0.76	0.02
		0.38	2.27	0.78	0.03
		0.40*	1.94	0.80	0.01

Total Deposition = 0.417 MeV ±0%

1. FMR is fraction of a mean range.
2. J is energy deposited in MeV/g/cm^2.
3. Estimated experimental uncertainty is 1.3%.

* Estimated one sigma statistical uncertainty exceeds 3% at larger FMR

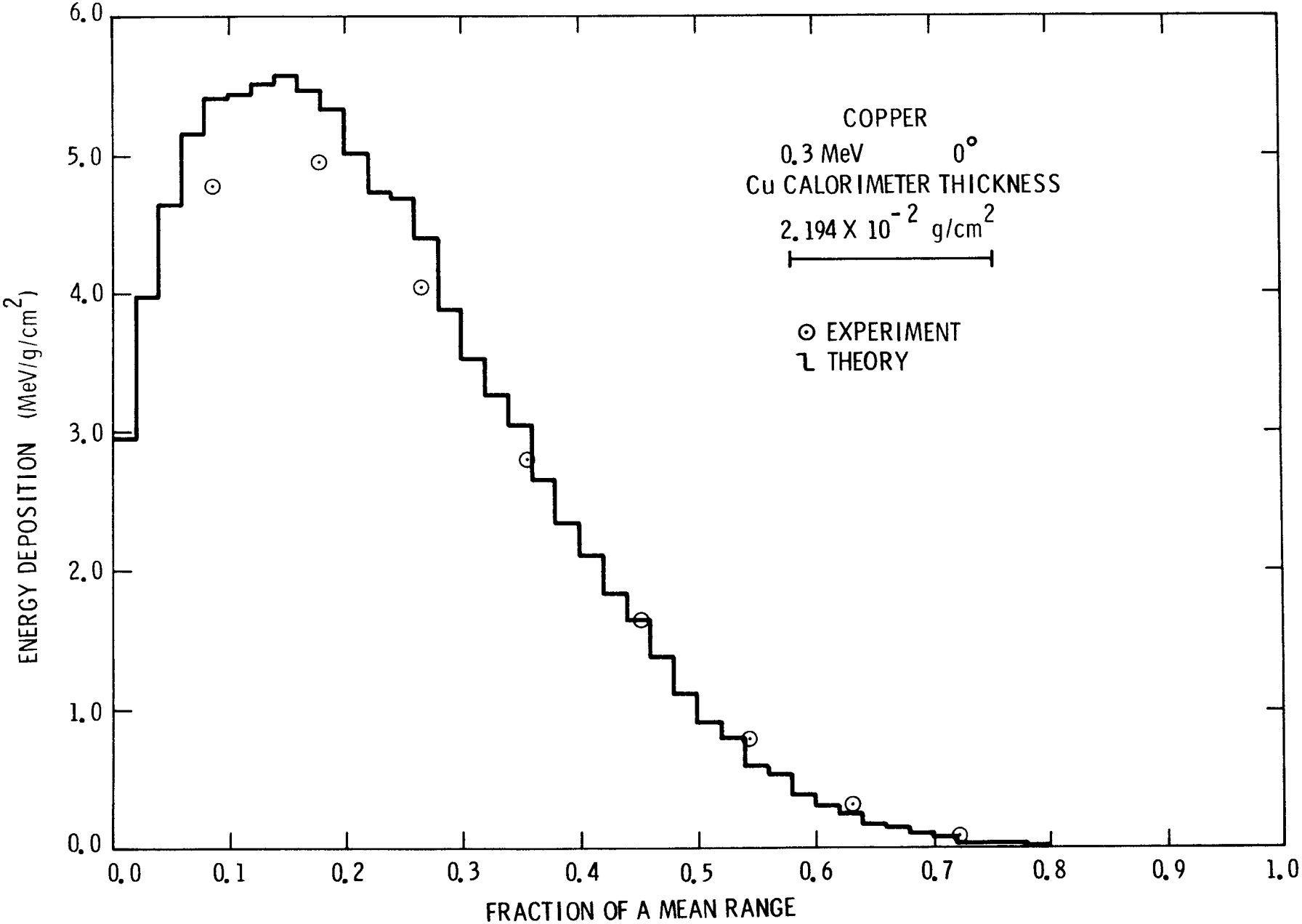

Figure V. E. 3. Comparison of Experimental and Theoretical Energy Deposition Profiles in Semi-Infinite Copper for 0.3-MeV Electrons Incident at an Angle of 0°

Table V. E. 3

Electron Energy Deposition in Copper[1, 2, 3]

Experimental Results 0.3 MeV, 0°		Theoretical Results 0.3 MeV, 0°			
FMR	J	FMR	J	FMR	J
0.087	4.77	0.02	2.95	0.42	2.11
0.178	4.95	0.04	3.97	0.44	1.83
0.266	4.04	0.06	4.64	0.46	1.64
0.357	2.80	0.08	5.15	0.48	1.37
0.453	1.64	0.10	5.41	0.50	1.11
0.544	0.78	0.12	5.43	0.52	0.91
0.632	0.31	0.14	5.51	0.54	0.79
0.723	0.09	0.16	5.57	0.56	0.59
		0.18	5.46	0.58	0.53
Total Deposition = 0.242 MeV		0.20	5.32	0.60	0.38
		0.22	5.01	0.62	0.30
		0.24	4.72	0.64	0.25
		0.26	4.68	0.66	0.17
		0.28*	4.40	0.68	0.14
		0.30	3.88	0.70	0.10
		0.32	3.53	0.72	0.07
		0.34	3.26	0.74	0.03
		0.36	3.05	0.76	0.03
		0.38	2.65	0.78	0.03
		0.40	2.34	0.80	0.01

Total Deposition = 0.248 MeV ±1%

1. FMR is fraction of a mean range.
2. J is energy deposited in MeV/g/cm^2.
3. Estimated experimental uncertainty is 1.3%.

*Estimated one sigma statistical uncertainty exceeds 3% at larger FMR

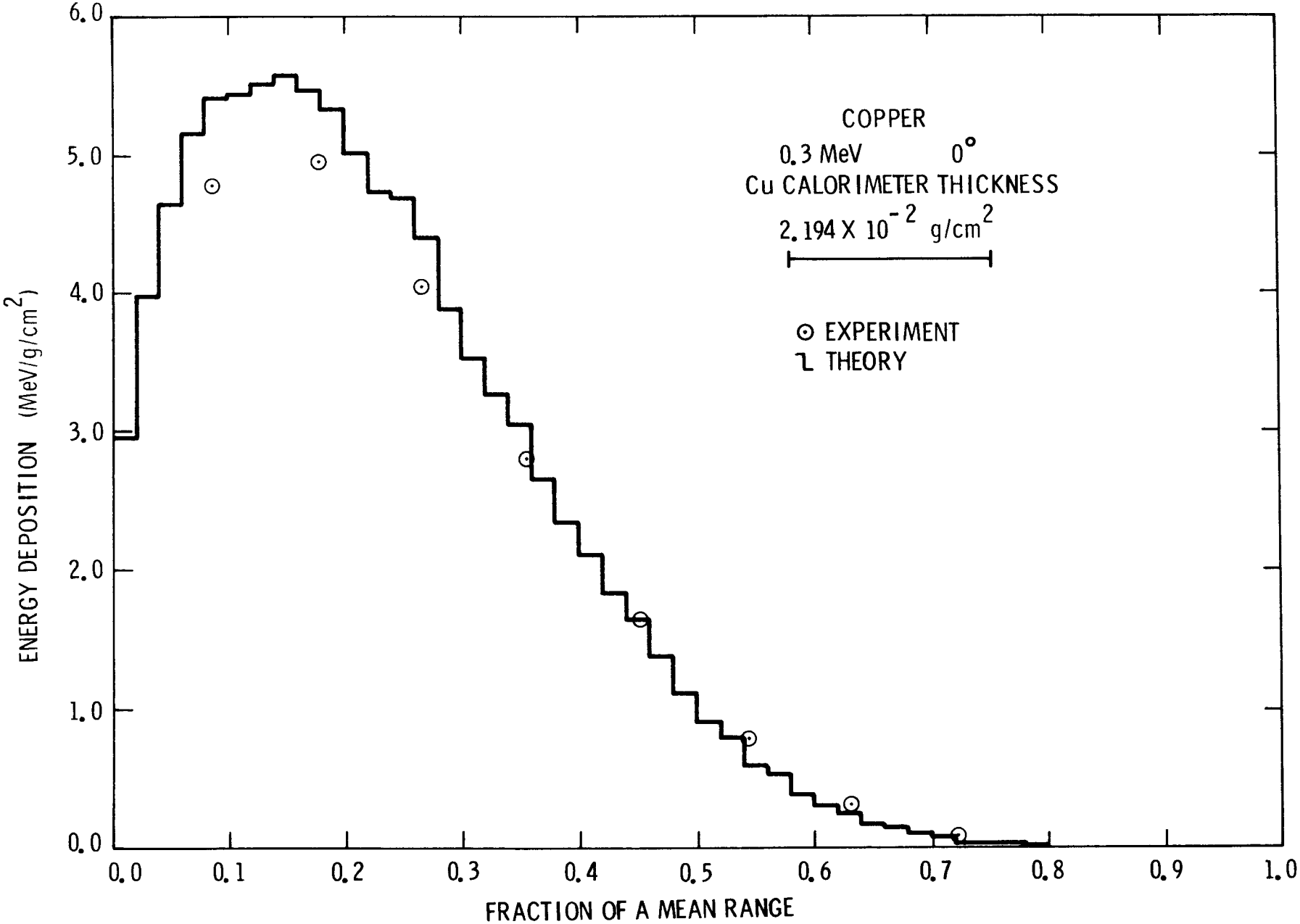

Figure V. E. 3. Comparison of Experimental and Theoretical Energy Deposition Profiles in Semi-Infinite Copper for 0.3-MeV Electrons Incident at an Angle of 0°

Table V. E.3

Electron Energy Deposition in Copper[1, 2, 3]

Experimental Results 0.3 MeV, 0°		Theoretical Results 0.3 MeV, 0°			
FMR	J	FMR	J	FMR	J
0.087	4.77	0.02	2.95	0.42	2.11
0.178	4.95	0.04	3.97	0.44	1.83
0.266	4.04	0.06	4.64	0.46	1.64
0.357	2.80	0.08	5.15	0.48	1.37
0.453	1.64	0.10	5.41	0.50	1.11
0.544	0.78	0.12	5.43	0.52	0.91
0.632	0.31	0.14	5.51	0.54	0.79
0.723	0.09	0.16	5.57	0.56	0.59
Total Deposition = 0.242 MeV		0.18	5.46	0.58	0.53
		0.20	5.32	0.60	0.38
		0.22	5.01	0.62	0.30
		0.24	4.72	0.64	0.25
		0.26	4.68	0.66	0.17
		0.28*	4.40	0.68	0.14
		0.30	3.88	0.70	0.10
		0.32	3.53	0.72	0.07
		0.34	3.26	0.74	0.03
		0.36	3.05	0.76	0.03
		0.38	2.65	0.78	0.03
		0.40	2.34	0.80	0.01
		Total Deposition = 0.248 MeV ±1%			

1. FMR is fraction of a mean range.
2. J is energy deposited in $MeV/g/cm^2$.
3. Estimated experimental uncertainty is 1.3%.

*Estimated one-sigma statistical uncertainty exceeds 3% at larger FMR.

F. Electron Energy Deposition in Molybdenum

Energies (MeV):	1.0, 0.5, 0.3, and 0.1
Angles (°):	0 and 60
Analysis Method:	C
Angle Determination Method:	B
Thermal Coupling Correction Method:	A

Continuous Slowing Down Approximation Range

Energy (MeV)	Range (g/cm^2)
1.0	6.73×10^{-1}
0.5	2.81×10^{-1}
0.3	1.37×10^{-1}
0.1	2.46×10^{-2}

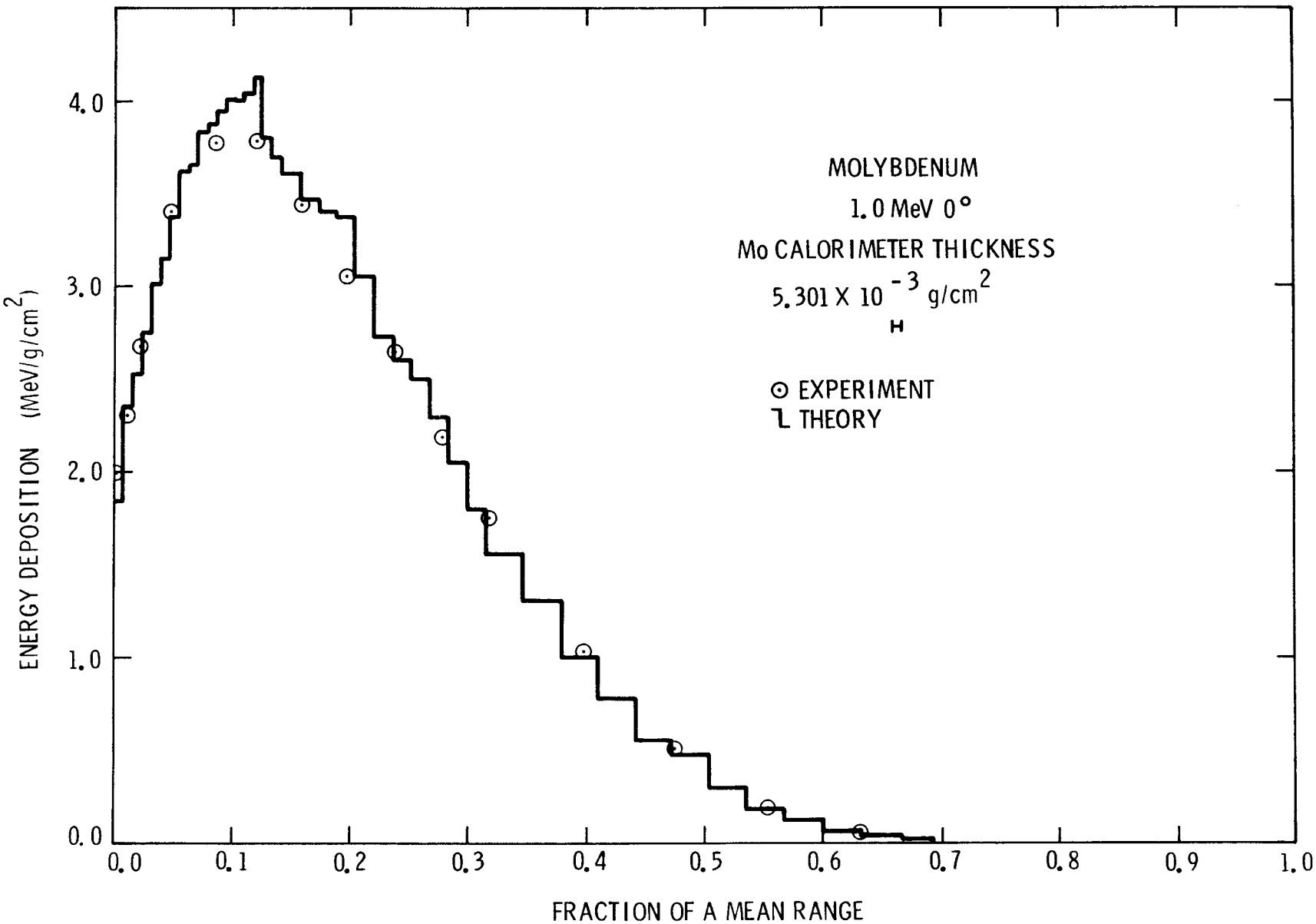

Figure V. F. 1. Comparison of Experimental and Theoretical Energy Deposition Profiles in Semi-Infinite Molybdenum for 1.0-MeV Electrons Incident at an Angle of 0°

Table V. F. 1

Electron Energy Deposition in Molybdenum[1,2,3]

Experimental Results 1.0 MeV, 0°		Theoretical Results 1.0 MeV, 0°			
FMR	J	FMR	J	FMR	J
0.004	1.99	0.008	1.84	0.205	3.37
0.012	2.30	0.016	2.36	0.221	3.06
0.022	2.68	0.024	2.53	0.237	2.73
0.049	3.40	0.032	2.76	0.252	2.59
0.088	3.77	0.039	3.01	0.268	2.49
0.122	3.78	0.047	3.15	0.284	2.29
0.159	3.45	0.055	3.38	0.300	2.04
0.198	3.04	0.063	3.62	0.315	1.80
0.240	2.64	0.071	3.65	0.347	1.56
0.280	2.18	0.079	3.83	0.379	1.31
0.319	1.75	0.087	3.88	0.410*	1.00
0.400	1.03	0.095	3.94	0.442	0.78
0.476	0.50	0.103	4.01	0.473	0.56
0.555	0.19	0.110	4.00	0.505	0.47
0.632	0.05	0.118	4.04	0.536	0.29
		0.126	4.13	0.568	0.18
Total Deposition = 0.779 MeV		0.134	3.80	0.599	0.12
		0.142	3.70	0.631	0.06
		0.158	3.61	0.663	0.04
		0.174	3.47	0.694	0.03
		0.189	3.41	0.726	0.01

Total Deposition = 0.791 MeV ±0%

1. FMR is fraction of a mean range.
2. J is energy deposited in MeV/g/cm^2.
3. Estimated experimental uncertainty is 1.6%.

*

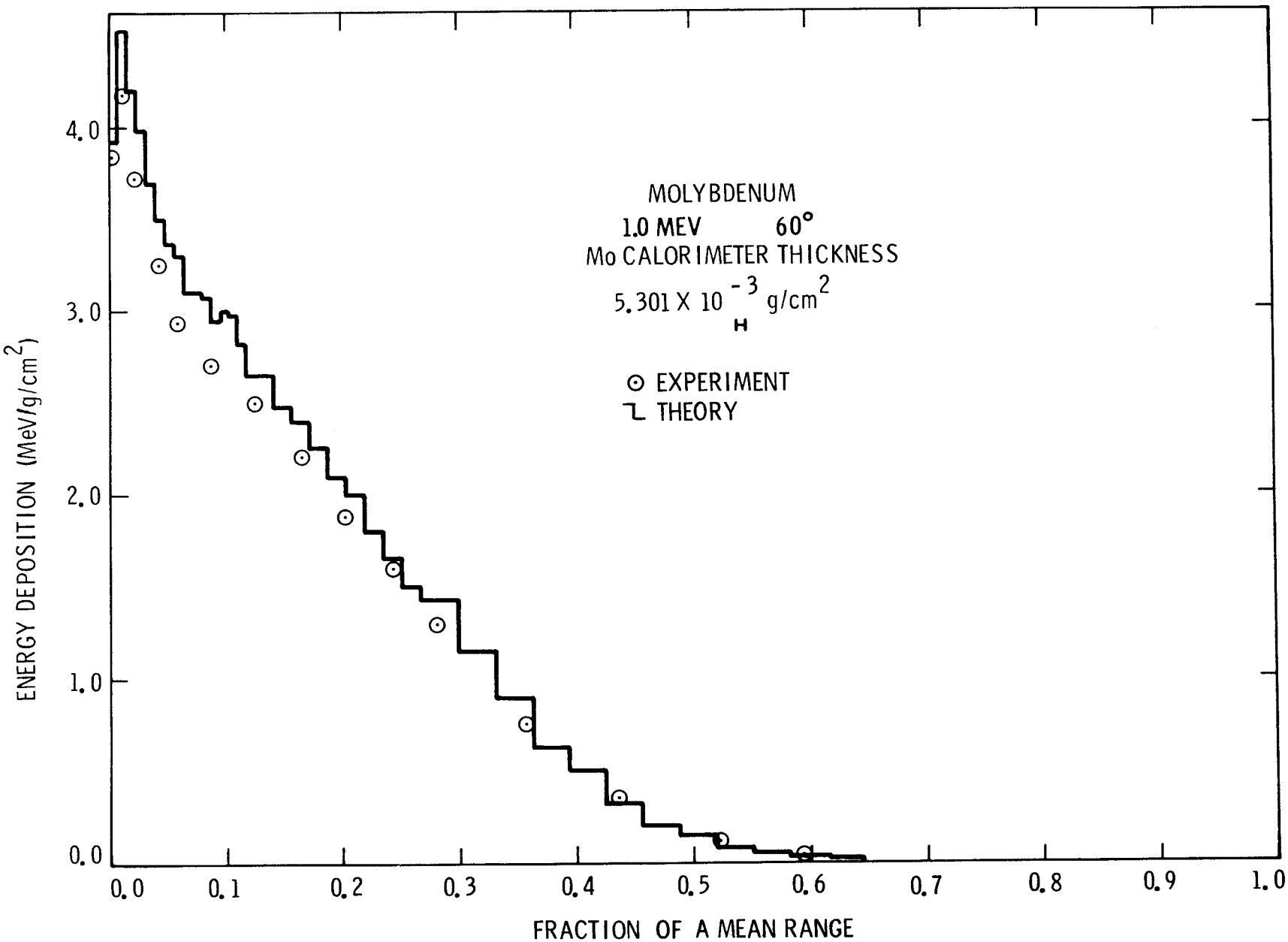

Figure V. F.2. Comparison of Experimental and Theoretical Energy Deposition Profiles in Semi-Infinite Molybdenum for 1.0-MeV Electrons Incident at an Angle of 60°

Table V. F. 2

Electron Energy Deposition in Molybdenum[1, 2, 3]

Experimental Results 1.0 MeV, 60°		Theoretical Results 1.0 MeV, 60°			
FMR	J	FMR	J	FMR	J
0.004	3.85	0.008	3.92	0.189	2.26
0.012	4.18	0.016	4.53	0.205	2.09
0.024	3.72	0.024	4.20	0.221	1.99
0.043	3.26	0.032	3.98	0.236	1.79
0.059	2.93	0.039	3.69	0.252	1.65
0.088	2.71	0.047	3.51	0.268	1.50
0.126	2.50	0.055	3.37	0.299	1.43
0.167	2.21	0.063	3.31	0.331	1.15
0.204	1.88	0.071	3.10	0.363	0.90
0.244	1.60	0.079	3.10	0.394	0.63
0.282	1.29	0.087	3.07	0.426	0.49
0.358	0.75	0.095	2.95	0.457	0.32
0.437	0.36	0.102	3.00	0.489	0.20
0.523	0.12	0.110	2.97	0.520	0.14
0.595	0.04	0.118	2.82	0.552	0.08
		0.126	2.65	0.583	0.05
Total Deposition = 0.557 MeV		0.142	2.64	0.615	0.03
		0.158*	2.48	0.646	0.02
		0.173	2.40	0.678	0.01

Total Deposition = 0.602 MeV ±1%

1. FMR is fraction of a mean range.
2. J is energy deposited in MeV/g/cm^2.
3. Estimated experimental uncertainty is 1.6%.

*Estimated one-sigma statistical uncertainty exceeds 3% at larger FMR.

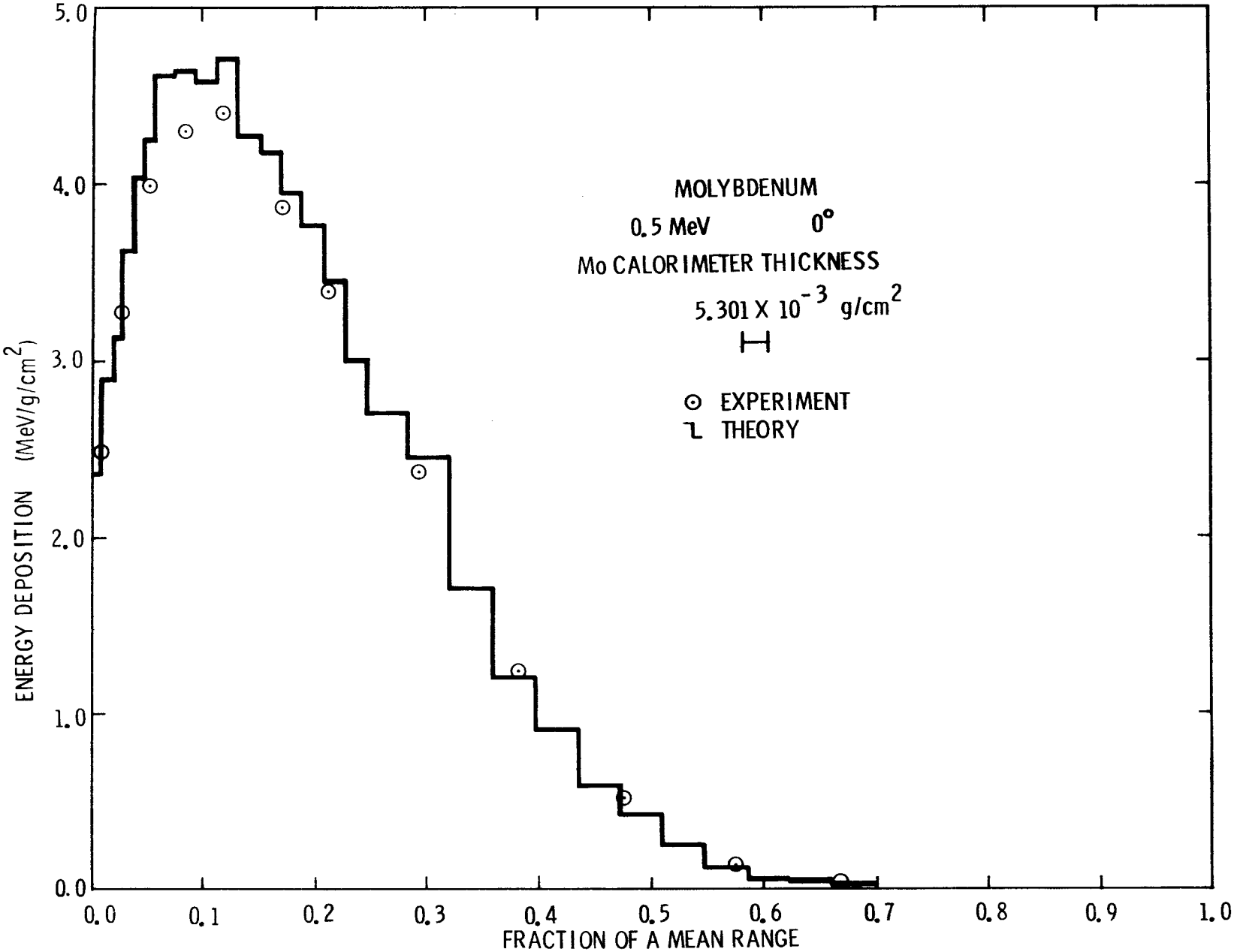

Figure V. F. 3. Comparison of Experimental and Theoretical Energy Deposition Profiles in Semi-Infinite Molybdenum for 0. 5-MeV Electrons Incident at an Angle of 0°

Table V. F.3

Electron Energy Deposition in Molybdenum[1, 2, 3]

Experimental Results 0.5 MeV, 0°		Theoretical Results 0.5 MeV, 0°			
FMR	J	FMR	J	FMR	J
0.009	2.48	0.009	2.36	0.246	3.00
0.028	3.27	0.019	2.89	0.283	2.69
0.052	3.99	0.028	3.13	0.321	2.19
0.083	4.31	0.038	3.63	0.359	1.71
0.118	4.40	0.047	4.03	0.397*	1.20
0.171	3.87	0.057	4.26	0.435	0.91
0.212	3.39	0.076	4.62	0.472	0.58
0.293	2.37	0.094	4.63	0.510	0.43
0.382	1.24	0.113	4.58	0.548	0.26
0.475	0.53	0.132	4.70	0.586	0.12
0.575	0.14	0.151	4.27	0.624	0.06
0.671	0.02	0.170	4.17	0.661	0.04
		0.189	3.95	0.699	0.02
Total Deposition = 0.373 MeV		0.208	3.77	0.737	0.00
		0.227	3.46		
		Total Deposition = 0.381 MeV ±1%			

1. FMR is fraction of a mean range.
2. J is energy deposited in MeV/g/cm^2.
3. Estimated experimental uncertainty is 1.6%.

*Estimated one-sigma statistical uncertainty exceeds 3% at larger FMR.

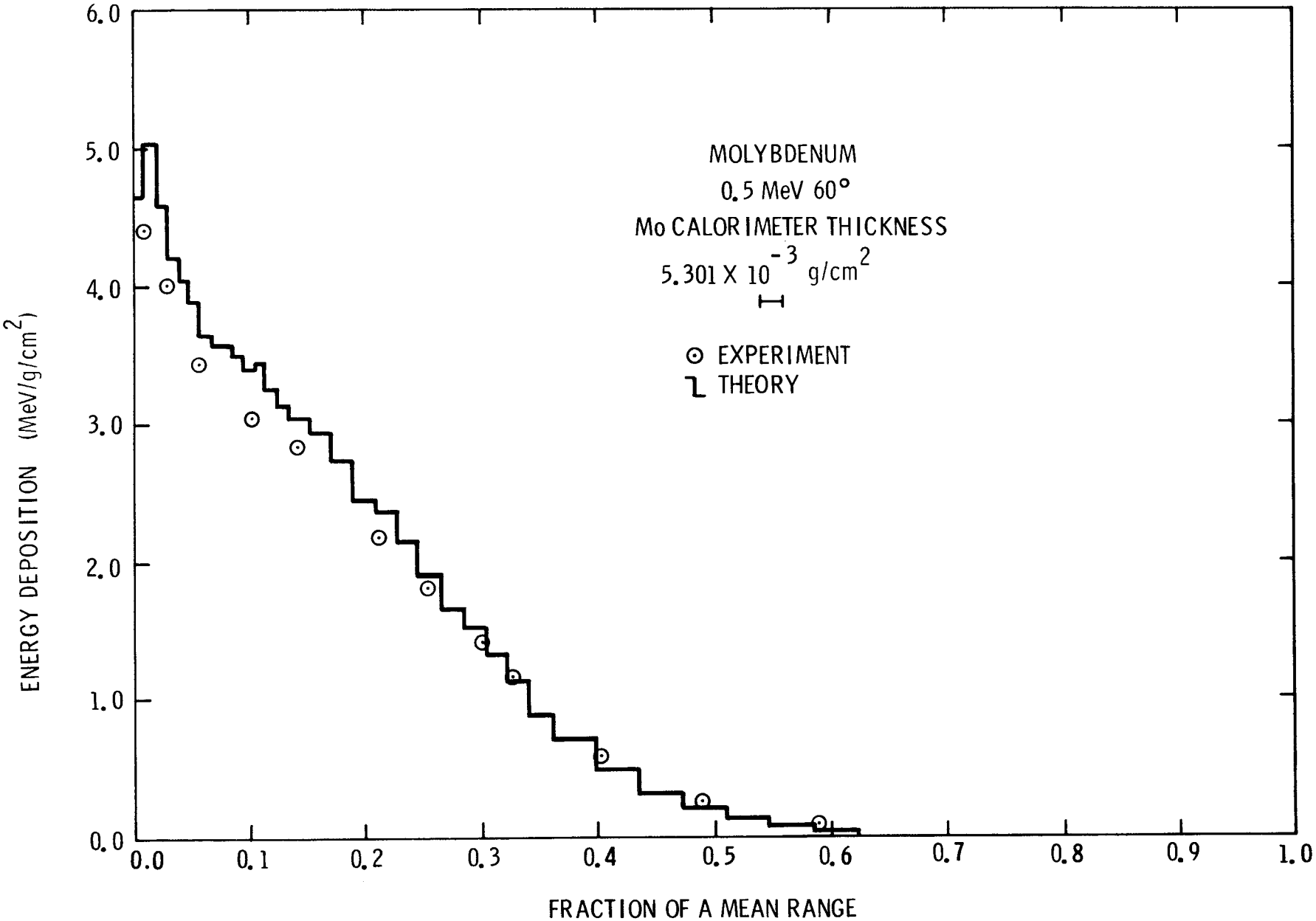

Figure V. F.4. Comparison of Experimental and Theoretical Energy Deposition Profiles in Semi-Infinite Molybdenum for 0.5-MeV Electrons Incident at an Angle of 60°

Table V. F.4

Electron Energy Deposition in Molybdenum[1,2,3]

Experimental Results 0.5 MeV, 60°		Theoretical Results 0.5 MeV, 60°			
FMR	J	FMR	J	FMR	J
0.009	4.40	0.009	4.65	0.208	2.44
0.028	4.01	0.019	5.02	0.227	2.37
0.057	3.42	0.028	4.57	0.245	2.15
0.102	3.04	0.038	4.20	0.264	1.91
0.142	2.83	0.047	4.04	0.283	1.65
0.212	2.17	0.057	3.88	0.302*	1.53
0.253	1.80	0.066	3.65	0.321	1.32
0.301	1.40	0.076	3.57	0.340	1.13
0.325	1.15	0.085	3.57	0.359	0.88
0.400	0.61	0.094	3.51	0.396	0.70
0.490	0.22	0.104	3.41	0.434	0.48
0.586	0.05	0.113	3.43	0.472	0.30
		0.123	3.25	0.510	0.19
Total Deposition = 0.272 MeV		0.132	3.12	0.548	0.12
		0.151	3.04	0.585	0.07
		0.170	2.94	0.623	0.03
		0.189	2.74	0.661	0.01
		Total Deposition = 0.290 MeV ±1%			

1. FMR is fraction of a mean range.
2. J is energy deposited in MeV/g/cm^2.
3. Estimated experimental uncertainty is 1.6%.

*Estimated one-sigma statistical uncertainty exceeds 3% at larger FMR.

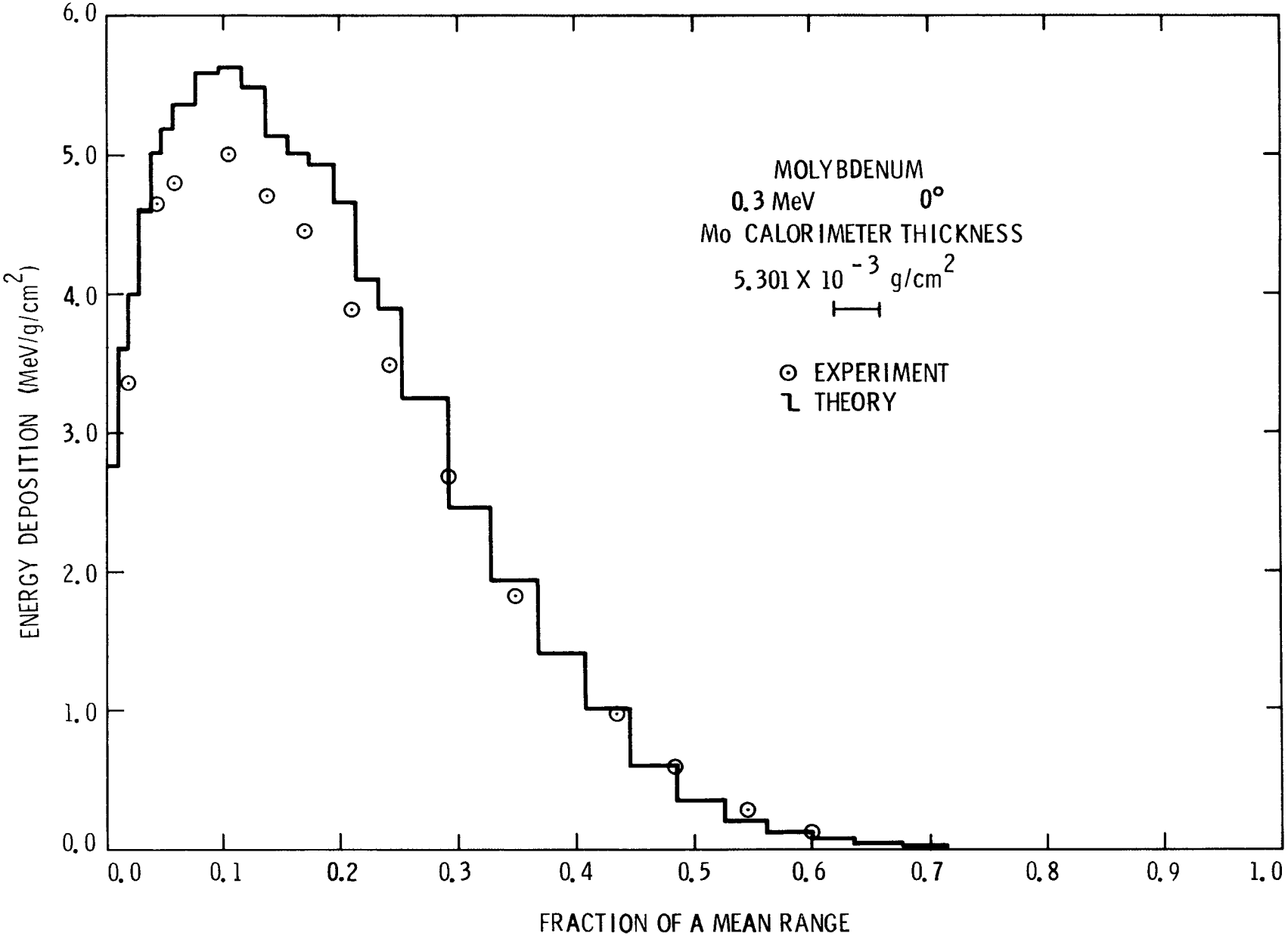

Figure V. F. 5 Comparison of Experimental and Theoretical Energy Deposition Profiles in Semi-Infinite Molybdenum for 0. 3-MeV Electrons Incident at an Angle of 0°

Table V. F.5

Electron Energy Deposition in Molybdenum[1,2,3]

Experimental Results 0.3 MeV, 0°		Theoretical Results 0.3 MeV, 0°			
FMR	J	FMR	J	FMR	J
0.019	3.35	0.010	2.76	0.252	3.88
0.041	4.63	0.019	3.60	0.291	3.25
0.058	4.78	0.029	3.98	0.329	2.47
0.106	4.99	0.039	4.60	0.368	1.93
0.139	4.68	0.048	5.01	0.407	1.41
0.171	4.44	0.058	5.18	0.445*	1.00
0.210	3.88	0.077	5.35	0.484	0.59
0.241	3.48	0.097	5.60	0.523	0.34
0.291	2.66	0.116	5.61	0.562	0.21
0.350	1.80	0.136	5.48	0.600	0.12
0.434	0.96	0.155	5.13	0.639	0.06
0.482	0.56	0.174	5.00	0.678	0.03
0.546	0.27	0.194	4.93	0.717	0.02
0.599	0.11	0.213	4.65	0.755	0.01
		0.232	4.09		
Total Deposition = 0.208 MeV		Total Deposition = 0.226 MeV ±0%			

1. FMR is fraction of a mean range.
2. J is energy deposited in MeV/g/cm^2.
3. Estimated experimental uncertainty is 1.6%.

*Estimated one-sigma statistical uncertainty exceeds 3% at larger FMR.

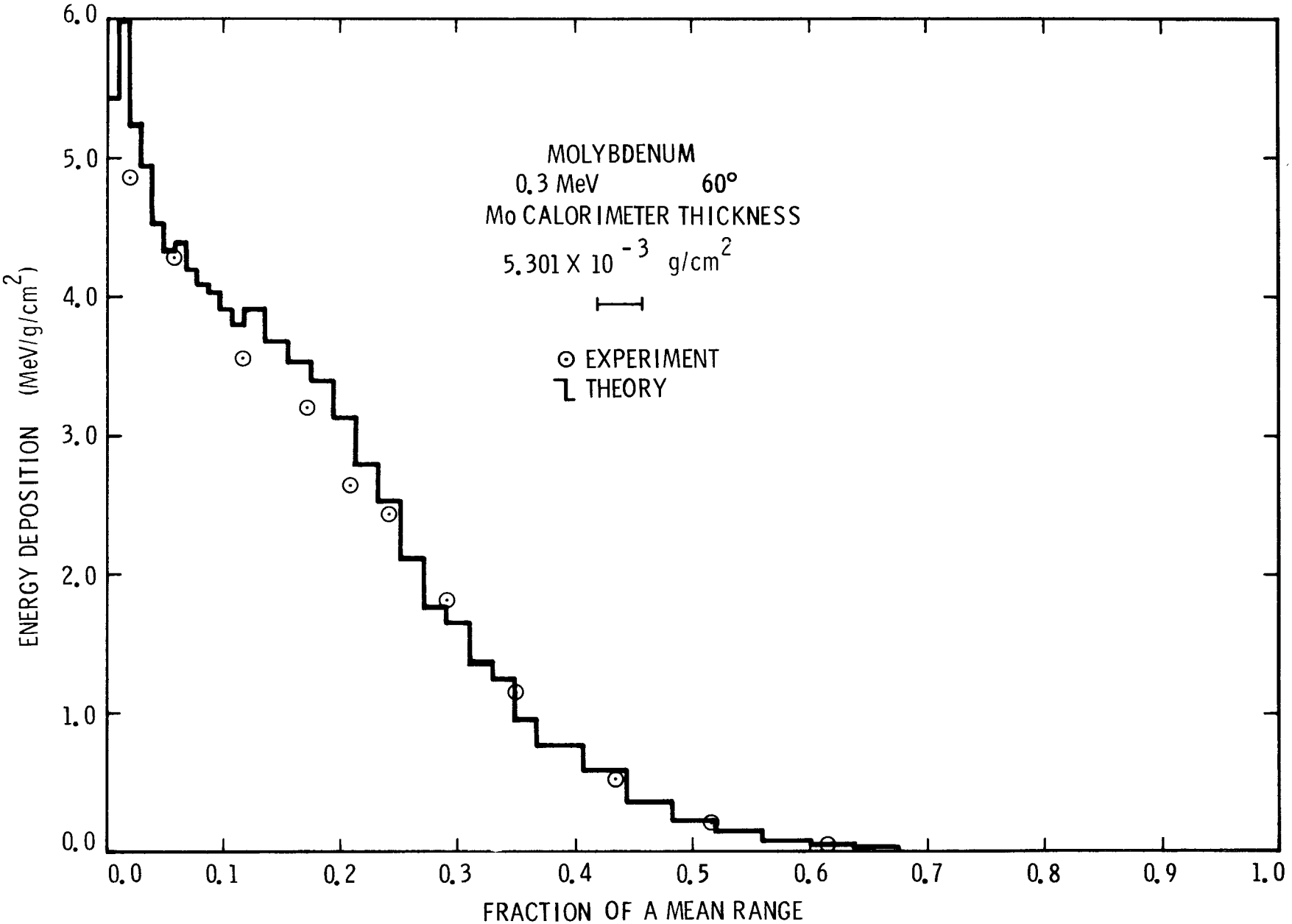

Figure V . F. 6. Comparison of Experimental and Theoretical Energy Deposition Profiles in Semi-Infinite Molybdenum for 0.3-MeV Electrons Incident at an Angle of 60°

Table V. F.6

Electron Energy Deposition in Molybdenum[1,2,3]

Experimental Results 0.3 MeV, 60°		Theoretical Results 0.3 MeV, 60°			
FMR	J	FMR	J	FMR	J
0.019	4.86	0.010	5.43	0.232	2.78
0.058	4.27	0.019	6.02	0.252*	2.53
0.117	3.56	0.029	5.24	0.271	2.11
0.171	3.21	0.039	4.94	0.290	1.76
0.210	2.64	0.048	4.53	0.310	1.65
0.241	2.43	0.058	4.33	0.330	1.37
0.291	1.81	0.068	4.38	0.348	1.25
0.350	1.15	0.077	4.20	0.368	0.95
0.434	0.51	0.087	4.07	0.406	0.79
0.518	0.20	0.097	4.05	0.445	0.58
0.616	0.04	0.106	3.90	0.484	0.35
Total Deposition = 0.160 MeV		0.116	3.81	0.522	0.22
		0.135	3.90	0.561	0.14
		0.155	3.68	0.600	0.07
		0.174	3.54	0.639	0.03
		0.194	3.41	0.677	0.02
		0.213	3.13		
		Total Deposition = 0.170 MeV ±1%			

1. FMR is fraction of a mean range.
2. J is energy deposited in MeV/g/cm^2.
3. Estimated experimental uncertainty is 1.6%.

*Estimated one-sigma statistical uncertainty exceeds 3% at larger FMR.

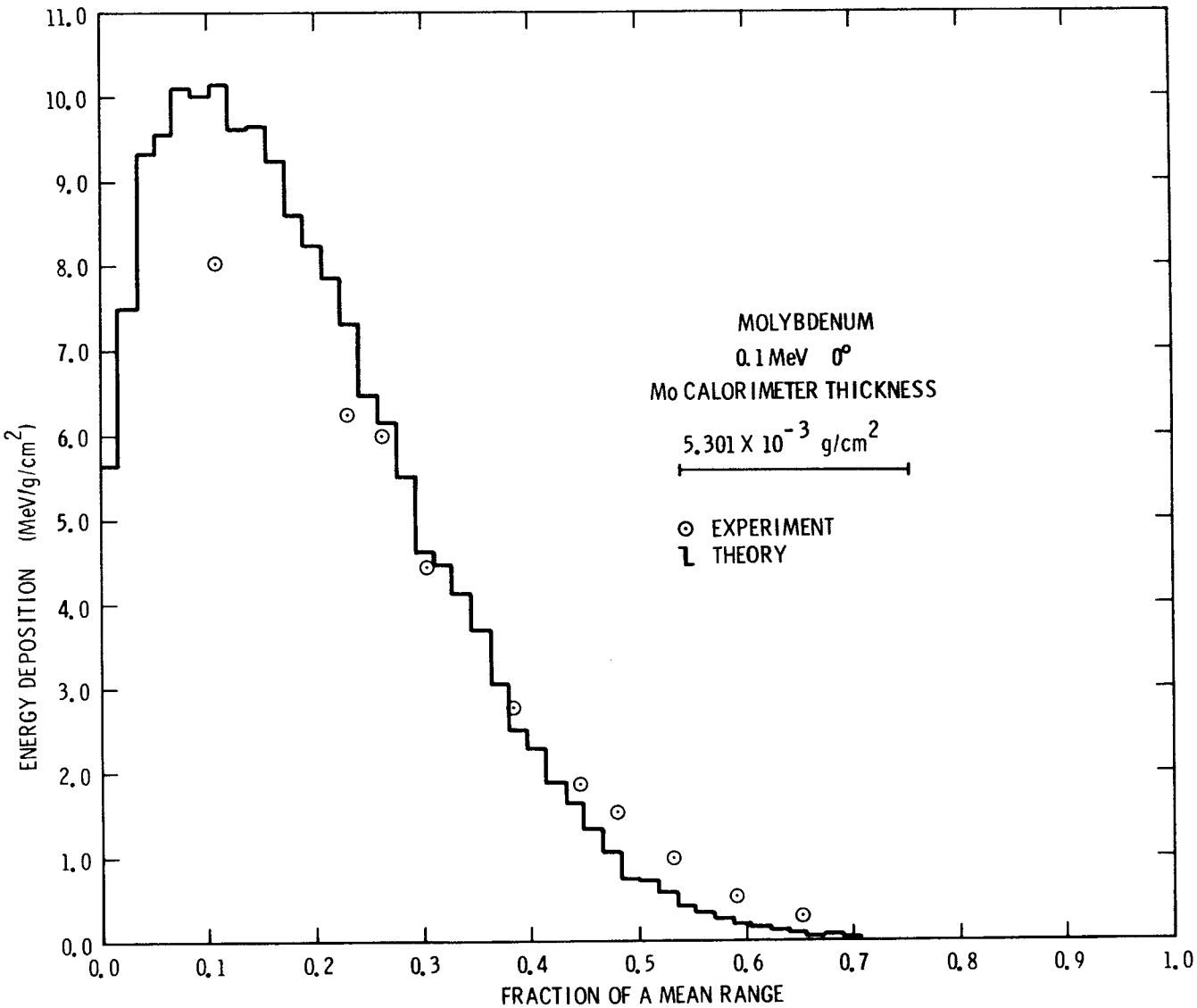

Figure V. F. 7. Comparison of Experimental and Theoretical Energy Deposition Profiles in Semi-Infinite Molybdenum for 0.1-MeV Electrons Incident at an Angle of 0°

Table V. F.7

Electron Energy Deposition in Molybdenum[1,2,3]

Experimental Results 0.1 MeV, 0°		Theoretical Results 0.1 MeV, 0°			
FMR	J	FMR	J	FMR	J
0.108	8.03	0.017	5.64	0.380	3.04
0.230	6.23	0.035	7.50	0.397	2.50
0.264	5.98	0.052	9.33	0.414	2.29
0.324	4.41	0.069	9.56	0.432	1.88
0.385	2.76	0.086	10.1	0.449	1.64
0.446	1.84	0.104	10.0	0.466	1.32
0.480	1.52	0.121	10.15	0.483	1.05
0.531	0.97	0.138	9.62	0.501	0.74
0.591	0.52	0.155	9.64	0.518	0.72
0.653	0.29	0.173	9.23	0.535	0.58
1.342	0.00	0.190	8.59	0.552	0.42
Total Deposition = 0.069 MeV		0.207	8.23	0.570	0.33
		0.224	7.86	0.587	0.28
		0.242	7.32	0.604	0.20
		0.259	6.46	0.622	0.17
		0.276	6.13	0.639	0.13
		0.294	5.51	0.656	0.12
		0.311	4.62	0.673	0.05
		0.328	4.46	0.691	0.06
		0.345*	4.12	0.708	0.04
		0.363	3.69	0.725	0.03
		Total Deposition = 0.074 MeV ±0%			

1. FMR is fraction of a mean range.
2. J is energy deposited in MeV/g/cm^2.
3. Estimated experimental uncertainty is 1.6%.

*Estimated one-sigma statistical uncertainty exceeds 3% at larger FMR.

G. Electron Energy Deposition in Tantalum

Energy (MeV):	1.033, 0.521, and 0.314*	1.0, 0.5, and 0.3
Angles (°):	0	0, 30, and 60
Analysis Method:	A	C
Angle Determination Method:	N/A	B
Thermal Coupling Correction Method	B**	A

Continuous Slowing Down Approximation Range

Energy (MeV)	Range (g/cm^2)	Energy (MeV)	Range (g/cm^2)
1.033	7.88×10^{-1}	1.0	7.63×10^{-1}
0.521	3.39×10^{-1}	0.5	3.25×10^{-1}
0.314	1.67×10^{-1}	0.3	1.60×10^{-1}

*Data plotted at nominal energy after adjusting FMR as discussed in introduction of this section.

**Aluminum shield 1.1×10^{-3} g/cm^2.

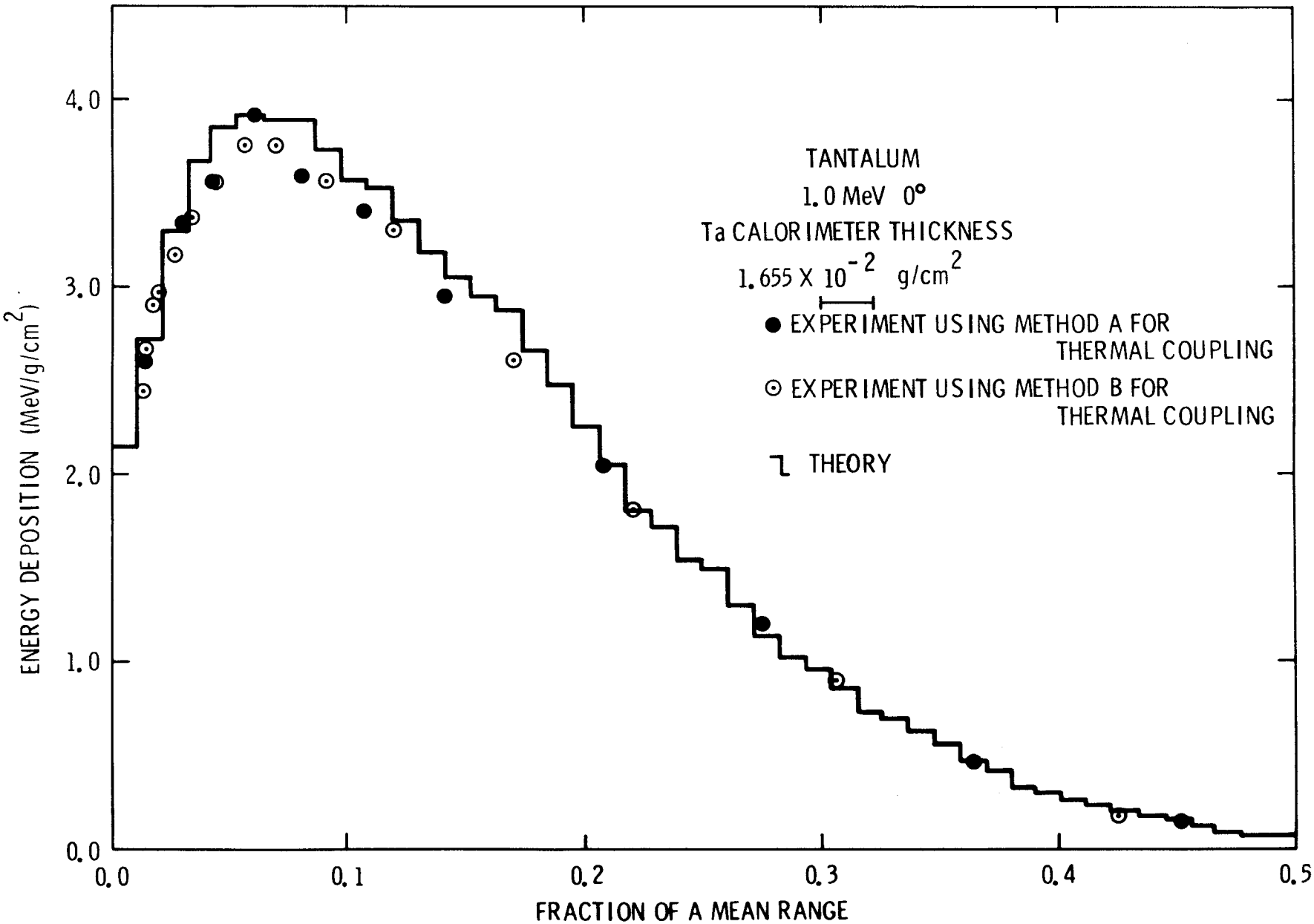

Figure V. G. 1. Comparison of Experimental and Theoretical Energy Deposition Profiles in Semi-Infinite Tantalum for 1.0-MeV Electrons Incident at an Angle of 0°

Table V. G.1

Electron Energy Deposition in Tantalum[1,2,3,4]

Experimental Results

1.0 MeV, 0°, Method A		1.033 MeV, 0°, Method B	
FMR	J	FMR	J
0.015	2.60	0.013	2.44
0.035	3.33	0.015	2.65
0.043	3.55	0.018	2.90
0.061	3.90	0.020	2.95
0.082	3.58	0.027	3.17
0.107	3.41	0.034	3.36
0.142	2.96	0.045	3.56
0.208	2.04	0.057	3.75
0.276	1.20	0.070	3.75
0.364	0.45	0.091	3.56
0.451	0.13	0.120	3.29
Total Deposition = 0.648 MeV		0.170	2.60
		0.221	1.81
		0.305	0.88
		0.426	0.17
		Total Deposition = 0.652 MeV	

Theoretical Results

1.0 MeV, 0°			
FMR	J	FMR	J
0.011	2.15	0.260	1.50
0.022	2.72	0.271*	1.29
0.033	3.31	0.282	1.13
0.043	3.67	0.293	1.02
0.054	3.86	0.304	0.96
0.065	3.91	0.315	0.85
0.076	3.90	0.325	0.72
0.087	3.90	0.336	0.69
0.098	3.73	0.347	0.62
0.108	3.57	0.358	0.55
0.119	3.53	0.369	0.47
0.130	3.35	0.380	0.42
0.141	3.18	0.390	0.32
0.152	3.05	0.401	0.29
0.163	2.96	0.412	0.24
0.174	2.87	0.423	0.23
0.184	2.66	0.434	0.19
0.195	2.47	0.445	0.17
0.206	2.26	0.456	0.16
0.217	2.05	0.466	0.11
0.228	1.81	0.477	0.08
0.239	1.72	0.488	0.08
0.249	1.55	0.499	0.07
Total Deposition = 0.670 MeV ±1%			

1. Experimental results obtained by using both methods (A and B) for thermal coupling correction.
2. FMR is fraction of a mean range.
3. J is energy deposited in MeV/g/cm^2.
4. Estimated experimental uncertainty is 2.2% for Method A and 1.2% for Method B.

*Estimated one-sigma statistical uncertainty exceeds 4% at larger FMR.

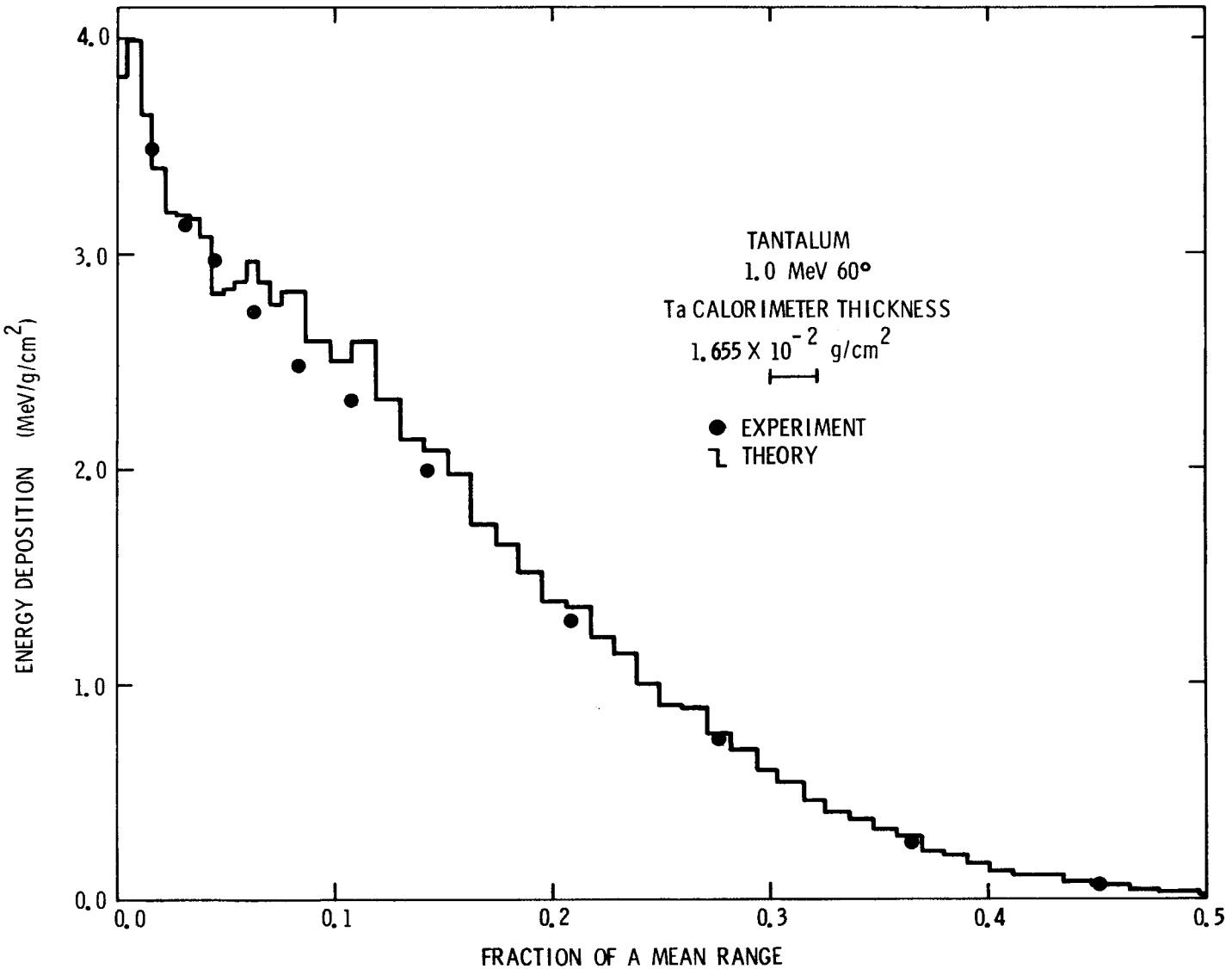

Figure V. G.2. Comparison of Experimental and Theoretical Energy Deposition Profiles in Semi-Infinite Tantalum for 1.0-MeV Electrons Incident at an Angle of 60°

Table V. G.2

Electron Energy Deposition in Tantalum[1, 2, 3, 4]

Experimental Results 1.0 MeV, 60°, Method A		Theoretical Results 1.0 MeV, 60°			
FMR	J	FMR	J	FMR	J
0.015	3.48	0.005	3.81	0.228	1.22
0.030	3.12	0.011	3.99	0.239	1.14
0.043	2.97	0.016	3.65	0.249	1.00
0.061	2.72	0.022	3.39	0.260	0.91
0.082	2.47	0.027	3.19	0.271	0.89
0.107	2.32	0.033	3.18	0.282*	0.77
0.142	1.99	0.038	3.17	0.293	0.69
0.208	1.29	0.043	3.08	0.304	0.60
0.276	0.74	0.049	2.81	0.315	0.54
0.364	0.26	0.054	2.83	0.325	0.48
0.451	0.07	0.060	2.87	0.336	0.40
		0.065	2.97	0.347	0.37
Total Deposition = 0.472 MeV		0.070	2.86	0.358	0.32
		0.076	2.76	0.369	0.29
		0.087	2.82	0.380	0.22
		0.098	2.59	0.390	0.20
		0.108	2.50	0.401	0.17
		0.119	2.59	0.412	0.12
		0.130	2.32	0.423	0.11
		0.141	2.14	0.434	0.11
		0.152	2.09	0.445	0.08
		0.163	1.98	0.456	0.07
		0.174	1.75	0.466	0.07
		0.184	1.65	0.477	0.05
		0.195	1.52	0.488	0.04
		0.206	1.38	0.499	0.04
		0.217	1.36	0.510	0.02

Total Deposition = 0.495 MeV ±1%

1. Experimental results obtained by using Method A for thermal coupling correction.
2. FMR is fraction of a mean range.
3. J is energy deposited in $MeV/g/cm^2$.
4. Estimated experimental uncertainty is 2.2% for Method A.

*Estimated one-sigma statistical uncertainty exceeds 4% at larger FMR

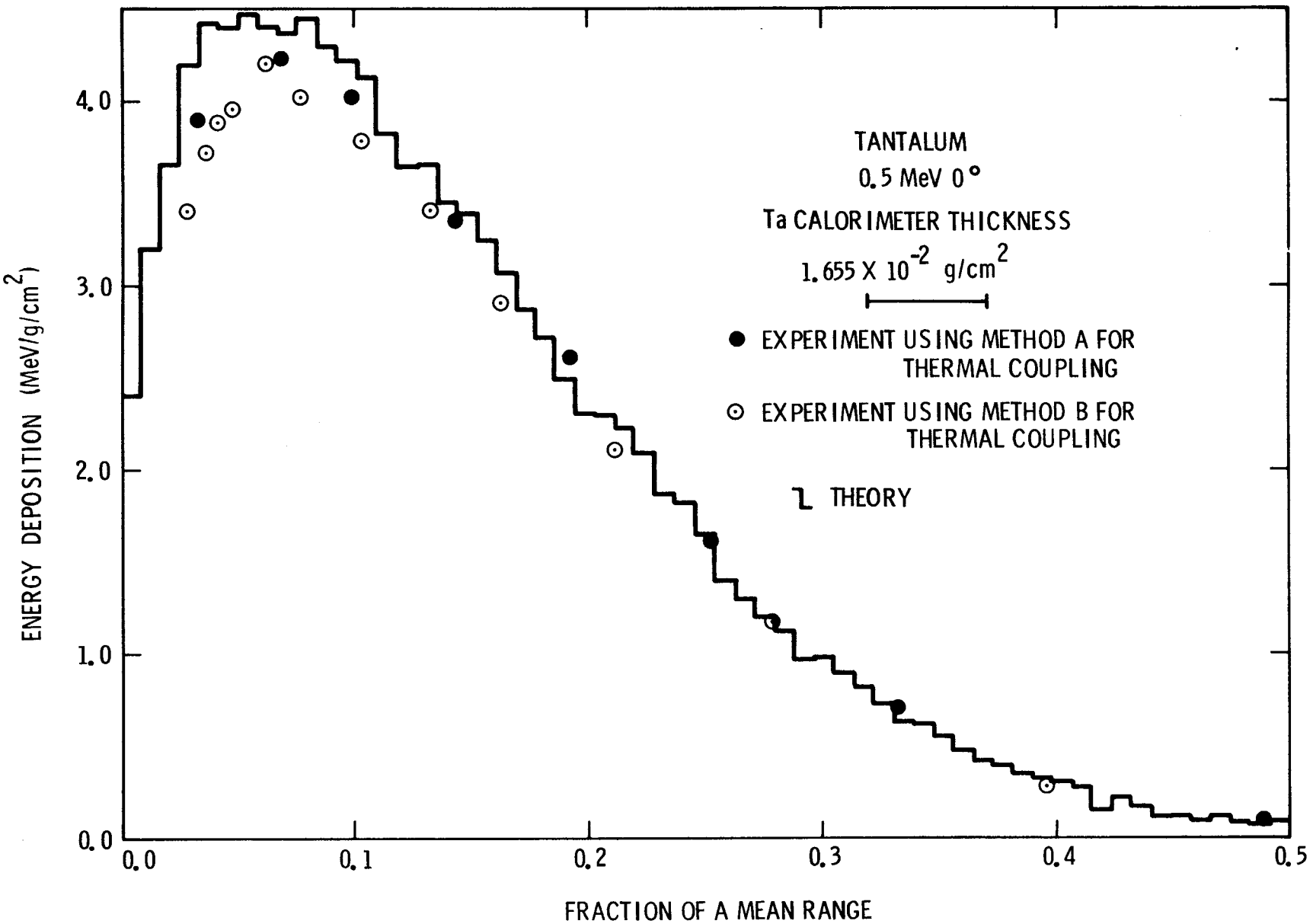

Figure V. G. 3. Comparison of Experimental and Theoretical Energy Deposition Profiles in Semi-Infinite Tantalum for 0.5-MeV Electrons Incident at an Angle of 0°

Table V. G.3

Electron Energy Deposition in Tantalum[1, 2, 3, 4]

Experimental Results
0.5 MeV, 0°, Method A

FMR	J
0.034	3.90
0.070	4.23
0.100	4.02
0.144	3.35
0.193	2.61
0.253	1.61
0.333	0.71
0.489	0.10

Total Deposition = 0.316 MeV

0.521 MeV, 0°, Method B

FMR	J
0.029	3.40
0.037	3.72
0.042	3.88
0.048	3.95
0.063	4.20
0.078	4.02
0.104	3.78
0.133	3.40
0.163	2.89
0.212	2.10
0.279	1.17
0.396	0.27
0.577	0.0
0.710	0.0

Total Deposition = 0.305 MeV

Theoretical Results
0.5 MeV, 0°

FMR	J	FMR	J
0.008	2.41	0.263	1.39
0.017	3.20	0.271	1.30
0.025	3.66	0.280	1.20
0.034	4.19	0.288	1.13
0.042	4.42	0.297	0.97
0.051	4.40	0.305	0.97
0.059	4.47	0.314	0.90
0.068	4.41	0.322	0.82
0.076	4.37	0.331	0.73
0.085	4.45	0.339	0.63
0.093	4.30	0.348	0.62
0.102	4.22	0.356	0.56
0.110	4.13	0.365	0.47
0.119	3.83	0.373	0.42
0.127	3.65	0.381	0.40
0.136	3.66	0.390	0.35
0.144	3.45	0.398	0.32
0.153	3.39	0.407	0.32
0.161*	3.25	0.415	0.27
0.170	3.07	0.424	0.15
0.178	2.87	0.432	0.19
0.186	2.72	0.441	0.17
0.195	2.49	0.449	0.11
0.203	2.31	0.458	0.12
0.212	2.30	0.466	0.09
0.220	2.23	0.475	0.12
0.229	2.09	0.483	0.08
0.237	1.87	0.492	0.07
0.246	1.82	0.500	0.09
0.254	1.65		

Total Deposition = 0.317 MeV ±1%

1. Experimental results obtained by using both methods (A and B) for thermal coupling correction.
2. FMR is fraction of a mean range.
3. J is energy deposited in MeV/g/cm^2.
4. Estimated experimental uncertainty is 2.2% for Method A and 1.2% for Method B.

*Estimated [illegible] uncertainty exceeds 4% at [illegible] FMR

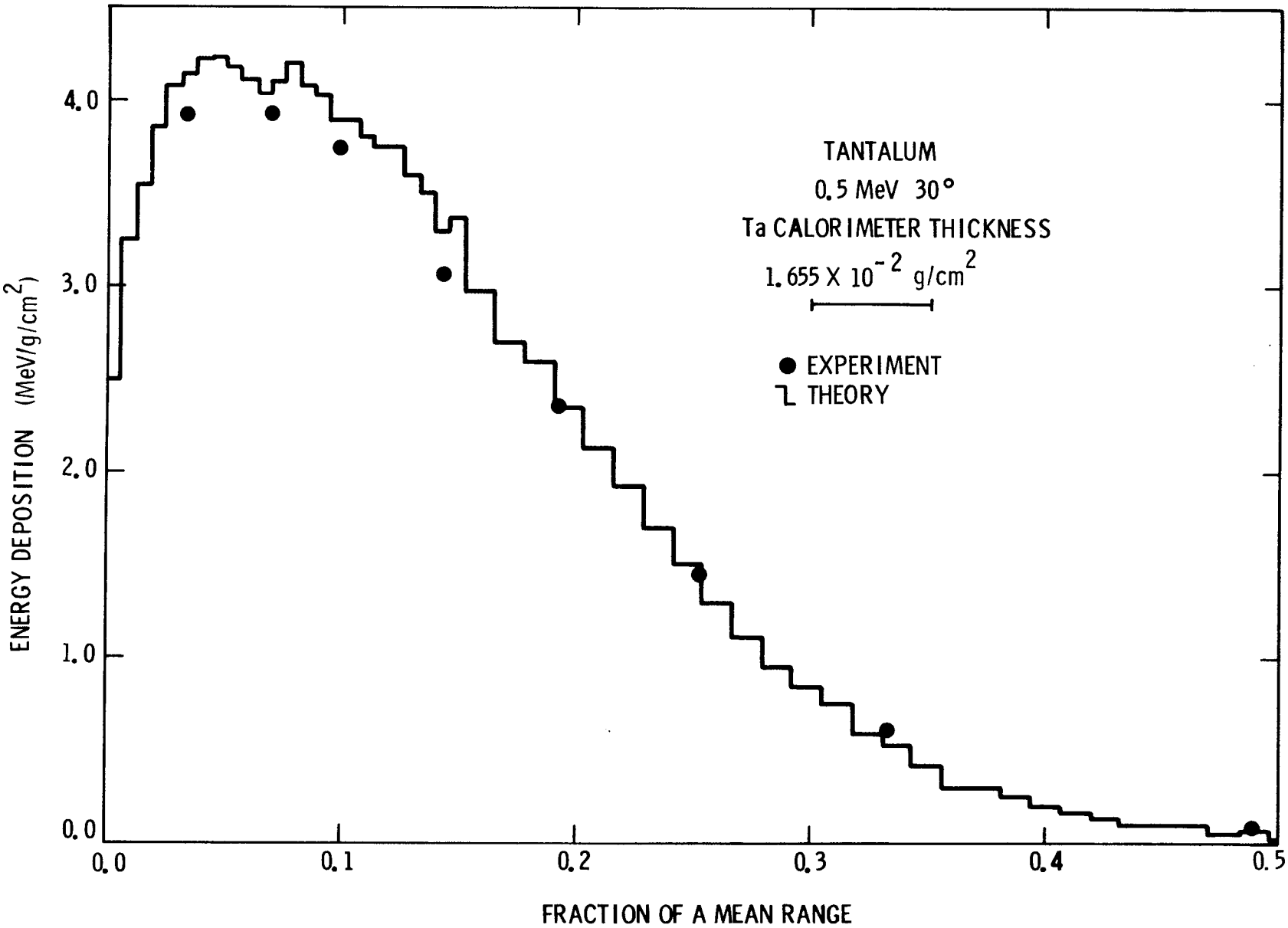

Figure V. G.4. Comparison of Experimental and Theoretical Energy Deposition Profiles in Semi-Infinite Tantalum for 0.5-MeV Electrons Incident at an Angle of 30°

Table V. G. 4

Electron Energy Deposition in Tantalum[1, 2, 3, 4]

Experimental Results
0.5 MeV, 30°, Method A

FMR	J
0.034	3.92
0.070	3.93
0.100	3.74
0.144	3.07
0.193	2.36
0.253	1.45
0.333	0.62
0.489	0.09

Total Deposition = 0.295 MeV

Theoretical Results
0.5 MeV, 30°

FMR	J	FMR	J
0.006	2.49	0.191	2.59
0.013	3.25	0.203	2.34
0.019	3.54	0.216*	2.13
0.025	3.86	0.229	1.92
0.032	4.08	0.242	1.70
0.038	4.14	0.254	1.51
0.045	4.22	0.267	1.29
0.051	4.23	0.280	1.11
0.057	4.18	0.292	0.95
0.064	4.11	0.305	0.84
0.070	4.03	0.318	0.75
0.076	4.10	0.331	0.59
0.083	4.20	0.343	0.53
0.089	4.08	0.356	0.42
0.095	4.03	0.369	0.30
0.102	3.89	0.381	0.30
0.108	3.89	0.394	0.25
0.114	3.81	0.407	0.21
0.121	3.75	0.420	0.17
0.127	3.75	0.432	0.14
0.134	3.60	0.445	0.10
0.140	3.51	0.458	0.10
0.146	3.29	0.470	0.10
0.153	3.37	0.483	0.06
0.165	2.97	0.496	0.08
0.178	2.70	0.509	0.03

Total Deposition = 0.298 MeV ±1%

1. Experimental results obtained by using Method A for thermal coupling correction.
2. FMR is fraction of a mean range.
3. J is energy deposited in MeV/g/cm^2.
4. Estimated experimental uncertainty is 2.2% for Method A.

*Estimated one-sigma statistical uncertainty exceeds 3% at larger FMR.

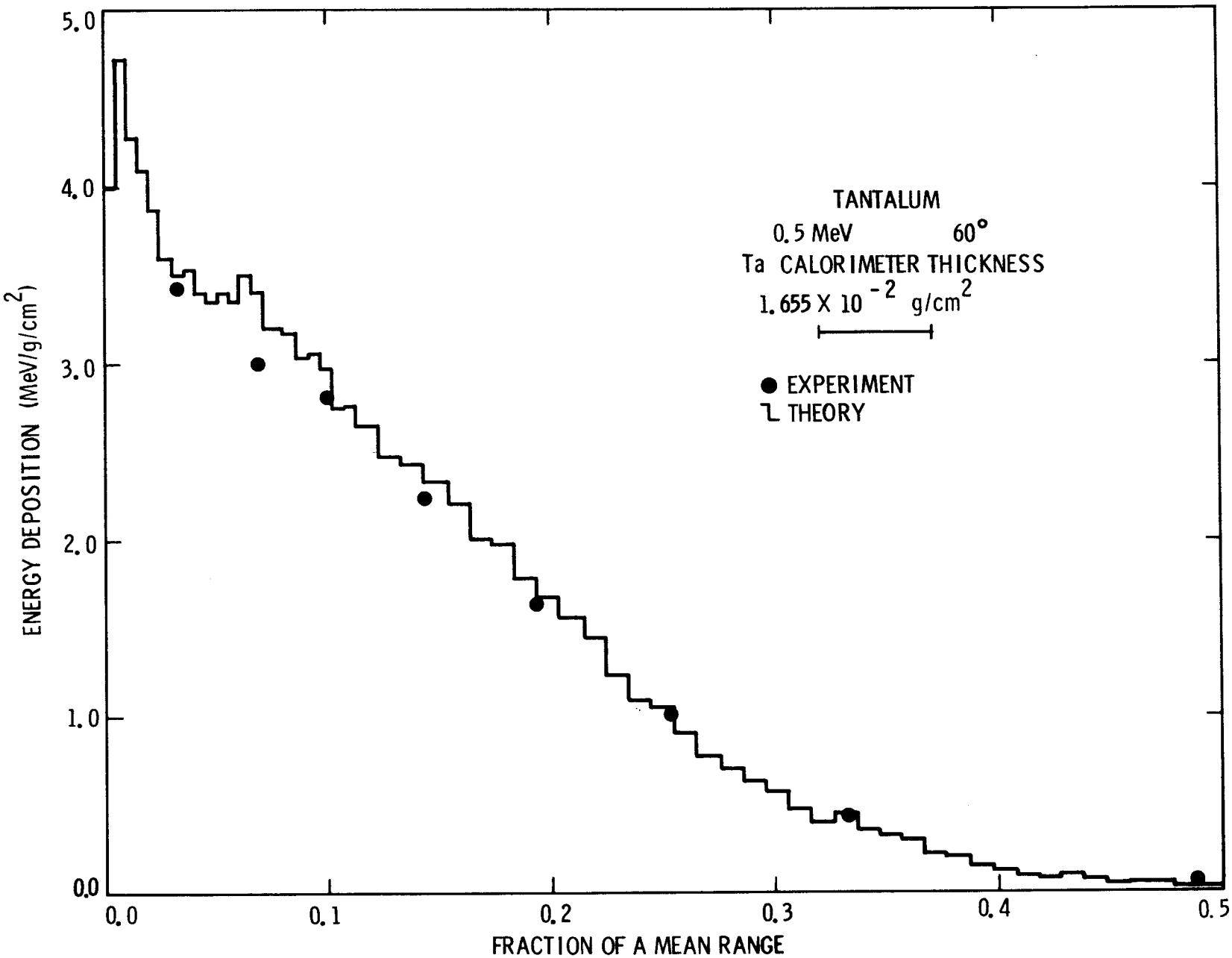

Figure V. G. 5. Comparison of Experimental and Theoretical Energy Deposition Profiles in Semi-Infinite Tantalum for 0.5-MeV Electrons Incident at an Angle of 60°

Table V. G. 5

Electron Energy Deposition in Tantalum[1, 2, 3, 4]

Experimental Results 0.5 MeV, 60°, Method A	
FMR	J
0.034	3.42
0.070	2.99
0.100	2.80
0.144	2.23
0.193	1.63
0.253	1.01
0.333	0.43
0.489	0.07

Total Deposition = 0.227 MeV

Theoretical Results 0.5 MeV, 60°			
FMR	J	FMR	J
0.005	4.00	0.214	1.56
0.010	4.72	0.224	1.44
0.015	4.28	0.234	1.23
0.020	4.09	0.244	1.09
0.025	3.87	0.254	1.05
0.031	3.59	0.264	0.91
0.036	3.49	0.275	0.77
0.041	3.53	0.285	0.71
0.046	3.39	0.295	0.63
0.051	3.34	0.305	0.57
0.056	3.39	0.315	0.47
0.061	3.36	0.326	0.39
0.066	3.50	0.336	0.45
0.071	3.41	0.346	0.36
0.076	3.20	0.356	0.32
0.081	3.19	0.366	0.29
0.086	3.17	0.376	0.22
0.092	3.03	0.387	0.21
0.097	3.06	0.397	0.15
0.102	2.97	0.407	0.12
0.107	2.74	0.417	0.09
0.112	2.76	0.427	0.08
0.122	2.64	0.437	0.10
0.132	2.47	0.448	0.07
0.142	2.43	0.458	0.04
0.153	2.33	0.468	0.06
0.163	2.21	0.478	0.06
0.173*	2.00	0.488	0.03
0.183	1.97	0.498	0.03
0.193	1.78	0.509	0.03
0.203	1.67		

Total Deposition = 0.235 MeV ±1%

1. Experimental results obtained by using Method A thermal coupling correction.
2. FMR is fraction of a mean range.
3. J is energy deposited in $MeV/g/cm^2$.
4. Estimated experimental uncertainty is 2.2% for Method A.

*Estimated one-sigma statistical uncertainty exceeds 4% at larger FMR.

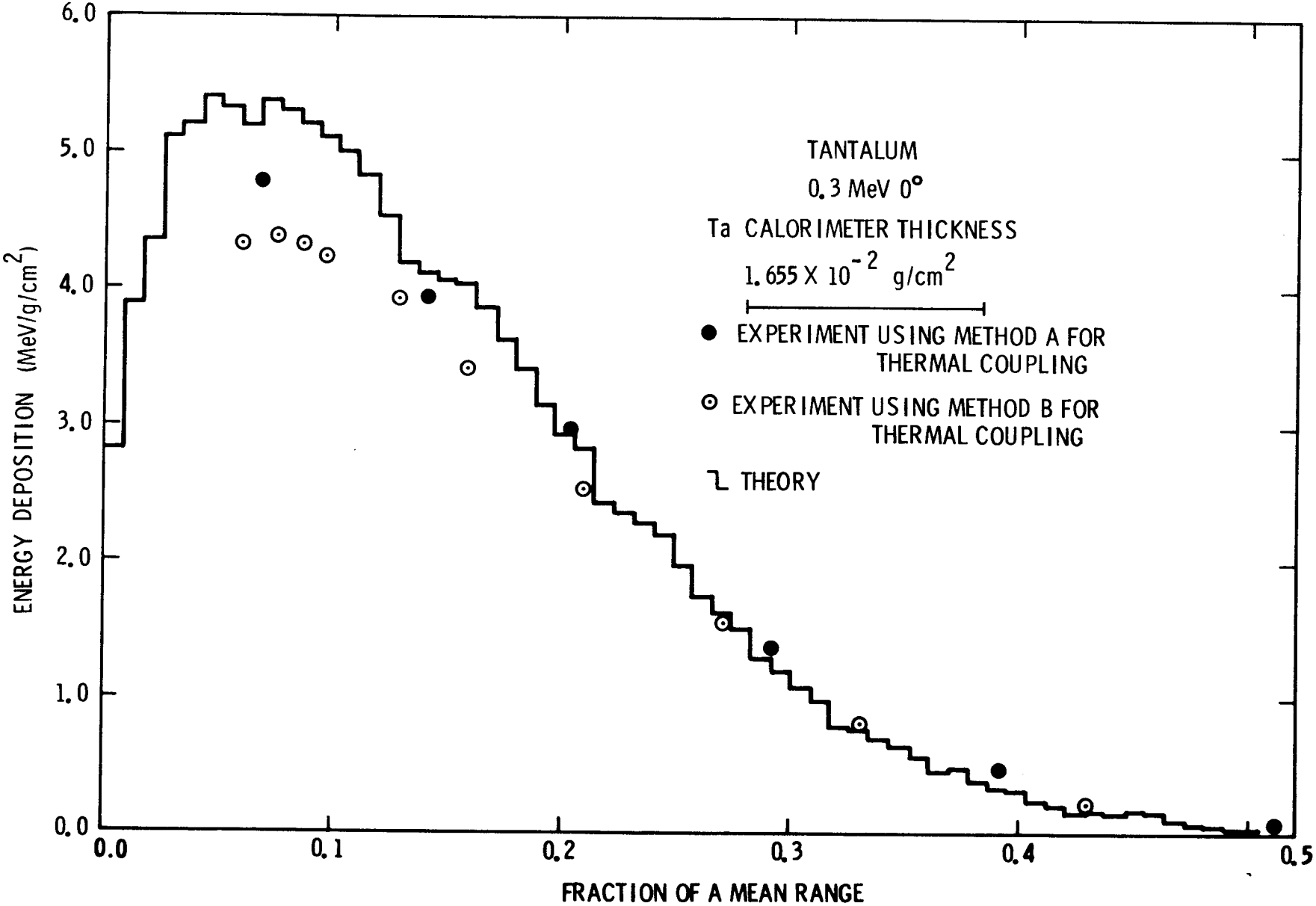

Figure V. G.6. Comparison of Experimental and Theoretical Energy Deposition Profiles in Semi-Infinite Tantalum for 0.3-MeV Electrons Incident at an Angle of 0°

Table V. G.6

Electron Energy Deposition in Tantalum[1, 2, 3, 4]

Experimental Results

0.3 MeV, 0°, Method A

FMR	J
0.069	4.78
0.142	3.94
0.204	2.97
0.292	1.37
0.392	0.48
0.511	0.08

Total Deposition = 0.184 MeV

0.314 MeV, 0°, Method B

FMR	J
0.060	4.32
0.076	4.38
0.087	4.32
0.097	4.23
0.129	3.92
0.159	3.41
0.210	2.52
0.271	1.54
0.331	0.82
0.429	0.22
0.566	0.02

Total Deposition = 0.177 MeV

Theoretical Results

0.3 MeV, 0°

FMR	J	FMR	J
0.009	2.82	0.266	1.74
0.017	3.89	0.274	1.63
0.026	4.35	0.283	1.51
0.034	5.11	0.292	1.28
0.043	5.21	0.300	1.20
0.051	5.41	0.309	1.08
0.060	5.32	0.317	0.98
0.069	5.19	0.326	0.79
0.077	5.37	0.334	0.76
0.086	5.29	0.343	0.70
0.094	5.21	0.352	0.65
0.103	5.12	0.360	0.57
0.111	5.00	0.369	0.46
0.120	4.82	0.377	0.48
0.129	4.52	0.386	0.39
0.137	4.18	0.394	0.34
0.146	4.14	0.403	0.33
0.154	4.06	0.412	0.25
0.163	4.03	0.420	0.21
0.172	3.85	0.429	0.16
0.180	3.62	0.437	0.17
0.189	3.41	0.446	0.15
0.197	3.14	0.454	0.17
0.206	2.92	0.463	0.16
0.214*	2.82	0.472	0.10
0.223	2.42	0.480	0.08
0.232	2.38	0.489	0.07
0.240	2.28	0.497	0.04
0.249	2.19	0.506	0.04
0.257	1.97		

Total Deposition = 0.189 MeV ±1%

1. Experimental results obtained by using both methods (A and B) for thermal coupling correction.
2. FMR is fraction of a mean range.
3. J is energy deposited in $MeV/g/cm^2$.
4. Estimated experimental uncertainty is 2.2% for Method A and 1.2% for Method B.

* Estimated one-sigma statistical uncertainty exceeds 4% of larger FMR.

H. Electron Energy Deposition in Uranium

Energies (MeV): 1.0, 0.5, and 0.3

Angles (°): 0 and 60

Analysis Method: C

Angle Determination Method: B

Thermal Coupling Correction Method: B

Continuous Slowing Down Approximation Range

Energy (MeV)	Range (g/cm^2)
1.0	8.09×10^{-1}
0.5	3.49×10^{-1}
0.3	1.74×10^{-1}

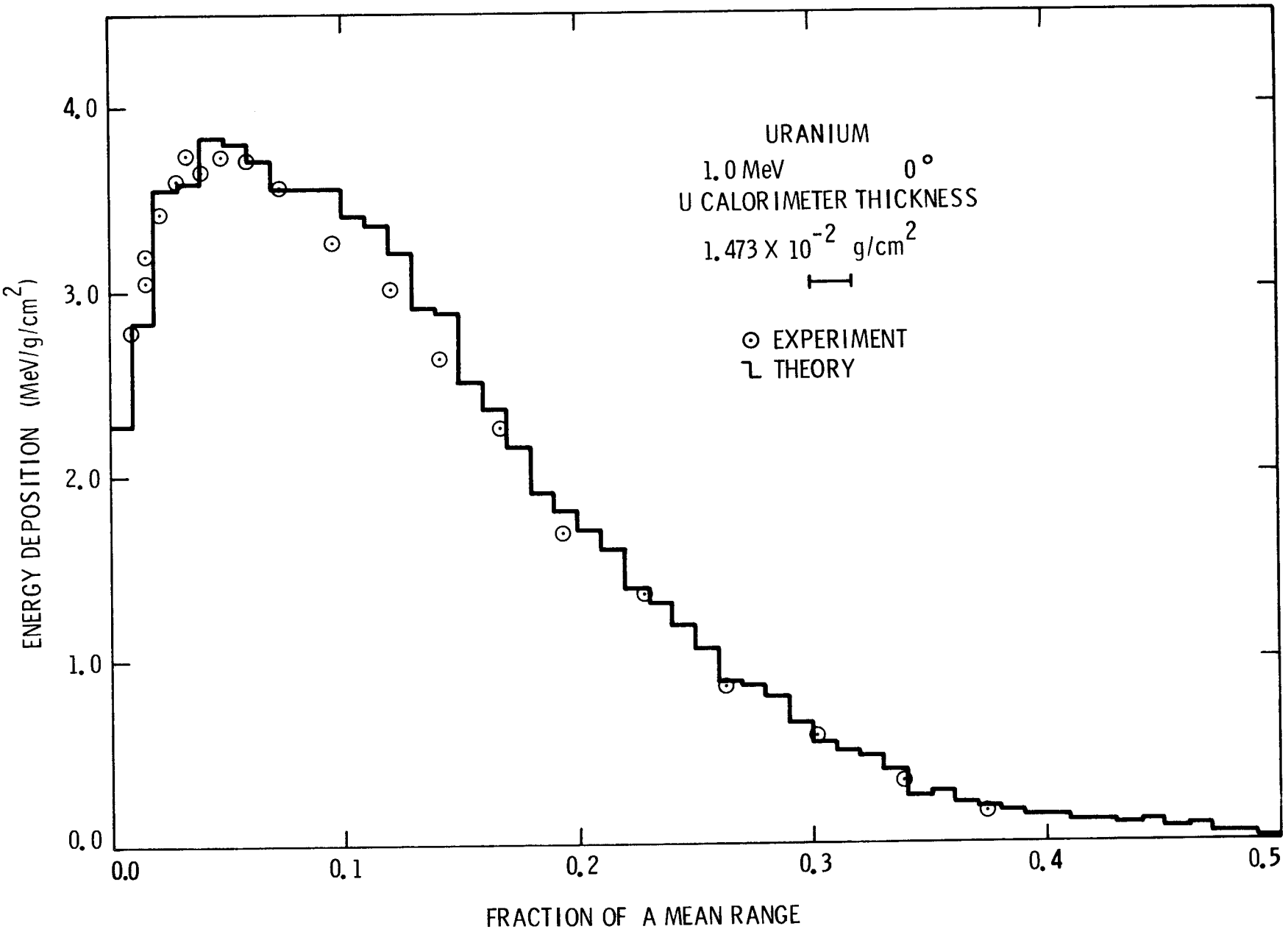

Figure V. H. 1. Comparison of Experimental and Theoretical Energy Deposition Profiles in Semi-Infinite Uranium for 1.0-MeV Electrons Incident at an Angle of 0°

Table V. H.1

Electron Energy Deposition in Uranium[1,2,3]

Experimental Results 1.0 MeV, 0°		Theoretical Results 1.0 MeV, 0°			
FMR	J	FMR	J	FMR	J
0.010	2.77	0.01	2.27	0.26	1.06
0.016	3.05	0.02	2.83	0.27	0.87
0.017	3.20	0.03	3.55	0.28	0.85
0.023	3.43	0.04	3.58	0.29	0.79
0.029	3.59	0.05	3.83	0.30	0.65
0.034	3.75	0.06	3.79	0.31	0.54
0.040	3.65	0.07	3.71	0.32	0.49
0.049	3.72	0.08	3.56	0.33	0.47
0.061	3.69	0.09	3.56	0.34	0.39
0.074	3.56	0.10	3.56	0.35	0.26
0.096	3.26	0.11	3.41	0.36	0.28
0.120	3.00	0.12	3.34	0.37	0.22
0.142	2.63	0.13	3.20	0.38	0.19
0.167	2.25	0.14	2.91	0.39	0.17
0.194	1.68	0.15	2.87	0.40	0.15
0.228	1.36	0.16	2.50	0.41	0.14
0.264	0.85	0.17*	2.36	0.42	0.12
0.303	0.58	0.18	2.14	0.43	0.12
0.338	0.32	0.19	1.90	0.44	0.10
0.374	0.15	0.20	1.81	0.45	0.12
		0.21	1.61	0.46	0.08
Total Deposition =		0.22	1.59	0.47	0.09
0.584 MeV		0.23	1.38	0.48	0.05
		0.24	1.30	0.49	0.05
		0.25	1.18	0.50	0.03

Total Deposition = 0.615 MeV ±1%

1. FMR is fraction of a mean range.
2. J is energy deposited in MeV/g/cm^2.
3. Estimated experimental uncertainty is 1.4%.

*Estimated one-sigma statistical uncertainty exceeds 4% at larger FMR.

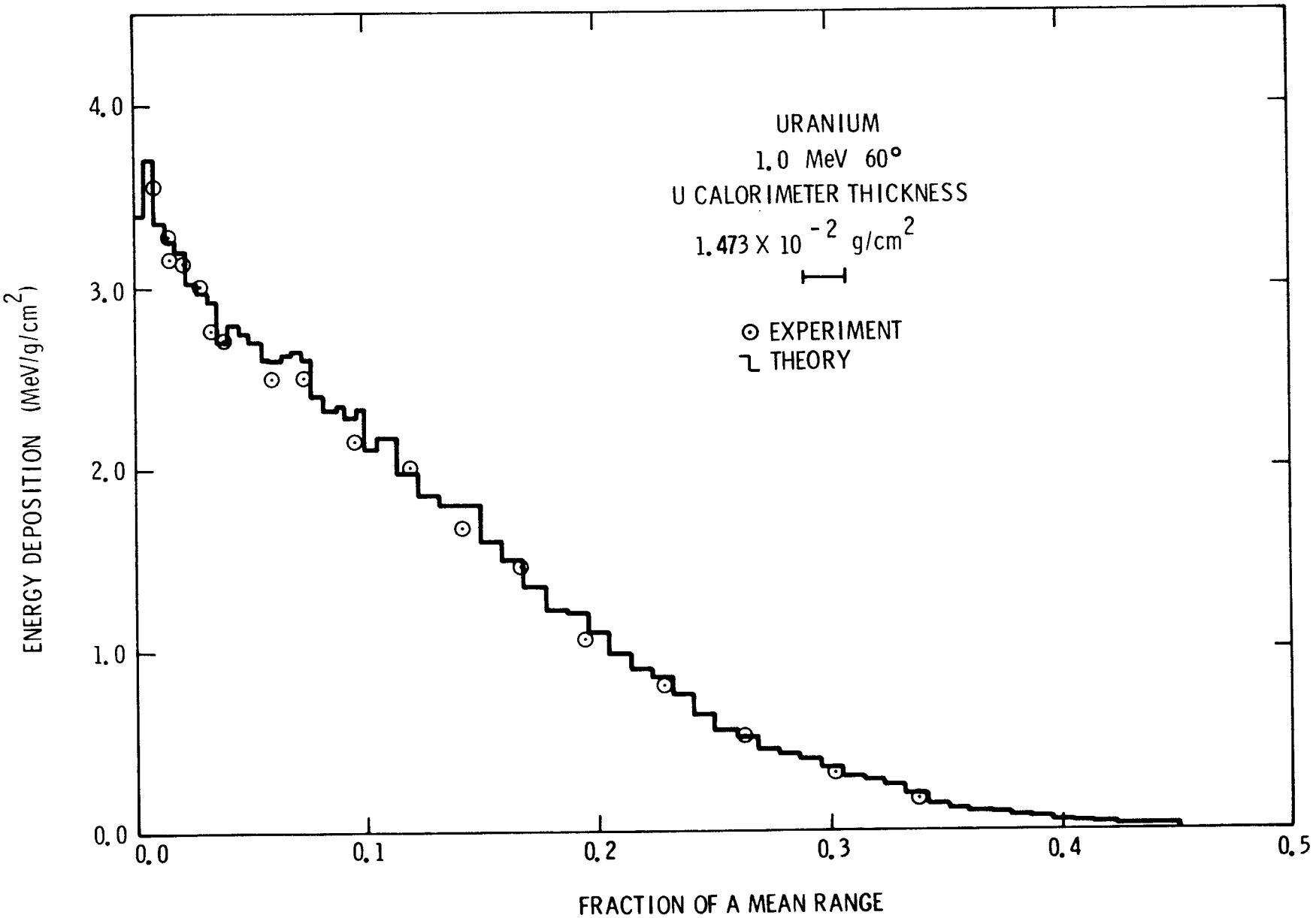

Figure V. H. 2. Comparison of Experimental and Theoretical Energy Deposition Profiles in Semi-Infinite Uranium for 1.0-MeV Electrons Incident at an Angle of 60°

Table V. H.2

Electron Energy Deposition in Uranium[1,2,3]

Experimental Results 1.0 MeV, 60°		Theoretical Results 1.0 MeV, 60°			
FMR	J	FMR	J	FMR	J
0.010	3.56	0.005	3.39	0.187	1.22
0.016	3.16	0.009	3.71	0.196	1.19
0.017	3.28	0.014	3.36	0.205	1.09
0.023	3.12	0.018	3.26	0.214	0.98
0.029	3.01	0.023	3.19	0.223	0.89
0.034	2.76	0.027	3.02	0.232	0.85
0.040	2.71	0.032	2.97	0.241	0.76
0.061	2.49	0.036	2.92	0.250	0.64
0.074	2.49	0.041	2.69	0.260	0.56
0.096	2.14	0.046	2.79	0.269	0.52
0.120	2.00	0.050	2.74	0.278	0.45
0.142	1.67	0.055	2.70	0.287	0.42
0.167	1.45	0.059	2.60	0.296	0.39
0.194	1.05	0.064	2.59	0.305	0.35
0.228	0.80	0.068	2.63	0.314	0.29
0.264	0.53	0.073	2.64	0.323	0.28
0.303	0.32	0.077	2.61	0.332	0.26
0.338	0.17	0.082*	2.39	0.342	0.21
		0.087	2.32	0.351	0.14
Total Deposition =		0.091	2.34	0.360	0.12
0.413 MeV		0.096	2.28	0.369	0.11
		0.100	2.33	0.378	0.10
		0.105	2.11	0.387	0.08
		0.114	2.17	0.396	0.07
		0.123	1.97	0.405	0.06
		0.132	1.85	0.414	0.05
		0.141	1.79	0.424	0.04
		0.150	1.79	0.433	0.03
		0.159	1.59	0.442	0.03
		0.168	1.49	0.451	0.03
		0.178	1.35		

Total Deposition = 0.427 MeV ±1%

1. FMR is fraction of a mean range.
2. J is energy deposited in MeV/g/cm^2.
3. Estimated experimental uncertainty is 1.4%.

*Estimated one-sigma statistical uncertainty exceeds 4% at larger FMR

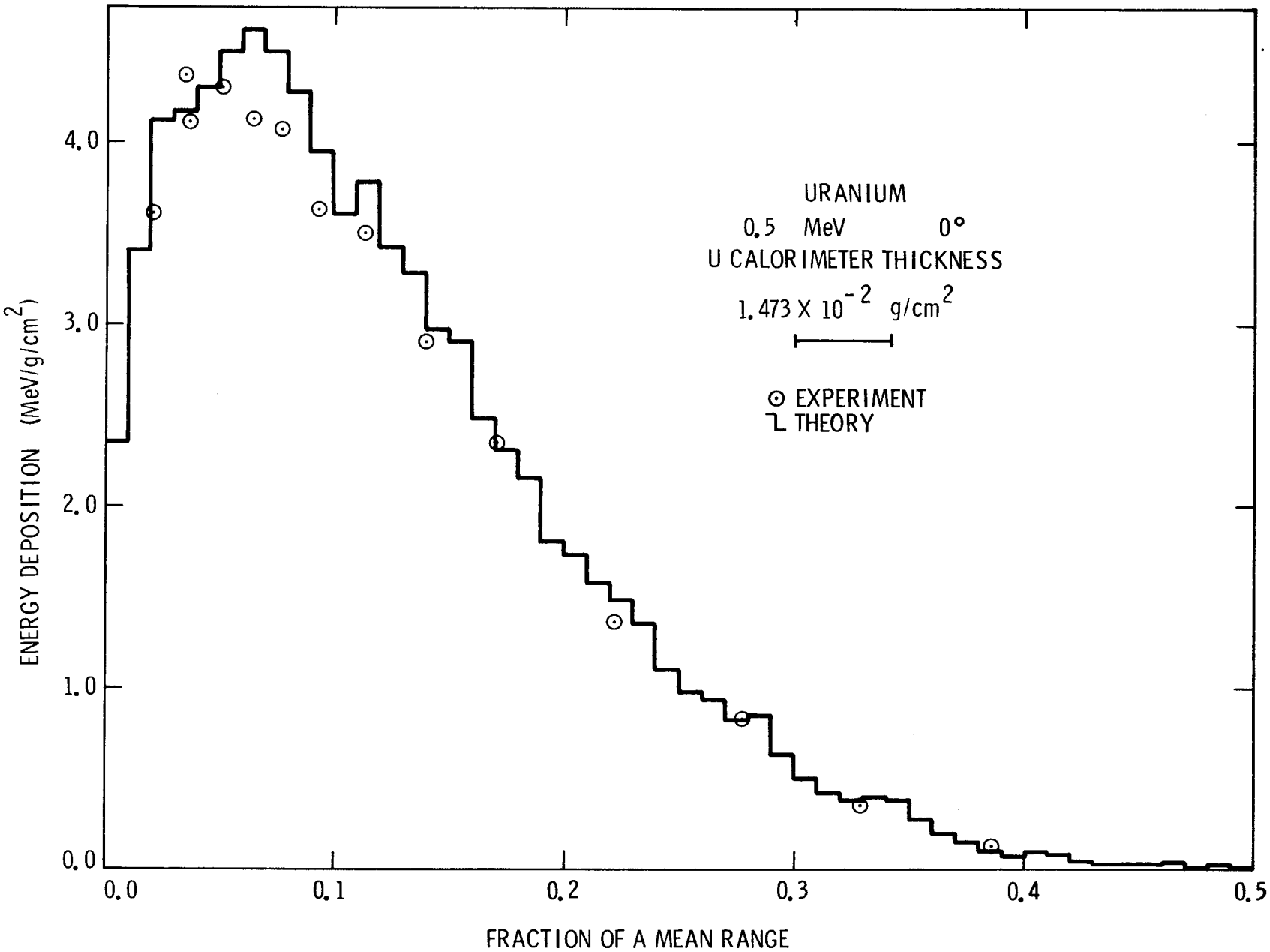

Figure V. H. 3. Comparison of Experimental and Theoretical Energy Deposition Profiles in Semi-Infinite Uranium for 0.5-MeV Electrons Incident at an Angle of 0°

Table V. H. 3

Electron Energy Deposition in Uranium[1, 2, 3]

Experimental Results 0.5 MeV, 0°		Theoretical Results 0.5 MeV, 0°			
FMR	J	FMR	J	FMR	J
0.022	3.61	0.01	2.35	0.26	0.97
0.037	4.37	0.02	3.41	0.27	0.93
0.038	4.09	0.03	4.12	0.28	0.82
0.053	4.31	0.04	4.17	0.29	0.84
0.067	4.13	0.05	4.30	0.30	0.63
0.079	4.07	0.06	4.49	0.31	0.50
0.094	3.63	0.07	4.62	0.32	0.42
0.115	3.49	0.08	4.50	0.33	0.38
0.141	2.89	0.09	4.27	0.34	0.39
0.172	2.35	0.10	3.94	0.35	0.38
0.223	1.35	0.11	3.61	0.36	0.27
0.278	0.83	0.12	3.78	0.37	0.19
0.330	0.35	0.13	3.42	0.38	0.15
0.387	0.13	0.14	3.28	0.39	0.09
		0.15	2.97	0.40	0.07
Total Deposition =		0.16	2.91	0.41	0.09
0.277 MeV		0.17*	2.48	0.42	0.08
		0.18	2.31	0.43	0.04
		0.19	2.16	0.44	0.03
		0.20	1.80	0.45	0.03
		0.21	1.73	0.46	0.03
		0.22	1.58	0.47	0.04
		0.23	1.48	0.48	0.02
		0.24	1.36	0.49	0.03
		0.25	1.10	0.50	0.02

Total Deposition = 0.291 MeV ±1%

1. FMR is fraction of a mean range.
2. J is energy deposited in MeV/g/cm^2.
3. Estimated experimental uncertainty is 1.4%.

*Estimated one-sigma statistical uncertainty exceeds 5% at larger FMR.

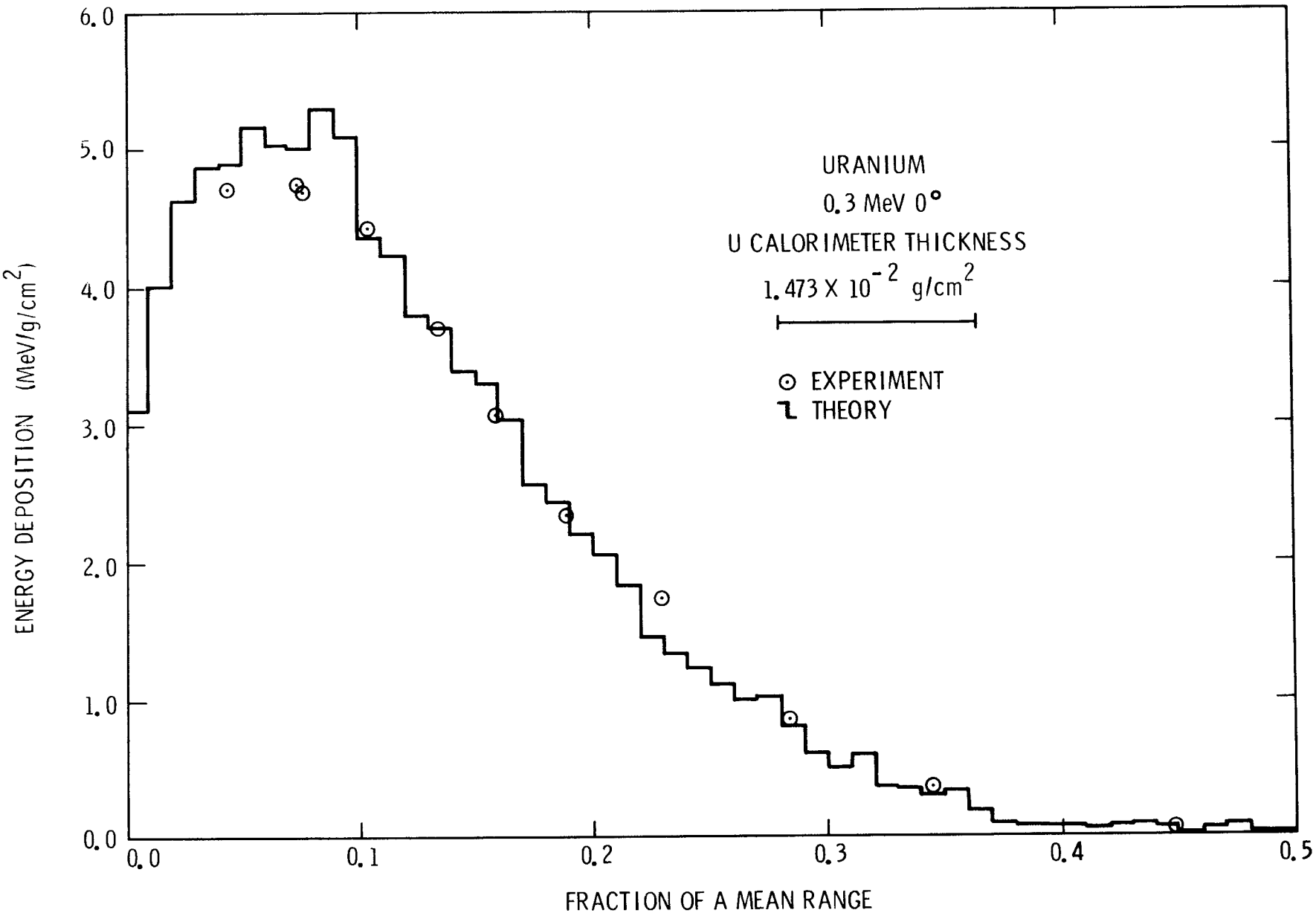

Figure V. H.4. Comparison of Experimental and Theoretical Energy Deposition Profiles in Semi-Infinite Uranium for 0.3-MeV Electrons Incident at an Angle of 0°

Table V. H.4

Electron Energy Deposition in Uranium[1,2,3]

Experimental Results 0.3 MeV, 0°		Theoretical Results 0.3 MeV, 0°			
FMR	J	FMR	J	FMR	J
0.044	4.69	0.01	3.11	0.26	1.11
0.075	4.73	0.02	4.01	0.27	0.99
0.077	4.67	0.03	4.63	0.28	1.01
0.105	4.42	0.04	4.87	0.29	0.80
0.135	3.68	0.05	4.89	0.30	0.60
0.159	3.04	0.06	5.16	0.31	0.51
0.189	2.33	0.07	5.03	0.32	0.59
0.230	1.72	0.08	5.01	0.33	0.36
0.284	0.84	0.09	5.29	0.34	0.36
0.345	0.35	0.10	5.08	0.35	0.29
0.448	0.04	0.11	4.35	0.36	0.33
		0.12	4.22	0.37	0.18
Total Deposition =		0.13	3.78	0.38	0.09
0.165 MeV		0.14*	3.70	0.39	0.08
		0.15	3.38	0.40	0.08
		0.16	3.29	0.41	0.07
		0.17	3.02	0.42	0.05
		0.18	2.56	0.43	0.08
		0.19	2.42	0.44	0.08
		0.20	2.20	0.45	0.07
		0.21	2.05	0.46	0.02
		0.22	1.82	0.47	0.05
		0.23	1.44	0.48	0.07
		0.24	1.33	0.49	0.02
		0.25	1.22	0.50	0.01

Total Deposition = 0.166 MeV ±2%

1. FMR is fraction of mean range.
2. J is energy deposited in MeV/g/cm^2.
3. Estimated experimental uncertainty is 1.4%.

*Estimated one-sigma statistical uncertainty exceeds 5% at larger FMR.

I. Electron Energy Deposition in Beryllium/Gold/Beryllium

Energies (MeV):	1.0
Angles (°):	0
Analysis Method:	C
Angle Determination Method:	N/A
Thermal Coupling Correction Method:	Beryllium (A), Gold none required

Continuous Slowing Down Approximation Range

Energy (MeV)	Range (g/cm^2)
1.0	5.36×10^{-1} (Be)
	7.72×10^{-1} (Au)

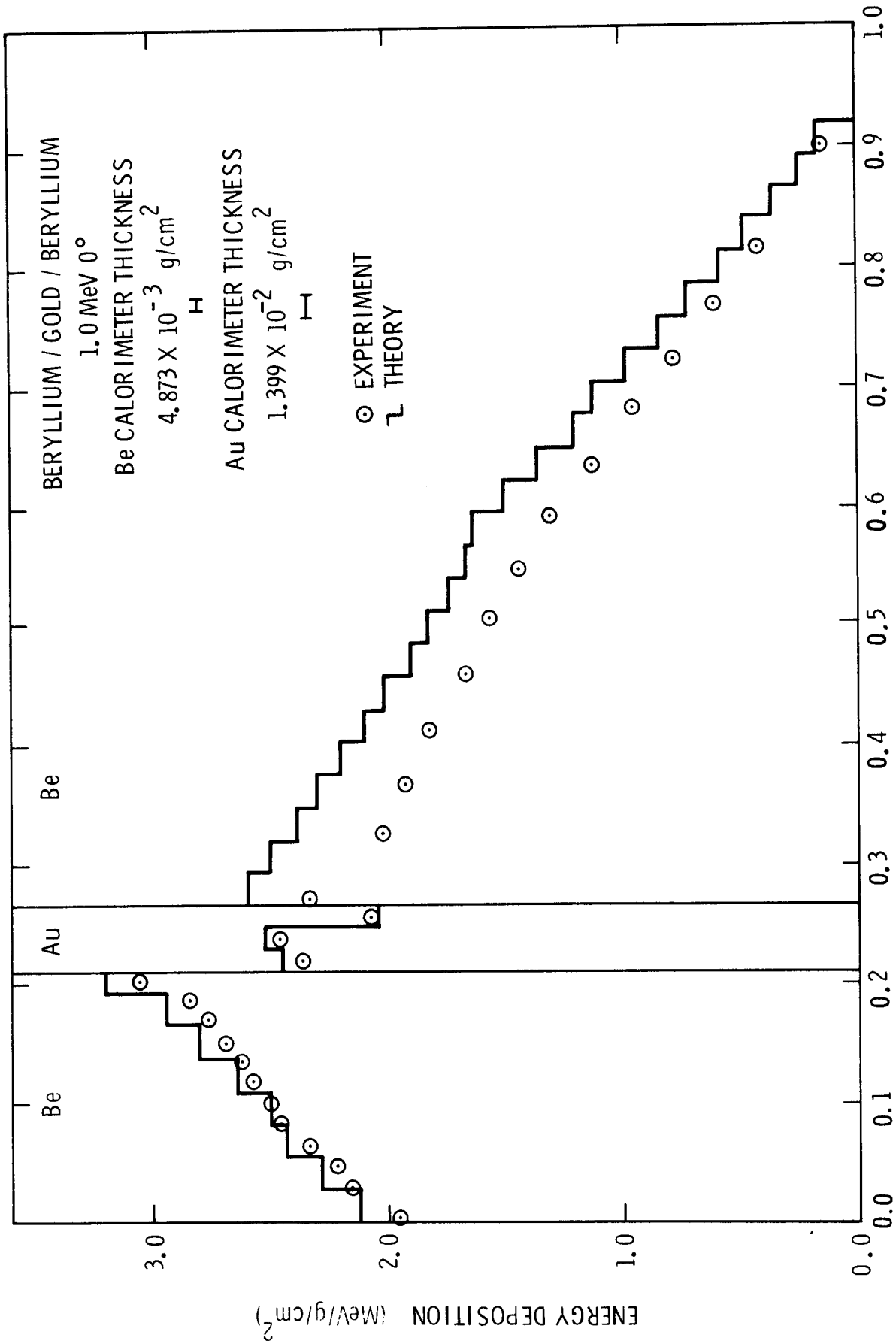

Figure V. I.1. Comparison of Experimental and Theoretical Energy Deposition Profiles in a Beryllium/Gold/Beryllium Configuration for 1.0-MeV Electrons Incident at an Angle of 0°

Table V. I.1

Electron Energy Deposition in Beryllium/Gold/Beryllium[1,2,3]

Experimental Results
1.0 MeV, 0°

FMR	J
In Be	
0.005	1.94
0.030	2.15
0.048	2.22
0.066	2.33
0.086	2.45
0.103	2.50
0.121	2.57
0.138	2.62
0.155	2.69
0.174	2.76
0.191	2.84
0.207	3.04
In Au	
0.220	2.44
0.239	2.57
0.257	2.08
In Be	
0.272	2.33
0.327	2.02
0.369	1.92
0.415	1.82
0.463	1.66
0.510	1.56
0.552	1.44
0.598	1.30
0.641	1.12
0.688	0.95
0.730	0.77
0.776	0.60
0.823	0.42
0.910	0.15

Theoretical Results
1.0 MeV, 0°

FMR	J
In Be	
0.027	2.12
0.054	2.28
0.082	2.43
0.111	2.50
0.138	2.64
0.166	2.80
0.193	2.94
0.211	3.19
In Au	
0.229	2.45
0.248	2.52
0.266	2.03
In Be	
0.293	2.59
0.321	2.47
0.348	2.38
0.375	2.29
0.403	2.19

FMR	J
In Be cont	
0.430	2.09
0.457	2.01
0.484	1.89
0.512	1.82
0.539	1.73
0.566	1.66
0.594	1.63
0.621	1.50
0.648	1.35
0.675	1.20
0.703	1.12
0.730	0.98
0.757	0.84
0.784*	0.72
0.812	0.58
0.839	0.48
0.866	0.36
0.893	0.25
0.921	0.17

Total Deposition = 0.894 MeV ±0%

1. FMR is fraction of a mean range.
2. J is energy deposited in MeV/g/cm^2.
3. Estimated experimental uncertainty is 1.6% in Be and 1.5% in Au.

*Estimated one-sigma statistical uncertainty exceeds 1% at larger FMR.

J. Electron Energy Deposition in Carbon/Copper/Carbon

Energies (MeV):	1.0
Angles (°):	0
Analysis Method:	C
Angle DeterminationMethod:	N/A
Thermal Coupling Correction Method:	Carbon (B); Copper, none required.

Continuous Slowing Down Approximation Range

Energy (MeV)	Range (g/cm^2)
1.0	4.89×10^{-1} (C)
	6.25×10^{-1} (Cu)

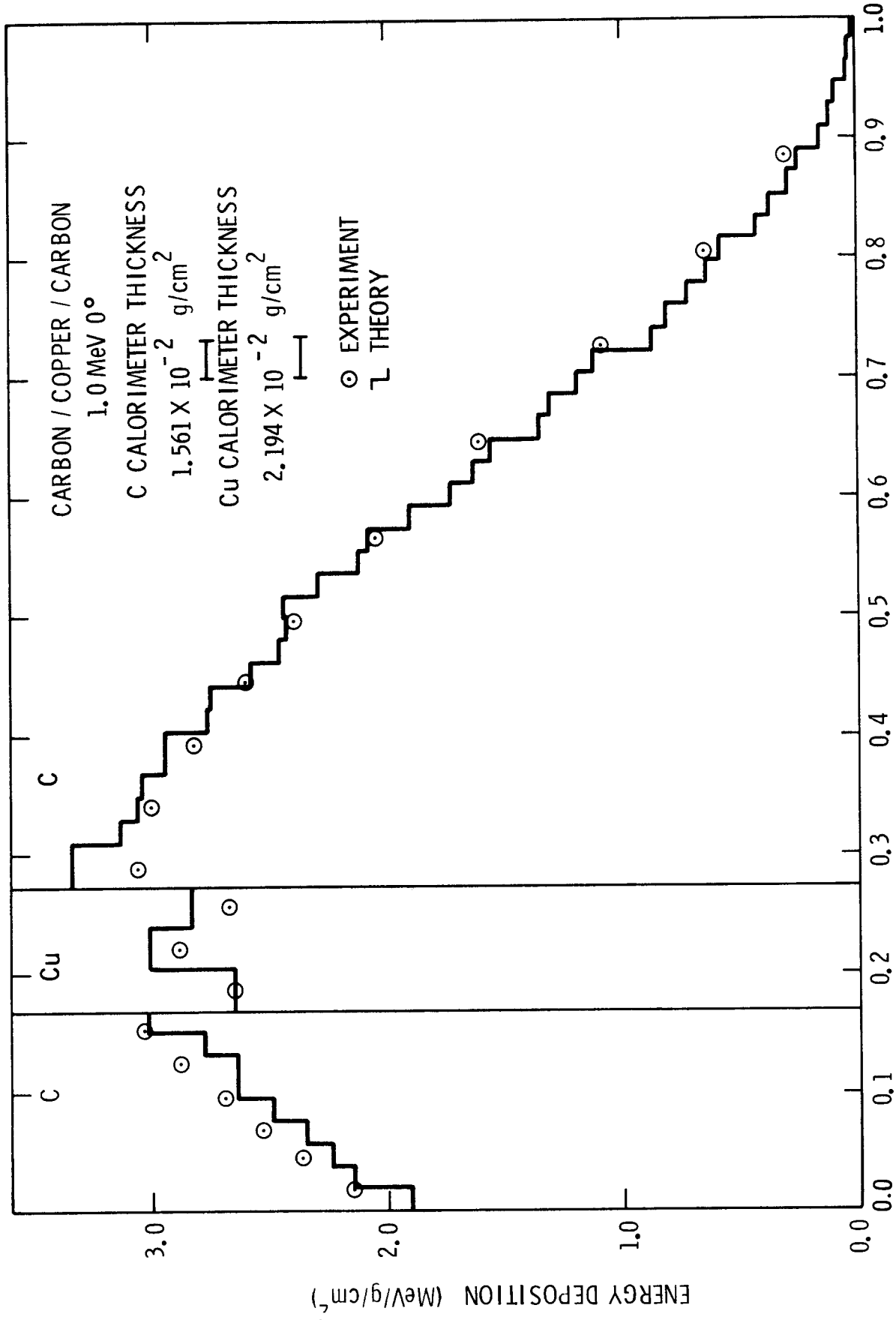

Figure V. J.1. Comparison of Experimental and Theoretical Energy Deposition Profiles in a Carbon/Copper/Carbon Configuration for 1.0-MeV Electrons Incident at an Angle of 0°

Table V. J. 1

Electron Energy Deposition in Carbon/Copper/Carbon[1, 2, 3]

Experimental Results
1.0 MeV, 0°

FMR	J
In C	
0.016	2.15
0.044	2.36
0.067	2.53
0.095	2.69
0.124	2.88
0.152	3.03
In Cu	
0.186	2.65
0.221	2.88
0.256	2.67
In C	
0.289	3.06
0.340	3.00
0.392	2.82
0.444	2.60
0.496	2.39
0.565	2.04
0.646	1.60
0.726	1.08
0.803	0.64
0.884	0.30

Theoretical Results
1.0 MeV, 0°

FMR	J	FMR	J
In C		In C cont	
0.019	1.90	0.516	2.44
0.037	2.15	0.535	2.29
0.056	2.24	0.554	2.12
0.075	2.35	0.572	2.09
0.094	2.49	0.591	1.90
0.112	2.64	0.610*	1.73
0.131	2.64	0.629	1.63
0.150	2.78	0.647	1.56
0.168	3.02	0.666	1.35
		0.685	1.31
In Cu		0.703	1.19
0.203	2.65	0.722	1.12
0.238	3.01	0.741	0.87
0.273	2.83	0.760	0.81
		0.778	0.72
In C		0.797	0.64
0.292	3.34	0.816	0.58
0.310	3.34	0.834	0.43
0.329	3.13	0.853	0.37
0.348	3.06	0.872	0.29
0.367	3.04	0.890	0.25
0.385	2.94	0.909	0.16
0.404	2.94	0.928	0.12
0.423	2.76	0.947	0.09
0.441	2.75	0.965	0.04
0.460	2.58	0.984	0.03
0.479	2.46	1.003	0.01
0.498	2.43		

Total Deposition = 0.945 ±0%

1. FMR is fraction of a mean range.
2. J is energy deposited in MeV/g/cm^2.
3. Estimated experimental uncertainty is 2.0% in C and 1.3% in Cu.

*Estimated one-sigma statistical uncertainty exceeds 3% at larger FMR.

K. Electron Energy Deposition in Carbon/Tantalum/Carbon

Energies (MeV):	1.0
Angles (°):	0
Analysis Method:	C
Angle Determination Method:	N/A
Thermal Coupling Correction Method:	Carbon (B), Tantalum (B)

Continuous Slowing Down Approximation Range

Energy (MeV)	Range (g/cm^2)
1.0	4.89×10^{-1} (C)
	7.63×10^{-1} (Ta)

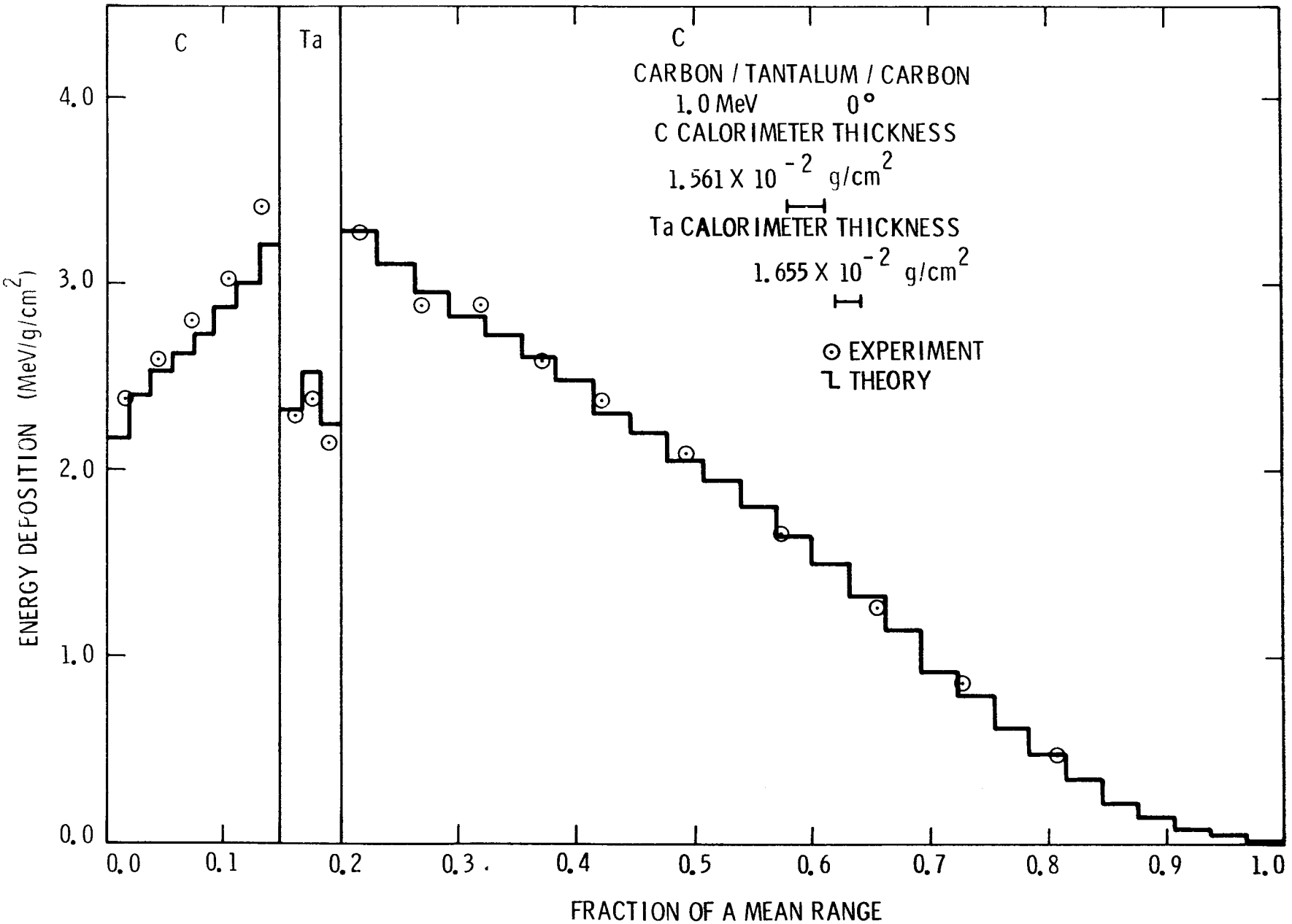

Figure V. K.1. Comparison of Experimental and Theoretical Energy Deposition Profiles in a Carbon/Tantalum/Carbon Configuration for 1.0-MeV Electrons Incident at an Angle of 0°

Table V. K. 1

Electron Energy Deposition in Carbon/Tantalum/Carbon[1, 2, 3]

Experimental Results 1.0 MeV, 0°		Theoretical Results 1.0 MeV, 0°			
FMR	J	FMR	J	FMR	J
In C		In C		In C cont.	
0.016	2.38	0.019	2.17	0.416	2.48
0.044	2.59	0.037	2.40	0.447	2.31
0.072	2.80	0.056	2.53	0.478	2.20
0.105	3.02	0.075	2.62	0.508	2.05
0.133	3.41	0.093	2.73	0.539	1.94
		0.112	2.87	0.570	1.81
In Ta		0.131	3.00	0.600	1.64
0.160	2.29	0.149	3.21	0.631	1.50
0.175	2.38			0.662	1.33
0.190	2.15	In Ta		0.692*	1.15
		0.167	2.32	0.723	0.93
In C		0.184	2.53	0.754	0.79
0.218	3.27	0.201	2.24	0.784	0.62
0.269	2.88			0.815	0.48
0.320	2.89	In C		0.846	0.34
0.372	2.58	0.232	3.28	0.877	0.22
0.424	2.38	0.263	3.10	0.907	0.15
0.494	2.09	0.293	2.95	0.938	0.08
0.574	1.66	0.324	2.82	0.969	0.05
0.654	1.27	0.355	2.72	0.999	0.02
0.728	0.87	0.385	2.61		
0.808	0.48	Total Deposition = 0.884 MeV ±0%			

1. FMR is fraction of a mean range.
2. J is energy deposited in MeV/g/cm^2.
3. Estimated experimental uncertainty is 2.0% in C and 1.2% in Ta.

L. Electron Energy Deposition in Carbon/Gold/Carbon

Energies (MeV):	1.0
Angles (°):	0
Analysis Method:	C
Angle Determination Method:	N/A
Thermal Coupling Correction Method:	Carbon (B); Gold, none required.

Continuous Slowing Down Approximation Range

Energy (MeV)	Range (g/cm^2)
1.0	4.89×10^{-1} (C)
	7.72×10^{-1} (Au)

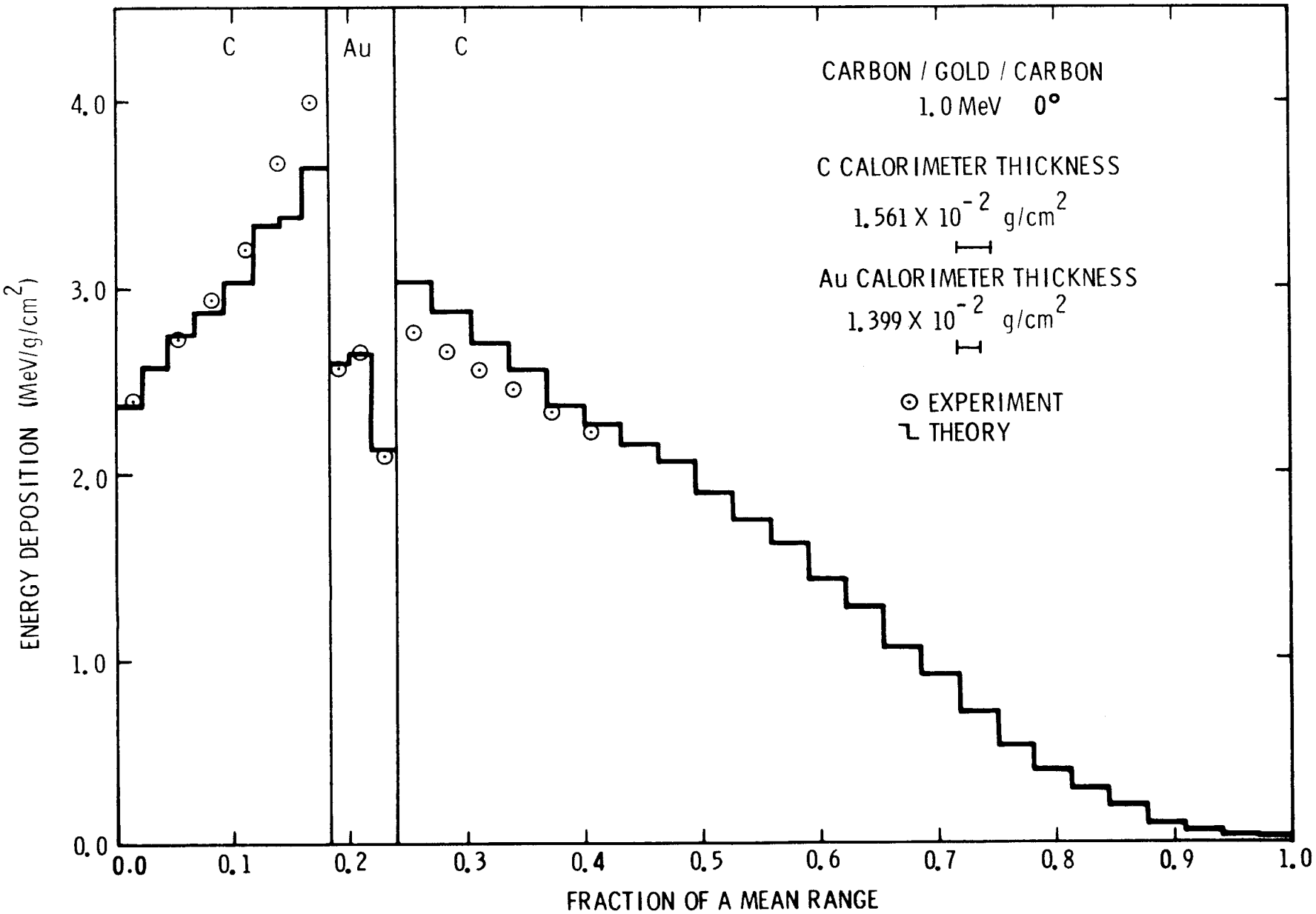

Figure V. L. 1. Comparison of Experimental and Theoretical Energy Deposition Profiles in a Carbon/Gold/Carbon Configuration for 1.0-MeV Electrons Incident at an Angle of 0°

Table V. L. 1

Electron Energy Deposition in Carbon/Gold/Carbon[1, 2, 3]

Experimental Results 1.0 MeV, 0°		Theoretical Results 1.0 MeV, 0°			
FMR	J	FMR	J	FMR	J
In C		In C		In C cont.	
0.016	2.42	0.022	2.37	0.430	2.27
0.049	2.78	0.045	2.57	0.462	2.16
0.081	2.98	0.067	2.75	0.493	2.07
0.110	3.26	0.093	2.87	0.525	1.89
0.138	3.73	0.115	3.03	0.557	1.75
0.166	4.07	0.138	3.34	0.589	1.62
		0.160	3.37	0.621*	1.43
In Au		0.182	3.64	0.653	1.28
0.191	2.57			0.685	1.06
0.210	2.65			0.717	0.91
0.228	2.09	In Au		0.749	0.71
		0.201	2.60	0.781	0.53
In C		0.219	2.64	0.813	0.40
0.254	2.81	0.238	2.13	0.845	0.29
0.282	2.70			0.877	0.21
0.310	2.60	In C		0.909	0.11
0.339	2.49	0.270	3.03	0.941	0.07
0.371	2.38	0.302	2.87	0.972	0.04
0.404	2.27	0.334	2.70	1.004	0.02
		0.366	2.56		
		0.398	2.36		

Total Deposition = 0.877 MeV ±0%

1. FMR is fraction of a mean range.
2. J is energy deposited in MeV/g/cm^2.
3. Estimated experimental uncertainty is 2.0% in C and 1.5% in Au.

M. Electron Energy Deposition in Carbon/Uranium/Carbon

Energies (MeV):	1.0
Angles (°):	0
Analysis Method:	C
Angle Determination Method:	N/A
Thermal Coupling Correction Method:	Carbon (B), Uranium (B)

Continuous Slowing Down Approximation Range

Energy (MeV)	Range (g/cm^2)
1.0	4.89×10^{-1} (C)
	8.09×10^{-1} (U)

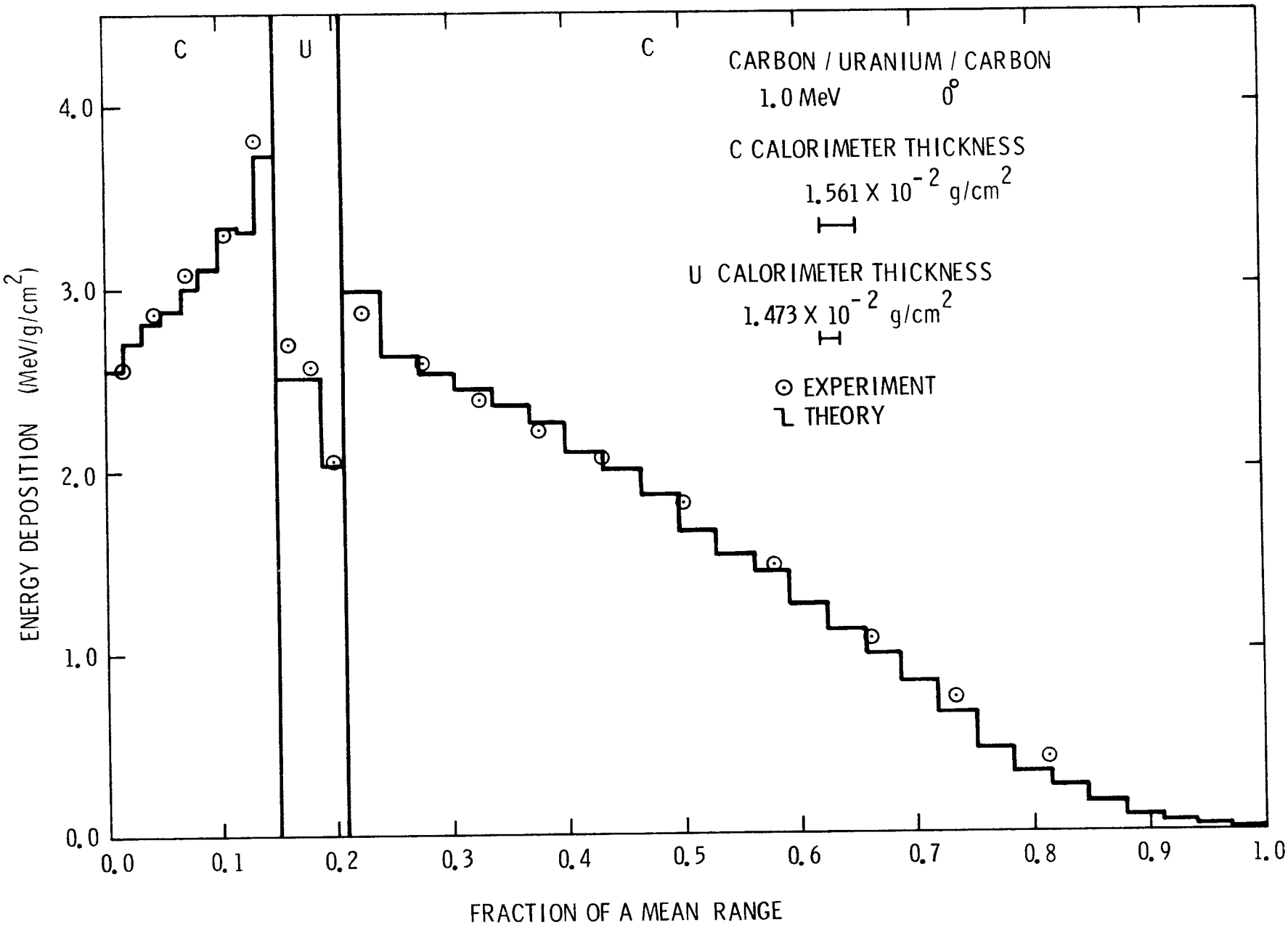

Figure V. M.1. Comparison of Experimental and Theoretical Energy Deposition Profiles in a Carbon/Uranium/Carbon Configuration for 1.0-MeV Electrons Incident at an Angle of 0°

Table V. M. 1

Electron Energy Deposition in Carbon/Uranium/Carbon[1, 2, 3]

Experimental Results 1.0 MeV, 0°		Theoretical Results 1.0 MeV, 0°			
FMR	J	FMR	J	FMR	J
In C		In C		In C cont	
0.016	2.57	0.017	2.56	0.367	2.35
0.044	2.87	0.033	2.71	0.399	2.26
0.072	3.07	0.050	2.82	0.431	2.09
0.105	3.30	0.066	2.88	0.463	1.99
0.133	3.79	0.083	3.00	0.495	1.86
		0.100	3.10	0.527*	1.66
In U		0.116	3.33	0.559	1.53
0.159	2.69	0.133	3.32	0.591	1.43
0.179	2.57	0.149	3.72	0.623	1.25
0.199	2.07			0.655	1.10
		In U		0.686	0.98
In C		0.169	2.51	0.718	0.83
0.223	2.86	0.188	2.51	0.750	0.65
0.274	2.59	0.207	2.03	0.782	0.46
0.325	2.38			0.814	0.32
0.377	2.21	In C		0.846	0.25
0.429	2.06	0.239	2.98	0.878	0.16
0.499	1.80	0.271	2.63	0.942	0.08
0.579	1.44	0.303	2.53	0.974	0.03
0.659	1.07	0.335	2.44	1.006	0.01
0.733	0.73	Total Deposition = 0.831 MeV ±0%			
0.813	0.40				

1. FMR is fraction of a mean range.
2. J is energy deposited in MeV/g/cm^2.
3. Estimated experimental uncertainty is 2.0% in C and 1.4% in U.

N. Electron Energy Deposition in Aluminum/Gold/Aluminum

Energies (MeV):	1.0
Angles (°):	0
Analysis Method:	C
Angle Determination Method:	N/A
Thermal Coupling Correction Method:	None required

Continuous Slowing Down Approximation Range

Energy (MeV)	Range (g/cm^2)
1.0	5.51×10^{-1} (Al)
	7.72×10^{-1} (Au)

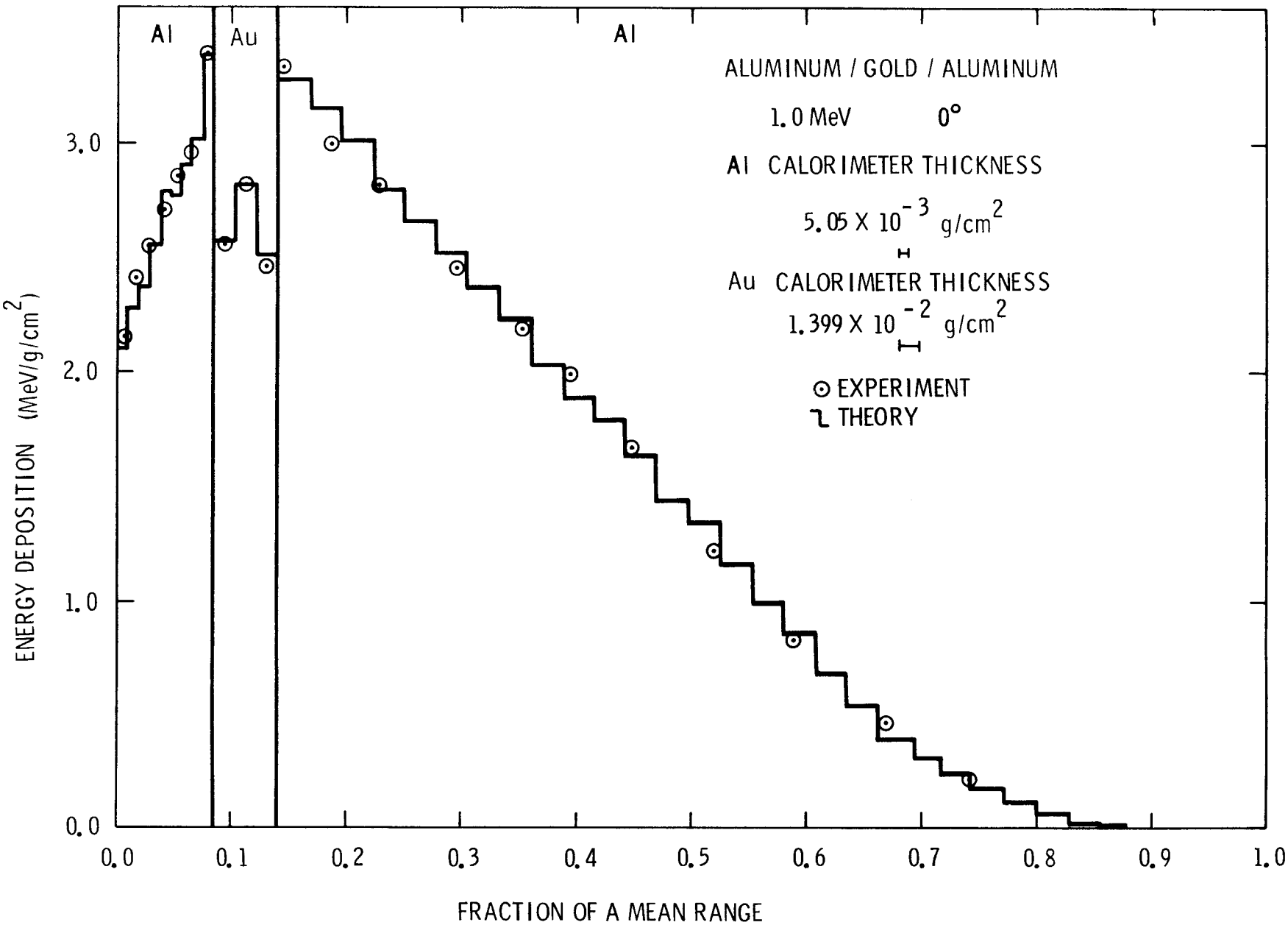

Figure V. N. 1. Comparison of Experimental and Theoretical Energy Deposition Profiles in an Aluminum/Gold/Aluminum Configuration for 1.0-MeV Electrons Incident at an Angle of 0°

Table V. N. 1

Electron Energy Deposition in Aluminum/Gold/Aluminum[1, 2, 3]

Experimental Results 1.0 MeV, 0°		Theoretical Results 1.0 MeV, 0°			
FMR	J	FMR	J	FMR	J
In Al		In Al		In Al cont.	
0.005	2.15	0.009	2.10	0.332	2.37
0.017	2.40	0.018	2.28	0.359	2.23
0.028	2.54	0.028	2.37	0.387	2.03
0.041	2.70	0.038	2.56	0.414	1.89
0.053	2.85	0.047	2.79	0.442	1.79
0.064	2.96	0.056	2.78	0.469	1.63
0.079	3.40	0.065	2.91	0.497	1.44
In Au		0.075	3.02	0.524	1.34
0.093	2.56	0.084	3.40	0.552	1.16
0.112	2.82			0.579	0.99
0.130	2.46	In Au		0.607	0.86
In Al		0.102	2.57	0.634*	0.68
0.145	3.34	0.121	2.82	0.662	0.54
0.186	3.00	0.139	2.51	0.689	0.39
0.226	2.82	In Al		0.717	0.31
0.296	2.46	0.167	3.28	0.744	0.24
0.353	2.19	0.194	3.15	0.772	0.18
0.394	1.99	0.222	3.01	0.799	0.11
0.447	1.66	0.249	2.80	0.827	0.06
0.520	1.21	0.277	2.66	0.854	0.02
0.590	0.83	0.304	2.52	0.882	0.01
0.668	0.46				
0.741	0.22	Total Deposition = 0.810 MeV ±0%			

1. FMR is fraction of mean range.
2. J is energy deposited in MeV/g/cm^2.
3. Estimated experimental uncertainty is 1.4% in Al and 1.5% in Au.

*

O. Electron Energy Deposition in Tantalum/Aluminum

Energies (MeV):[1]	1.033, 0.521, and 0.314
Angles (°):	0
Analysis Method:	Aluminum (A), Tantalum (A and B)
Angle Determination Method:	N/A
Thermal Coupling Correction Method:	Aluminum, none required;[2] Tantalum (B)[3]

Continuous Slowing Down Approximation Range

Energy (MeV)	Range (g/cm^2)
1.033	7.88×10^{-1} (Ta)
	5.69×10^{-1} (Al)

1. Data plotted at nominal energy after adjusting FMR as discussed in introduction of this section.
2. First data point in aluminum at interface is high because of thermal coupling between front tantalum and aluminum calorimeter.
3. Aluminum shield 1.1×10^{-3} g/cm^2.

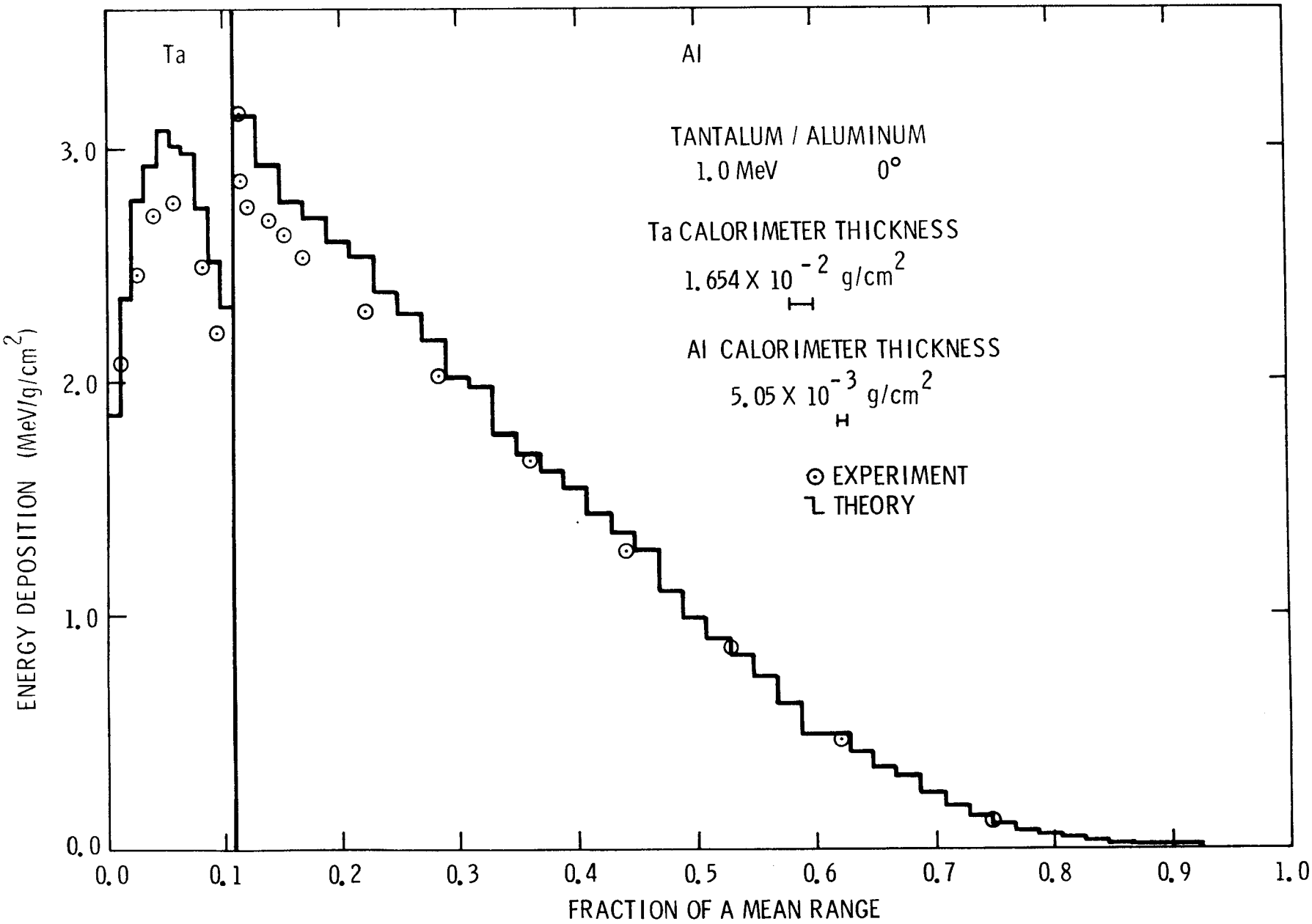

Figure V. O. 1. Comparison of Experimental and Theoretical Energy Deposition Profiles in a Tantalum/ Aluminum Configuration for 1.0-MeV Electrons Incident at an Angle of 0°

Table V. O. 1

Electron Energy Deposition in Tantalum/Aluminum[1, 2, 3]

Experimental Results
1.033 MeV, 0°

FMR	J
In Ta	
0.013	2.08
0.026	2.46
0.040	2.72
0.058	2.77
0.081	2.49
0.095	2.21
In Al	
0.112	3.15
0.115	2.86
0.121	2.75
0.139	2.69
0.153	2.63
0.167	2.53
0.219	2.30
0.282	2.02
0.360	1.67
0.439	1.27
0.529	0.85
0.620	0.46
0.747	0.12

Theoretical Results
1.0 MeV, 0°

FMR	J	FMR	J
In Ta		In Al cont	
0.011	1.87	0.427	1.43
0.021	2.36	0.447	1.39
0.032	2.78	0.467	1.28
0.043	2.93	0.487	1.10
0.054	3.08	0.507*	0.99
0.064	3.01	0.527	0.90
0.075	2.98	0.547	0.83
0.086	2.75	0.567	0.74
0.096	2.52	0.587	0.62
0.107	2.32	0.607	0.49
		0.627	0.49
In Al		0.647	0.41
0.127	3.14	0.667	0.35
0.147	2.92	0.687	0.31
0.167	2.77	0.707	0.24
0.187	2.71	0.727	0.18
0.207	2.60	0.747	0.14
0.227	2.54	0.767	0.11
0.247	2.38	0.787	0.08
0.267	2.29	0.807	0.06
0.287	2.18	0.827	0.05
0.307	2.02	0.847	0.03
0.327	1.98	0.867	0.02
0.347	1.78	0.887	0.01
0.367	1.69	0.907	0.01
0.387	1.62	0.927	0.01
0.407	1.55		

Total Deposition = 0.729 MeV ±0%

1. FMR is fraction of a mean range.
2. J is energy deposited in MeV/g/cm^2.
3. Estimated experimental uncertainty is 1.2% in Ta and 1.4% in Al.

*Estimated one-sigma statistical uncertainty exceeds 3% at larger FMR.

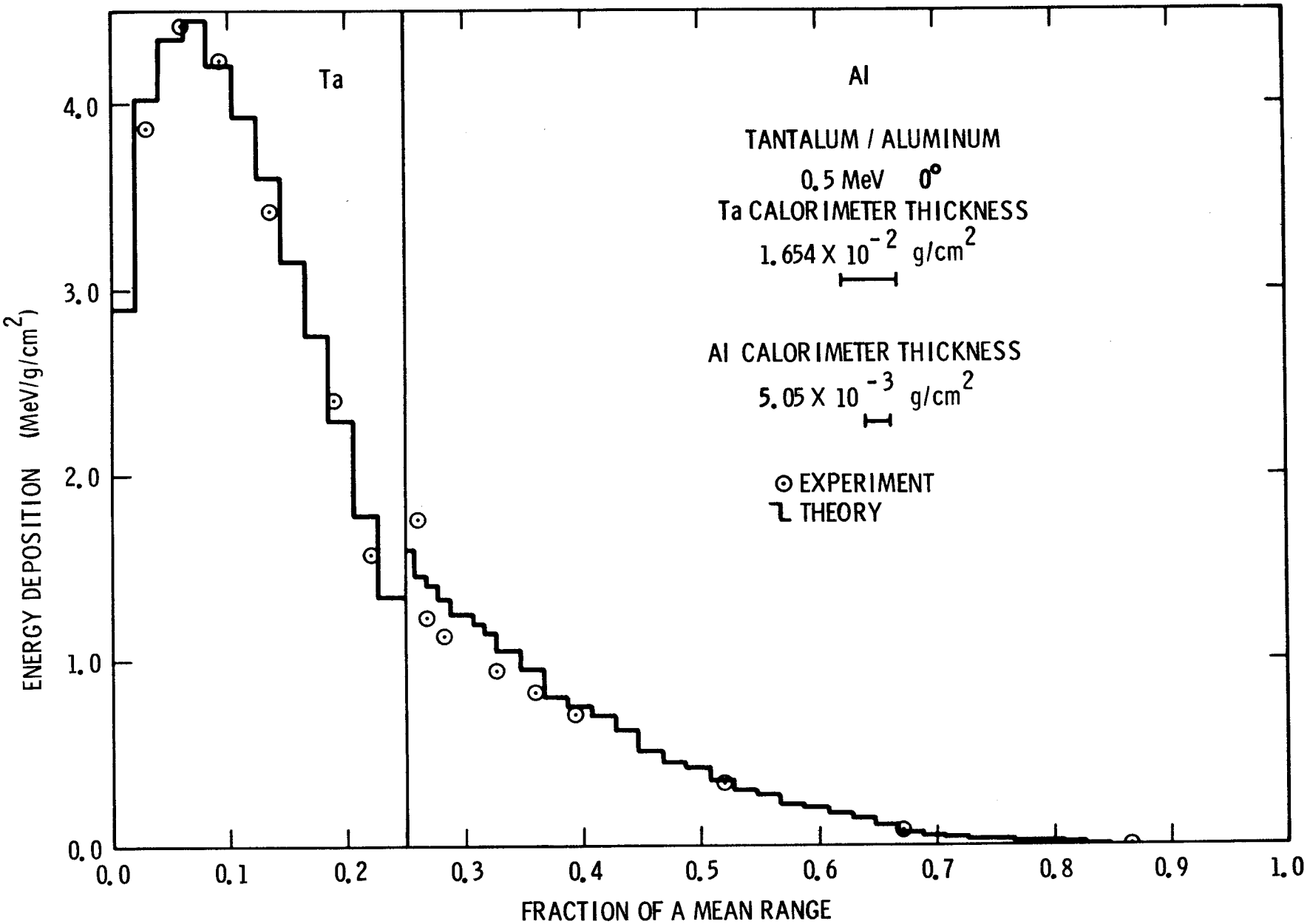

Figure V. O. 2. Comparison of Experimental and Theoretical Energy Deposition Profiles in a Tantalum/ Aluminum Configuration for 0.5-MeV Electrons Incident at an Angle of 0°

Table V. O. 2

Electron Energy Deposition in Tantalum/Aluminum[1, 2, 3]

Experimental Results 0.521 MeV, 0°		Theoretical Results 0.5 MeV, 0°			
FMR	J	FMR	J	FMR	J
In Ta		In Ta		In Al cont.	
0.030	3.87	0.021	2.89	0.387	0.81
0.060	4.42	0.041	4.03	0.407	0.75
0.093	4.23	0.062	4.35	0.427*	0.69
0.135	3.42	0.082	4.46	0.447	0.62
0.190	2.48	0.103	4.21	0.467	0.51
0.221	1.57	0.123	3.93	0.487	0.45
		0.144	3.61	0.507	0.42
In Al		0.165	3.15	0.527	0.35
0.261	1.76	0.185	2.74	0.547	0.30
0.268	1.23	0.206	2.29	0.567	0.27
0.282	1.13	0.226	1.78	0.587	0.22
0.327	0.94	0.247	1.34	0.607	0.20
0.359	0.83	In Al		0.627	0.17
0.393	0.71	0.257	1.60	0.647	0.14
0.520	0.33	0.267	1.46	0.667	0.11
0.673	0.08	0.277	1.41	0.687	0.07
0.865	0.00	0.287	1.33	0.707	0.06
		0.297	1.24	0.727	0.04
		0.307	1.25	0.747	0.03
		0.317	1.19	0.767	0.03
		0.327	1.14	0.787	0.02
		0.347	1.05	0.807	0.02
		0.367	0.94	0.827	0.01
			Total Deposition = 0.320 MeV ±1%	0.847	0.01

1. FMR is fraction of a mean range.
2. J is energy deposited in MeV/g/cm^2.
3. Estimated experimental uncertainty is 1.2% in Ta and 1.4% in Al.

*

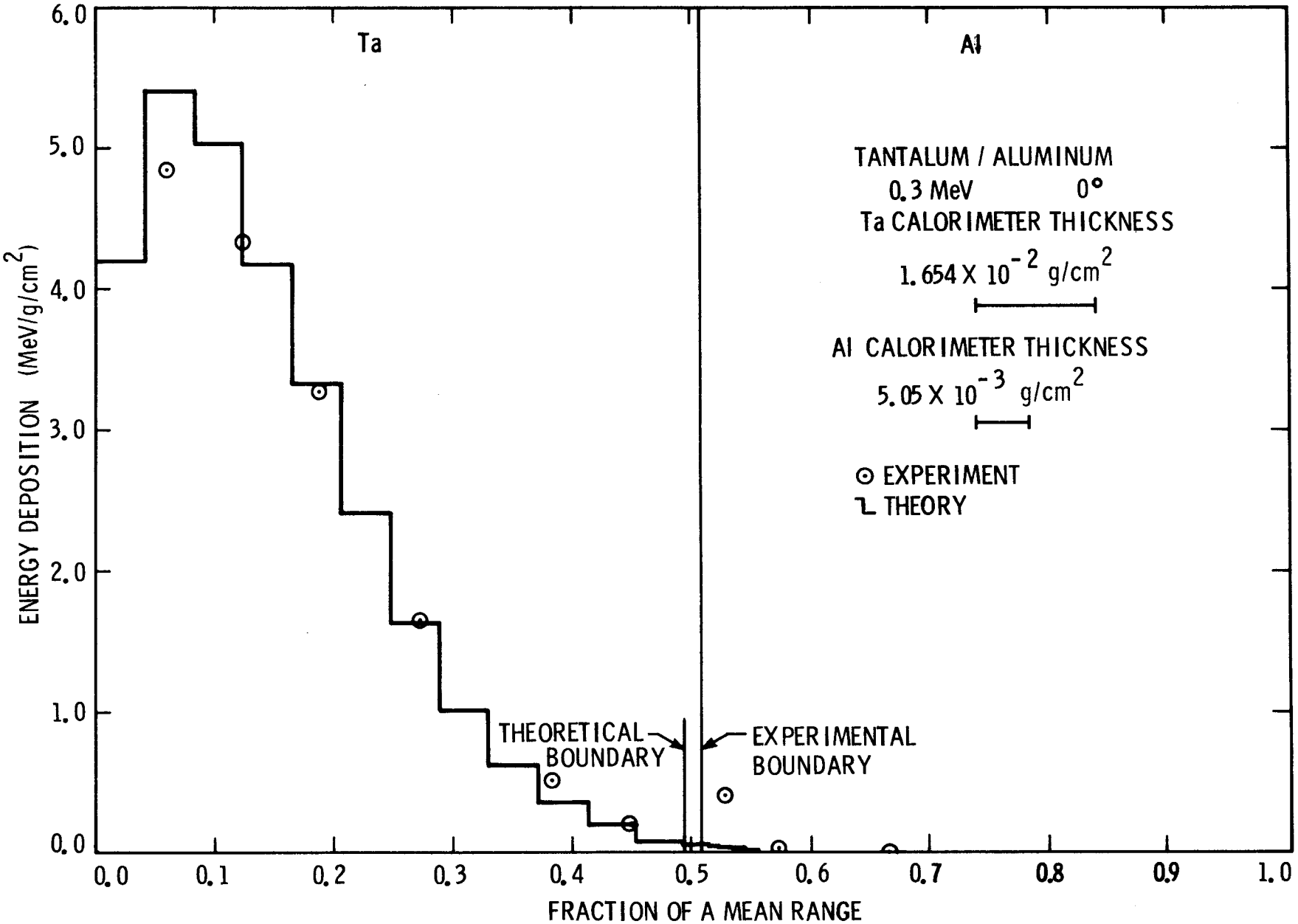

Figure V. O.3. Comparison of Experimental and Theoretical Energy Deposition Profiles in a Tantalum/Aluminum Configuration for 0.3-MeV Electrons Incident at an Angle of 0°

Table V. O.3

Electron Energy Deposition in Tantalum/Aluminum[1,2,3]

Experimental Results 0.314 MeV, 0°		Theoretical Results 0.3 MeV, 0°			
FMR	J	FMR	J	FMR	J
In Ta		In Ta		In Ta cont	
0.060	4.84	0.041	4.20	0.453	0.18
0.123	4.33	0.082	5.41	0.494	0.07
0.188	3.26	0.123	5.03		
0.273	1.63	0.165	4.17	In Al	
0.384	0.49	0.206	3.32	0.504	0.04
0.447	0.19	0.247	2.41	0.514	0.05
		0.288	1.63	0.524	0.04
In Al		0.329	1.01	0.534	0.03
0.528	0.38	0.370*	0.61	0.544	0.03
0.572	0.02	0.412	0.35	0.554	0.01
0.666	0.00				

Total Deposition = 0.188 MeV ±1%

1. FMR is fraction of a mean range.
2. J is energy deposited in MeV/g/cm^2.
3. Estimated experimental uncertainty is 1.2% in Ta and 1.4% in Al.

*Estimated one-sigma statistical uncertainty exceeds 8% at larger FMR.

VI. Conclusions

A new calorimetric method has been developed for the measurement of electron energy deposition profiles in one-dimensional, thermally conducting media available in the form of thin foils. This method has several advantages over more traditional techniques such as ionization chambers, passive dosimetry, solid-state detectors, and luminescence. A specially developed method for analyzing data obtained from a modulated source beam by an on-line computer minimizes sensitivity to beam alignment and beam profile. System calibration with a positive-ion machine eliminates uncertainties due to thermophysical parameters.

The technique has been used to measure electron energy deposition profiles in a number of conducting media spanning the periodic table, as a function of the kinetic energy (≤ 1.0 MeV) and angle of incidence ($\leq 60°$) of the source electrons. Results have been obtained for both semi-infinite and multilayer configurations. In every case, these results have been compared with the predictions of a sophisticated, one-dimensional coupled electron/photon Monte Carlo transport code. Overall agreement between theory and experiment is very good. There is a tendency for the theoretical predictions to be higher near the backscatter peak and lower in the straggling tail; this discrepancy is usually larger at lower source energies and higher target atomic numbers. Another less systematic, but somewhat more serious discrepancy occurs in low-Z media near high-Z/low-Z interfaces.

The present technique becomes less accurate as the thermal conductivity of the stopping medium decreases. For example, unsatisfactory results have been obtained for stainless steel and titanium. In an attempt to overcome this problem, we are studying a new quasi-integral technique which involves mechanical modulation of the electron beam by thin foils in front of a total-stopping calorimeter.

References

[1] Y. Nakai, Jap J Appl Phys, 2, 743 (1963).

[2] J. G. Trump, K. A. Wright, and A. M. Clarke, J Appl Phys, 21, 345 (1950).

[3] F. N. Huffman, J. S. Cheka, B. G. Saunders, R. H. Ritchie, and R. D. Birkhoff, Phys Rev, 106, 435 (1957).

[4] D. Harder, Habilitationsschrift, University of Würzburg (1965).

[5] Y. Nakai, K. Matsuda, T. Takagaki, and K. Kimura, AEC-TR-6806, 7 (1965); Annual Report of the Japanese Association for Radiation Research on Polymers, 6, 7 (1964-1965).

[6] F. N. Huffman, ORNL Report 2137 (1958).

[7] H. Aiginger and E. Gonauser, Atomkernenergie, 13, 33 (1968)

[8] F. Parak and K. Luchner, Nukleonik, 9, 25 (1967).

[9] H. Aiginger and H. Hubney, Atomkernenergie, 10, 479 (1965).

[10] J. G. Trump, R. J. Van de Graaff, and R. W. Cloud, Am J of Roent, 43, 728 (1940).

[11] F. Frantz, excerpted from L. V. Spencer, Phys Rev, 98, 1597 (1955).

[12] M. Rosenstein (PhD dissertation, University of Maryland, 1971).

[13] H. Eisen (PhD dissertation, University of Maryland, 1971).

[14] M. Rosenstein, H. Eisen, and J. Silverman, J Appl Phys, 43, 3191 (1972).

[15] H. Eisen, M. Rosenstein, and J. Silverman, 11th Symposium on Electron, Ion, and Laser Beam Technology, Boulder, CO (1971).

[16] H. Eisen, M. Rosenstein, and J. Silverman, Intl J Appl Radiation and Isotopes (1972).

[17] A. Brynjolfson and G. Thaarup, Fanish Atomic Energy Commission, RISO-53, 1963.

[18] W. L. McLaughlin and E. K. Hussmann, IAEA-SM-123/43, International Atomic Energy Agency, p. 579, 1969.

[19] P. H. Hoff and T. E. Everhardt, Proceedings 10th Symposium on Electron, Ion, and Laser Beam Technology, May 21-23, 1969, P. 454.

[20] S. E. Chappell and J. C. Humphreys, IEEE Trans Nucl Sci NS-17, 272 (1970).

[21] J. M. Davies and B. McQue, Int J Appl Radiation and Isotopes, 21, 283 (1970).

[22] A. E. Grün, Z. Naturforschung, 12A, 89 (1957).

[23] L. V. Spencer, Phys Rev, 98, 1597 (1955).

[24] M. J. Berger, "Monte Carlo Calculations of the Penetration and Diffusion of Fast Charged Particles," Methods in Computational Physics, (New York: Vol. 1, Academic, 1963).

[25] G. H. Miller, G. J. Lockwood, and J. A. Halbleib, IEEE Trans Nucl Sci, NS-21, 359 (1974).

[26]J. A. Halbleib, Sr., and W. H. Vandevender, Nucl Sci Eng, 57, 94 (1975).

[27]G. J. Lockwood, G. H. Miller, and J. A. Halbleib, IEEE Trans Nucl Sci, NS-20, 326 (1973).

[28]G. J. Lockwood, G. H. Miller, and J. A. Halbleib, IEEE Trans Nucl Sci, NS-23, 1862 (1976).

[29]G. J. Lockwood, J. A. Halbleib, Sr., G. H. Miller, IEEE Trans Nucl Sci, NS-25, 1581 (1978).

[30]H. S. Carslaw and J. C. Jaeger, Conduction of Heat in Solids, p 493 (London: Clarendon Press, 1959).

[31]G. J. Lockwood and G. H. Miller, SAND74-0190 (Albuquerque: Sandia Laboratories, 1974).

[32]G. H. Miller and G. J. Lockwood, IEEE Trans Nucl Sci, NS-22, 1072 (1975).

[33]M. J. Berger and S. M. Seltzer, ETRAN Monte Carlo Code System for Electron and Photon Transport Through Extended Media, CCC-107, Radiation Shielding Information Center, Computer Code Collection, Oak Ridge National Laboratory (1968).

[34]F. Biggs, and R. Lighthill, Analytical Approximations for X-Ray Cross Sections II, SC-RR-71-0507 (Albuquerque: Sandia Laboratories, 1971); also F. Biggs and R. Lighthill, Analytical Approximations for Total Pair Production Cross Sections, SC-RR-68-619 (Albuquerque: Sandia Laboratories 1968).

APPENDIX

Differential Equation for Heat Flow

We assume in the following that the calorimeter system possesses circular symmetry. By this we mean not only that the calorimeter is circular in shape but that heat input and removal occurs with no angular dependence. Further, we assume that the thickness of the calorimeter is small enough so that there is no Z-dependence. Thus the calorimeter is a thin circular disc. Although the above assumption of angular independence in heat input and removal is not rigorously fulfilled, the approximation obtained as a result of the assumption is quite satisfactory. In practice, the angular dependence arises from (1) the noncircular shape of the calorimeters (they are generally octagonal in contour) and (2) the noncircular heat input profiles which result when the angle of incidence of the electron beam is deliberately chosen to be other than zero. In general, the calorimeters are so thin that the approximation resulting from the assumption that there is no Z-dependence is very good (generally $w/r_o < 10^{-2}$).

Consider then an annular element, having radii r and $r + \Delta r$, of a circular sheet of radius r_o and thickness w. Let the material have the following properties:

K_1 = thermal conductivity

ρ = density

c = specific heat

ϵ = total emissivity .

Further, assume that the temperature difference between any point on the circular sheet and some reference temperature T_o is given by u(r, t), so that $u(r, t) = T(r, t) - T_o$. Then at radius r the rate at which heat flows into the element is given by

$$-2\pi r w K_1 \left.\frac{\partial u}{\partial r}\right|_r \quad .$$

Likewise, the rate at which it leaves the element at $r + \Delta r$ is given by

$$-2\pi (r + \Delta r) w K_1 \left.\frac{\partial u}{\partial r}\right|_{r + \Delta r} \quad .$$

Thus, the net heat flow into the element by conduction is

$$-2\pi w K_1 \left[r \frac{\partial u}{\partial r}\bigg|_r - (r + \Delta r) \frac{\partial u}{\partial r}\bigg|_{r+\Delta r} \right]$$

$$= 2\pi w K_1 \frac{\partial}{\partial r} \left(r \frac{\partial u}{\partial r} \right) \Delta r \quad .$$

Heat also leaves by radiation. The rate is (for both sides) $4\pi r \Delta r \sigma \epsilon (T^4 - T_o^4)$. The usual approximation is that $T^4 - T_o^4 \approx 4T_o^3 u$, resulting in heat loss at the rate of

$$16\pi r \Delta r \sigma \epsilon T_o^3 u \quad ,$$

where σ is the Stefan-Boltzmann radiation constant.

The final heat-flow terms are the source and sink terms. For the source we assume a heat input rate $(\dot{q})$ per unit area such that

$$\dot{q} = \dot{q}(r, t) \quad .$$

As noted, $\dot{q}$ is assumed to be independent of azimuthal angle. The heat input rate to the element is then:

$$2\pi r \Delta r \dot{q}(r, t) \quad .$$

The sink is represented by the heating of the material. The rate at which heat is deposited is related to the rate of temperature rise by

$$2\pi r \Delta r \, w \rho c \frac{\partial u}{\partial t} \quad .$$

We now collect terms, putting heat input terms on the left (with appropriate attention to the algebraic signs) and the material heating term on the right:

$$2\pi w K_1 \frac{\partial}{\partial r} \left(r \frac{\partial u}{\partial r} \right) \Delta r - 16\pi r \Delta r \sigma \epsilon T_o^3 u + 2\pi r \Delta r \dot{q}(r, t)$$

$$= 2\pi r \Delta r w \rho c \frac{\partial u}{\partial t} \quad .$$

This results in

$$\frac{1}{r}\frac{\partial}{\partial r}\left(r\frac{\partial u}{\partial r}\right) - \frac{8\sigma\epsilon T_o}{wK_1}u + \frac{\dot{q}(r,t)}{wK_1} = \frac{\rho c}{K_1}\frac{\partial u}{\partial t} \quad .$$

If we define

$$\alpha^2 = \frac{8\sigma\epsilon T_o^3}{wK_1} \quad \text{and} \quad \beta^2 = \frac{\rho c}{K_1} \quad ,$$

then further rearrangement results in

$$\frac{1}{r}\frac{\partial}{\partial r}\left(r\frac{\partial u}{\partial r}\right) - \alpha^2 u = \beta^2\frac{\partial u}{\partial t} - \frac{\dot{q}(r,t)}{wK_1} \quad ,$$

which is Eq (1) in this report.

DISTRIBUTION:

Air Force Weapons Lab
Kirtland Air Force Base
Albuquerque, NM 87115
Attn: J. F. Janni, DYC

Oak Ridge National Lab (2)
Union Carbide Corp
P.O. Box X
Oak Ridge, TN 37830
Attn: R. D. Birkoff
R. H. Ritchie

Science Applications, Inc
1651 Old Meadow Rd
McLean, VA 22101
Attn: W. L. Chadsey

US Department of Commerce (3)
National Bureau of Standards
Washington, DC 20234
Attn: M. J. Berger
S. M. Seltzer
L. V. Spencer

US Naval Research Lab (3)
Code 770
Washington, DC 20390
Attn: J. L. Block
J. B. Langworthy
S. K. Searles

Harry Diamond Lab (2)
2800 Powder Mill Rd
Aurora Facility
Adelphi, MD
Attn: S. Graybill
K. Karas

Los Alamos Scientific Lab (2)
P.O. Box 1663
Los Alamos, NM 87544
Attn: J. Mack, J-15
Report Librarian

SPIRE Corp
Patriots Park
Bedford, MA 01730
Attn: R. Little

Maxwell Laboratories, Inc
9244 Balboa Ave
San Diego, CA 92123
Attn: A. Kolb

Physics International
2700 Merced St
San Leandro, CA 94577
Attn: A. J. Toepfer

Department of Physics
University of Texas
System Cancer Center
M. D. Anderson Hospital
and Tumor Institute
6723 Bertner
Houston, TX 77030
Attn: J. R. Marbach

US Naval Research Lab (2)
Code 6680
Washington, DC 20375
Attn: J. Criss
D. Brow

Brookhaven National Lab (2)
Upton, NY 11973
Attn: R. M. Sternheimer
R. F. Peierls

L'Garde, Inc
1555 Placentia Ave.
Newport Beach, CA 92663
Attn: M. Thomas

Kaman Sciences Corp
P.O. Box 7463
Colorado Springs, CO 80933
Attn: W. E. Ware

Mathematical Applications Group, Inc
180 South Broadway
White Plains, NY
Attn: W. Gruber
R. Nagle
R. Goldstein
P. S. Mittelman
M. H. Kalos

Science Applications, Inc
P.O. Box 2351
1250 Prospect St
La Jolla, CA 92037
Attn: E. A. Straker
W. H. Scott, Jr
N. R. Byrn

Mission Research Corp
735 State St
Santa Barbara, CA 93101
Attn: C. L. Longmire

Peter Almond
Physics Dept
M. D. Anderson Hospital
Texas Medical Center
Houston, TX 77030

DISTRIBUTION (Cont):

Anders Brahme
Dept of Radiation Physics
Karolinska Institute
Fack
S-104 01 Stockholm, Sweden

Andree Dutreix
Institut Gustave Roussy
94 800 Villejuif, France

Dietrich Harder
Institut fur Medizinische Physik
und Biophysik
D 3400 Gottingen
Gosslerstr. 10, West Germany

Mr. and Mrs. Hans Leetz
Institut f. Biophysik
Univ Kliniken
D-6650 Homberg 3, West Germany

Hans Svensson
Radiation Physics Dept
Regional Hospital
S-901 85 Umea, Sweden

Andre Wanbersie
Unite de Radiotherapie et de
Neutrontherapie
Centre des Tumerus UCL 54.69
av. Hippocrate, 54
B. 1200 Bruxelles, Belgium

Air Force Cambridge Research Lab (4)
L. G. Hanscom Field
Bedford, MA 01730
Attn: J. N. Bradford
E. A. Burke
A. R. Frederickson
J. C. Garth

Northrup Research & Technology Center (2)
3401 W. Broadway
Hawthorne, CA 90250
Attn: W. Hant
G. Duckworth

The Aerospace Corp (4)
P.O. Box 92957
Los Angeles, CA 90009
Attn: D. G. Swanson
C. Crummer
R. Pruett
C. Greenhow

Experimental & Mathematical
Physics Consultants
Box 66331
Los Angeles, CA 90066
Attn: T. M. Jordan

1111 J. Harris
1112 C. R. Mehl
1112 K. M. Glibert
1112 J. J. Hohlfelder
1116 J. D. Plimpton
1759 L. W. Kruse
2140 B. L. Gregory
2623 W. H. Vandevender
4000 A. Narath
Attn: 4300 R. L. Peurifoy
4400 A. W. Snyder
4500 E. H. Beckner
4700 J. H. Scott
4200 G. Yonas
4210 J. B. Gerardo
4211 E. J. McGuire
4211 M. K. Matzen
4211 M. E. Riley
4211 T. A. Green
4211 J. M. Peek
4212 R. A. Gerber
4212 J. K. Rice
4216 G. H. Miller
4216 A. W. Johnson
4230 J. E. Powell
4231 J. H. Renken
4231 F. Biggs
4231 S. A. Dupree
4231 J. A. Halbleib, Sr.
4231 C. J. MacCallum
4231 P. J. McDaniel
4231 J. E. Morel
4231 C. N. Vittitoe
4232 W. Beezhold
4232 G. J. Lockwood (25)
4232 L. E. Ruggles
4232 L. W. Kruse
4234 R. E. Palmer
4240 G. W. Kuswa
4241 J. R. Freeman
4242 L. P. Mix
4244 P. A. Miller
4247 M. M. Widner
4247 M. J. Clauser
4247 A. V. Farnsworth
4247 M. A. Sweeney
4250 T. H. Martin
4252 J. P. Vandevender
4252 D. L. Johnson
4253 K. R. Prestwich
4253 M. T. Buttram
4253 J. J. Ramirez
4254 S. A. Goldstein
4362 E. F. Hartman
4420 J. V. Walker
4423 D. A. McArthur
4441 L. D. Buxton
4442 W. H. Buckalew
5531 L. D. Bertholf
5534 D. A. Benson

DISTRIBUTION (Cont):

8266 E. A. Aas
8341 L. G. Haggmark
3141 T. L. Werner (5)
3151 W. L. Garner (3)
for DOE/TIC (Unlimited Release)
DOE/TIC (25)
(R. P. Campbell, 3154-3)

Second Printing, February 1987

7112 G. J. Lockwood (50)

ILLUSTRATIONS